4-14-2021 1:00 PM

# Probing the Role of Silicates for Corrosion Control in Lead Plumbing

Hailey Holmes, *The University of Western Ontario*

Supervisor: Herrera, Jose E., *The University of Western Ontario*

A thesis submitted in partial fulfillment of the requirements for the Master of Engineering Science degree in Chemical and Biochemical Engineering

## Abstract

Lead service lines and fittings were installed in Canada's drinking water networks until 1986 and currently pose severe health risks. As pipes corrode over decades of use, lead is released into drinking water resulting in dangerous exposure to elevated lead levels. Sodium silicates can be used for corrosion control of lead, however a basic understanding of how they work is lacking. This thesis describes the results of experiments conducted to determine how silicates interact with lead and aluminum in drinking water, using microscopic and spectroscopic techniques. The results show the presence of silicates inhibited $Pb^{2+}$ carbonates from oxidizing into less soluble $Pb^{4+}$ oxides. Furthermore, aluminum interacts with silicates resulting in allophane formation on the lead surface and extending into the bulk. Allophane did not protect against lead dissolution. Silicates may not be adequate as a corrosion control option in drinking water systems rich in solid lead carbonate ($Pb^{2+}$) phases.



## Keywords

Lead, drinking water, corrosion control, sodium silicates, silicates, aluminosilicates, water treatment, lead in drinking water

## Summary for Lay Audience

Exposure to lead from drinking water can pose serious health concerns. Lead was used for drinking water service lines and fittings in Canada until 1986; the majority are still in place today and have corroded over time with use. Health Canada has set the maximum allowable concentration for lead in drinking water at 5 ppb, as research has shown exposure to even very small amounts of lead can have dire consequences for infant and child development. Corrosion control strategies are needed to reduce human exposure and provide safe drinking water to Canadians. Current methods of corrosion control for lead include pH adjustment and orthophosphate treatment. Lower lead release rates are observed at more basic pH values, resulting in lower dissolved lead concentrations. When water is treated with orthophosphate, a lead-phosphate layer is formed on the pipe wall that prevents lead dissolution. Unfortunately, both methods of corrosion control include drawbacks such as build up of calcium along the pipe wall and increased environmental risk.

Sodium silicate treatment is a third method of corrosion control for lead. Many studies have investigated the effectiveness of silicate treatment; however, few have focused on determining how it works. This thesis examines how silicates interact with lead compounds and the effects on dissolved lead levels. We found that in the presence of lead carbonate in chlorinated drinking water silicates stopped lead from oxidizing to insoluble lead oxides, resulting in higher dissolved lead levels. We also investigated the role of aluminum, as aluminum is often found in drinking water due to use of alum in the water treatment process. We found that in the presence of aluminum, silicates will precipitate out of water and form an aluminosilicate layer. In the short term, this layer does not protect against lead dissolution or result in lower dissolved lead levels. As a result of findings from this research, we do not suggest implementing sodium silicates as a corrosion control option for lead in lead carbonate-rich systems. Future long-term studies on dissolved lead levels during the formation of the aluminosilicate layer in lead oxide rich systems are suggested.

# Acknowledgements

I would like to extend my sincere appreciation to my supervisor, Dr. José Herrera, for the opportunity to conduct research with him over the past two years. His support and encouragement has enabled me to learn so much and I am very grateful for his guidance. This work would not have been possible without him.

I would also like to thank Wei Tian and Chantal Walker for their patience and advice with my many questions as I learned to use our lab equipment, and to Dr. Pjontek for his suggested improvements to my work and use of his laboratory space. Furthermore, I am grateful to Caitlin Corcoran for her help with access to megapure water and guidance with aqueous characterization techniques.

Finally, I would like to express my deepest gratitude to my husband, parents and parents-in-law for their unending love and support.

# Table of Contents

# List of Tables

# List of Figures

# Chapter 1

# 1 Background Information

## 1.1 Lead in Drinking Water

Health concerns linked to lead poisoning in adults and children in 1986 resulted in the ban of lead use in paints, gasoline, drinking water service lines and connections including solder and brass (HealthCanada, 2017; Kitman, 2000; O'Connor et al., 2018). The US Centers for Disease Control and Prevention (CDC) report that lead is adsorbed and stored in bone, blood and tissue in the body. Short term health effects of lead exposure in adults and children include abdominal pain, tiredness, headaches, memory loss and weakness. Long term chronic exposure can cause kidney and brain damage, depression, reduced fertility, high blood pressure, heart and kidney disease and is likely carcinogenic (CDC, 2018). High blood lead levels have been shown to increase blood pressure and renal dysfunction in adults. Further severe effects of high blood lead levels in children include reduced cognition, neurological development issues, behavioral problems and reduced intelligence quotient (Hanna-Attisha et al., 2016; HealthCanada, 2017).

The CDC reports that there is no safe level of lead exposure (CDC, 2018). Countries and provinces have implemented guidelines and restrictions on the acceptable level for lead measured from the tap. In Canada, the maximum allowable concentration (MAC) for lead in tap water is 5 μg/L. Replacing lead service lines is not a simple solution. There are many boundaries to removing and replacing the lines including jurisdictional complexities, insufficient data regarding Canada's inventory of lead service lines, and cost to both the homeowner and municipality (Sgro, 2017). Municipalities that have drinking water distribution networks with lead service lines must treat their water with a form of corrosion control in order to keep lead levels below the MAC. Commonly used forms of corrosion control include pH adjustment and. orthophosphate treatment. A proposed additional measure of corrosion control for lead is sodium silicate treatment.

While many studies have been conducted to analyze the effectiveness of sodium silicate treatment for lead service lines or other metallic pipes at both bench and pilot scale, few have focused on explaining how silicates might inhibit lead corrosion and decrease dissolved lead levels at consistent pH (Kogo et al., 2017; Lintereur et al., 2010; Michael R. Schock et al., 2005).

Thus, improved knowledge on the mechanisms that control the interaction between lead corrosion scale and silicates is required to develop thorough corrosion control strategies to address elevated lead levels in drinking water networks. We have attempted to fill these knowledge gaps by studying the pure phase lead compounds commonly found in corrosion scale, cerussite, minium, and plattnerite, and their behaviour in chlorinated drinking water at consistent pH in the presence of sodium silicate and aluminum. We comprehensively analyzed the solid precipitate formed in these systems after exposure to silicate-dosed synthetic drinking water using UV-Vis, FTIR, and Raman spectroscopy as well as XRD, XPS and SEM-EDX to determine the mechanistic details describing the relationship between lead corrosion scale and the presence of sodium silicate in the aqueous phase. We found that sodium silicates inhibit the oxidation of $Pb^{2+}$ to the less soluble $Pb^{4+}$, resulting in elevated lead levels in systems with scale rich in $Pb^{2+}$ carbonates. Furthermore, in the presence of aqueous aluminum resulted in the formation of the aluminosilicate allophane on the surface of the lead solid phase and extending into the bulk. This aluminosilicate did not prevent lead dissolution.

## 1.2 Thesis Outline

Chapter 1 presents background information and research objectives.

Chapter 2 presents a literature review on methods of corrosion control, studies that have investigated the effects of silicate as a corrosion inhibitor and studies that have attempted to explain how silicates interact with lead.

Chapter 3 presents the experimental design and experimental methodologies.

Chapter 4 presents and discusses the experimental results relating to inhibition of lead oxidation in the presence of silicates, and role of aluminum in aqueous silicate precipitation.

Chapter 5 summarizes the experimental results and provides recommendations for future work.

# Chapter 2

# 2 Literature Review

## 2.1 Current Issues Associated with Lead in Drinking Water

Historically, lead has been used extensively in piping networks, gasoline, paint, and for other industrial purposes due to its properties as a soft, malleable and inexpensive heavy metal. In the past, the primary sources of human lead exposure were gasoline fumes, chips and dust from lead-based paints in the home and lead in soil from anthropogenic and geological sources (O'Connor et al., 2018). In 1986, lead was outlawed for use in paints, gasoline, and drinking water service lines in North America. Paints and gasoline were developed with new formulations and drinking water service lines were no longer installed using lead pipes. Drinking water delivered to buildings with lead service lines installed before 1986 currently presents a main source of human lead exposure (HealthCanada, 2017; Kitman, 2000).

The health effects that result from exposure to lead in drinking water are severe. In adults, these include headache, memory loss, reduced fertility, and heart and kidney disease (CDC, 2018). Infants and children exposed to lead can experience reduced cognition, neurological development issues, behavioral problems and reduced intelligence quotient (Government of Canada, 2013; Hanna-Attisha et al., 2016). In 1992 in Canada, the drinking water maximum allowable concentration (MAC) for lead was set to 10 ppb or 0.01 mg/L. In 2019, the MAC was halved to 5 ppb due to new research that showed the threshold below which lead cannot cause neurological development issues in infants and children cannot be identified (HealthCanada, 2017). In the United States, the Environmental Protection Agency (USEPA) Safe Drinking Water Act Lead and Copper Rule (LCR) set a lead action level of 15 ppb or 0.15 mg/L in 1991, and more recently a maximum contaminant level goal of zero (USEPA, 2020).

Washington D.C. and Flint, Michigan are the most notorious examples of major lead problems in drinking water networks. Washington's lead in drinking water crisis was triggered by a switch in disinfectant from free chlorine to chloramines in November 2000. This resulted from an attempt to reduce the formation of disinfection by-products caused by the secondary disinfectant free chlorine (Edwards et al., 2009). However, chloramines altered water chemistry in such a way that lead was released from corrosion scales built up along the pipe wall (Lin and Valentine,

2008). In April 2014, the city of Flint switched their drinking water supply from Lake Huron to the Flint River as a temporary cost-saving measure until a new pipeline could be installed in 2016 (Hanna-Attisha et al., 2016). The water quality of the Flint River is significantly more corrosive than that of Lake Huron, and the City of Flint did not add any corrosion inhibitors to the water. As a result, the city experienced fast leaching of lead into their water, exposing residents to dangerous lead levels and causing potentially irreversible health problems (Hanna-Attisha et al., 2016).

Lead exposure from lead service lines is not just a problem in the United States; elevated lead levels in drinking water have been documented across Europe and Canada and are a potential public health threat in any community with lead service lines. In November 2019, the major Canadian newspaper the Toronto Star put out an exposé on lead levels across the country, discussing the extent of Canada's lead problem with data showing high lead levels in tap water in every Canadian province. Unfortunately, installation of lead service lines was not well documented; most water authorities do not know where and how many are in their water network (Hanna-Attisha et al., 2016; HealthCanada, 2017; Kim et al., 2011; Van Der Leer et al., 2002).

Many water utilities have plans to eventually replace lead service lines, however the process is costly and expenses are split between homeowner and municipality. Further complicating the matter is the completion of partial lead service line replacements, when the municipality replaces only their portion of the line, resulting in the creation of a galvanic couple that can cause increased lead release (Zhou et al., 2015). Corrosion control of lead service lines is critical to ensure safe drinking water until full replacement of all pipes is completed.

## 2.2 Dissolution of Lead Corrosion Scale

Over time, lead corrosion scale forms on lead service lines through reactions of metallic lead with aqueous species, in turn dependent on water quality. Dissolution of this corrosion scale occurs via reactions that involve electron (redox processes) and/or proton transfer (acid/base process). Leaching of particulate lead can also occur due to changes in water usage patterns or simple mechanical shock to the pipe (LaRose Thompson et al., 1997). The chemical stability of lead corrosion scale is determined by drinking water quality. Most commonly, lead corrosion scale consists of hydrocerussite ($Pb(CO_3)_2(OH)_2$), cerussite ($PbCO_3$) or lead (II) and (IV) oxides ($PbO_2$, PbO and $Pb_3O_4$) (Guo and Herrera, 2018).

Water quality parameters such as pH, alkalinity, oxidation-reduction potential (ORP), and hardness affect the formation and speciation of lead corrosion scale, which further affects how and how much lead dissolves into drinking water. In general, alkalinity and pH have the highest influence on the formation of lead carbonates (hydrocerussite and cerussite) and aluminosilicates on the inner layers of scale. On the other hand, free chlorine seems to have the highest influence on the formation of $PbO_2$ and hydrocerussite in the outermost scale layers (Guo and Herrera, 2018; Kim and Herrera, 2010). These results direct the type of corrosion control method that is most useful for a given water quality. A potential mechanism for the dissolution of lead from lead service lines containing a lead carbonate rich corrosion scale is shown in Equation 1 (Kim and Herrera, 2010). Figure 1 shows the Pourbaix diagram for a lead carbonate system, where it can be seen that lead oxides and carbonates are stable under drinking water conditions (pH range 6 – 9).

$$Pb(s) + 1/2O_2 + H_2O \leftrightarrows Pb^{2+} + 2OH^-$$

$$3Pb^{2+} + 2CO_3^{2-} + 2OH^- \leftrightarrows Pb_3(CO_3)_2(OH)_2$$

$$Pb_3(CO_3)_2(OH)_2 + H_2CO_2 \leftrightarrows 3PbCO_3 + 2H_2O$$

$$3PbCO_3 + HOCl + 3H_2O \leftrightarrows Pb_3O_4 + HCl + 3H_2CO_3$$

$$Pb_3O_4 + 2HOCl \leftrightarrows 3PbO_2 + 2HCl$$

Equation 1

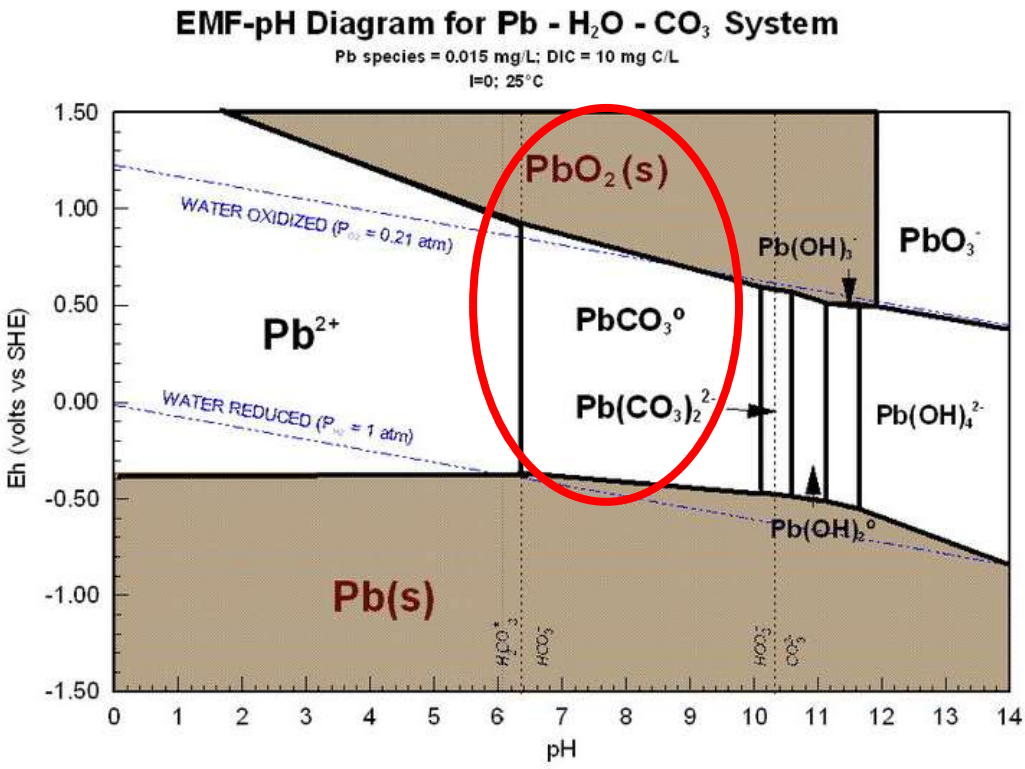


*Figure 1: Pourbaix diagram for lead carbonate system – adapted from (Michael R Schock et al., 2005)*

In some cases, corrosion scale contains mainly lead oxides and the solid phase is rich in $PbO_2$. $Pb^{4+}$ is a strong oxidant that forms in systems exposed to water with a high ORP, regulated mainly by free chlorine. The presence of other reductants found in drinking water such as natural organic matter, manganese ions, and iron ions decrease ORP, potentially triggering the dissolution of $PbO_2$. As shown by the red circle in Figure 1, even the reductive dissolution of $PbO_2$ under drinking water conditions is thermodynamically favorable. This process is, however, kinetically controlled and under well-mixed conditions, the dissolution of $PbO_2$ seems to be controlled by surface reactions rather than mass transport processes (Wang et al., 2013).

Disinfectants, dissolved inorganic carbon (DIC), and pH are important parameters for controlling lead release (Xie and Giammar, 2011). The most used secondary disinfectants in drinking water distribution systems are free chlorine and chloramines. Free chlorine can oxidize Pb(II) to Pb(IV) oxides, however chloramines do not have a high enough ORP to maintain lead in the +4 oxidation state (Switzer et al., 2006). Thus, in water systems with a history of elevated free chlorine usage, $PbO_2$ is the dominant form of lead in the outer layers of corrosion scale (Xie and

Giammar, 2011). Some distribution systems have historically used free chlorine as a disinfectant, then switched to chloramines to reduce the formation of toxic disinfection by-products such as trihalomethanes. In systems that have experienced this switch, the dissolution of $PbO_2$ occurs more quickly due to the lower water ORP when monochloramine is used instead of free chlorine, thus resulting in elevated lead release to municipal drinking water (Edwards et al., 2009; Xie and Giammar, 2011).

Although the redox dissolution process involving aqueous and solid lead species is quite complex, minium ($Pb_3O_4$) has been identified as an intermediate solid phase formed during the oxidation of Pb(II) to Pb(IV) (Guo et al., 2016; Kim and Herrera, 2010). Minium can potentially affect dissolved lead levels in drinking water; reactions from Pb(II) to Pb(IV) affect the stability of corrosion scale and it is well known that free chlorine will oxidize Pb(II) phases to the Pb(IV) phase $PbO_2$ (Edwards and Dudi, 2004; Lytle and Schock, 2005). Solid phase analysis has been used to determine $Pb_3O_4$ may dissolve through a dissolution mechanism that involves continuous formation of $PbO_2$ with co-precipitation of lead carbonates. When a continuous source of free chlorine is present, the final products in the dissolution are $PbO_2$ and lead carbonates (Guo et al., 2016).

## 2.3 Methods for Lead Corrosion Control in Drinking Water Networks

### 2.3.1 pH Adjustment

Lead release rates are lower at higher pH, increasing pH from neutral to basic values in the range of 8 to 9 has been widely applied to control lead release (Kim et al., 2011; Noel et al., 2014; Xie and Giammar, 2011). Multiple studies and pipe loop experiments have shown increasing pH reduced lead release from lead pipe corrosion scale (Kim et al., 2011; Xie and Giammar, 2011). However, pH adjustment is only effective if the dominant lead phase in the corrosion scale is a lead carbonate rather than a lead oxide, and is dependent on water quality parameters such as alkalinity (Guo and Herrera, 2018; Tam and Elefsiniotis, 2009).

At pH values between 7.0 and 7.5, increased alkalinity results in a substantial increase in lead release. In fact, a fivefold increase in alkalinity leads to three- to fivefold increase in lead concentrations (Tam and Elefsiniotis, 2009). However, as inferred from Figure 1, lead dissolution thermodynamically lessens as pH increases to the point of almost being eliminated by

pH 9. At neutral pH, an increase in alkalinity promotes lead dissolution. At basic pH values, the effect of alkalinity on lead leaching is negligible (Tam and Elefsiniotis, 2009).

Characterization performed on lead pipes delivering drinking water that experienced a pH decrease from 8.0 to 7.0 shows destabilization of corrosion scale at lower pH values. The main lead phase in the system was hydrocerussite, with cerussite, minium and aluminosilicate present as secondary components. In batch dissolution experiments, the solubility of lead scale was highest at pH 6 and decreased as pH increased to 8. Furthermore, dissolved lead concentrations were two orders of magnitude greater at pH 6 compared to higher pH values, suggesting that the dissolution of corrosion products is fast and strongly affected by solution pH (Kim et al., 2011; Kim and Herrera, 2010). The dissolution of corrosion scale was slower as pH increased from 6 to 9. Therefore, the reduced lead concentration at higher pH values is assumed to be due to both the lower solubility and slower dissolution of lead at elevated pH values.

### 2.3.2 Orthophosphate Treatment

Orthophosphate is a commonly used corrosion inhibitor for lead systems. It limits lead release by forming low solubility Pb(II) phosphate solids such as hydroxypyromorphite and chloropyromorphite that form films on the corrosion scale depending on pH, DIC and temperature (Guo and Herrera, 2018; Lytle et al., 2009; Noel et al., 2014; Michael R. Schock et al., 2005; Schock, 1989). Orthophosphate may also adsorb to surfaces of lead corrosion products and inhibit their dissolution without forming new solid phases (Noel et al., 2014; Xie, 2010). However, orthophosphate functions best as a corrosion inhibitor for lead systems only within a specific range of pH and DIC (Guo and Herrera, 2018). For low DIC environments, less than 1 mg C/L, the optimum pH for orthophosphate film formation is 8.0. As DIC concentration increases and orthophosphate concentration increases, the optimum pH decreases to 7.0 (Schock, 1989). Orthophosphate is especially effective at pH values greater than 7.5 where up to 70% reduction in lead release is achievable (Tam and Elefsiniotis, 2009).

Orthophosphate inhibits the formation of Pb(IV) in chlorinated waters. In the absence of orthophosphate, cerussite and hydrocerussite, with lead in the +2 oxidation state, transform over time to form Pb(IV) oxides and a rapid change in colour of lead precipitate from white to orange-red occurs. Under the same environmental conditions but with orthophosphate, the formation of Pb(IV) oxides is inhibited and the precipitate stays white (Lytle et al., 2009). This colour change

indicates lead particle transformations occur between hydrocerussite and $Pb_3O_4$ in the absence of orthophosphate. With orthophosphate, the dominant lead phase remains white, which is the colour of hydrocerussite (Lytle et al., 2009). However, the presence of the protective layer of lead-phosphate compound(s) inhibits lead dissolution when it is in the more soluble +2 state (Schock and Celement, 1998).

Ng et al. attempted to determine the mechanistic role of orthophosphate as a corrosion inhibitor in controlling lead release from $PbO_2$ in chlorinated systems experiencing a disinfectant change from free chlorine to monochloramine (Ng et al., 2012). Thermodynamically, lead solids should be transformed to chloropyromorphite via a dissolution-reprecipitation mechanism if there is adequate orthophosphate and chloride concentration. It is well-known that free chlorine reduces Pb(II) ions to form $PbO_2$, however in the presence of orthophosphate, $PbO_2$ formation is inhibited and other lead phosphate compounds such as hydroxypyromorphite and secondary lead phosphate are formed (Ng et al., 2012). These lead phosphate minerals are less thermodynamically stable than chloropyromorphite; in the presence of chlorine, they should transform to the more stable phase. The precipitation of chloropyromorphite occurs below pH 7, whereas precipitation of hydroxypyromorphite occurs below pH 8. Ng and collaborators found that soluble Pb(II) release remained under the USEPA LCR action level of 15 ppb when orthophosphate was added and pH was above 8, due to the slow decomposition of monochloramine throughout the length of their experiment. At lower pH values when orthophosphate was added, they observed a spike in soluble lead followed by a slow decrease back down below the action level (Ng et al., 2012). The authors also used SEM-EDX and XRD to characterize the solid compounds present and the elemental composition changes of lead solid phases. Through this analysis, they were able to determine that the most likely phases to form under drinking water conditions in chloraminated water with orthophosphate are hydroxypyromorphite and secondary lead phosphate. If chloride exists, then chloropyromorphite will form rather than hydroxypyromorphite. They also found an indication of orthophosphate ion adsorption on the $PbO_2$ surface; adsorption of orthophosphate on $PbO_2$ may provide some degree of protection against reductive dissolution by preventing direct contact with reducing agents (Ng et al., 2012). They did not provide any possible reactions or reaction mechanisms for the conversion of $PbO_2$ to hydroxypyromorphite or chloropyromorphite.

There are environmental concerns with adding more phosphates to our water systems. Eutrophication is one of the largest global pollution problems (Gilbert et al., 2005). The main driver of cultural eutrophication, that is eutrophication induced by the actions of humans, is increased nutrient loading to lakes and rivers. Rising fertilizer use for agriculture and food production, discharge of animal waste, atmospheric and aquatic industry emissions, and municipal wastewater, sewage and septic systems all contribute large volumes of phosphorus to environmental water networks (Steffen et al., 2014). Reducing the addition of phosphates to municipal drinking water treatment can help limit challenges for wastewater treatment plants and the effect of increased phosphorus loading on toxic algae blooms. Furthermore, increased phosphorus load in the DWDS could impact bacterial regrowth and biofilm formation (Aghasadeghi et al., 2021).

### 2.3.3 Sodium Silicate Treatment

Sodium silicate is another alternative water additive that can be used for lead corrosion control in drinking water systems and has demonstrated effectiveness in both pilot and full scale studies (Lintereur et al., 2010; Michael R. Schock et al., 2005; Zhou et al., 2015). Sodium silicate solutions consist of mono- and polymeric silicate species and are attractive for use as corrosion inhibitors due to their low toxicity and environmental impact. Their respective concentrations depend on the silicate content and $SiO_2/Na_2O$ ratio, typically 3.22 for water treatment applications (LaRose Thompson et al., 1997). Furthermore, for very dilute solutions such as drinking water where silicate levels are 4-25 ppm as $SiO_2$, depolymerization occurs and the sodium silicate monomer is the dominant species (LaRose Thompson et al., 1997; Lehrman and Shuldener, 1952). The silicate film-forming mechanism is hypothesized to be adsorption of silica to existing oxide or hydroxide films on a metal surface. Initially, high doses of silicates in the range of 20-40 mg/L as $SiO_2$ are required. Once the film is formed and sites are saturated, the dosage of silicate can be dropped significantly lower to maintenance doses in the range of 5-15 mg/L as $SiO_2$ (Scheetz et al., 1997).

In 1990, a town in Massachusetts investigated well-water treatment by sodium silicates for a municipality with lead service lines and found that a silicate treatment of 25-30 mg/L as $SiO_2$ elevated the pH from 6.3 to 7.1 and reduced lead concentrations by 55%. An increased dose of 45-55 mg/L as $SiO_2$ further elevated the pH to 7.5 and reduced lead concentrations by 95%,

meeting LCR action levels (Michael R. Schock et al., 2005). However, these results are complicated in that pH increase is a well documented lead corrosion control mechanism therefore the observed decrease in lead levels from silicate dosing cannot be attributed solely to silicate treatment.

In 1989, Schock and collaborators reported findings with soft, low alkalinity waters at pH 8.2 and silicate dosages between 10 – 20 mg/L as $SiO_2$. The experimental results indicated the slow formation of a surface silicate film over a period of eight to nine months. They reported no decrease in lead dissolution with a silicate dosage of 10 mg/L as $SiO_2$, and experiments suggested that minimum dosage of 20 mg/L as $SiO_2$ would be necessary to achieve a decrease in lead dissolution, along with a long induction period to form a protective film prior to any noticeable decrease in dissolved lead concentrations (Schock, 1989).

In 2005, Schock et al. discussed possible mechanisms for silicates in corrosion control applications based on new research and results from the 1990 Massachusetts event. Claims made as early as 1945 report that a thin silicate coating may form and act as a protective barrier to lead diffusion, however there is no strong analytical evidence to support this claim (Michael R. Schock et al., 2005; Stericker, 1945, 1938). Sodium silicate undergoes basic hydrolysis, increasing water pH which is also beneficial for lead corrosion control (Michael R. Schock et al., 2005). To carry a proper assessment of the effectiveness of silicate in lead corrosion control, a protocol for the systematic isolation of the pH effect from that of silicate addition needs to be developed. The scales from Massachusetts were found to contain chloropyromorphite, a compound originating from poly- or orthophosphate that had been previously used to treat this water system without success prior to silicate treatment in 1990. Through XRD and SEM analysis of the scales, Schock et. al showed that chloropyromorphite was not protective and did not inhibit lead release (Michael R. Schock et al., 2005). When the Massachusetts water was treated with phosphates, they first used an average polyphosphate dose of 3.4 mg/L $PO_4$ at pH 6.1. They treated the water with orthophosphate, with an average dose of 1.2 mg/L $PO_4$ at pH 6.1, and reported elevated lead levels resulting from suspected sequestration of polyphosphate and ineffectiveness of orthophosphate at low pH (Michael R. Schock et al., 2005). When the system was treated with 25-30mg/L as $SiO_2$, they observed a significant increase in pH alongside a large decrease in lead levels to below the LCR action level as evidenced by the graphs shown

in Figure 2 and Figure 3. The data appears consistent with the slow formation of protective silicate films, the hypothesized mechanism of corrosion control with silicates. After continuous monitoring from 1992 to 2000, the data showed a 97% decrease in lead levels from 0.077 mg/L to 0.002 mg/L (Michael R. Schock et al., 2005). However, they did not determine any mechanisms or models that explain how silicates may function as corrosion inhibitors.

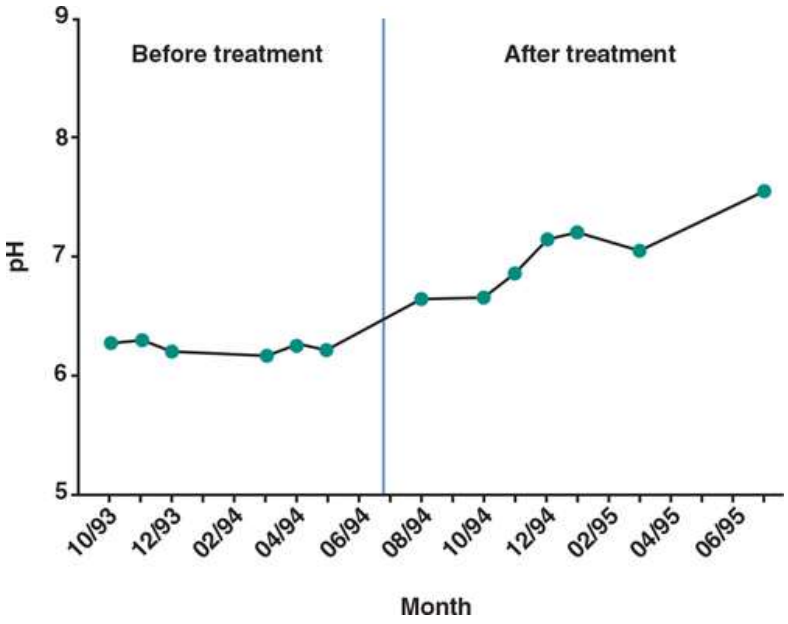


*Figure 2: pH Increase with Silicate Treatment* (Michael R. Schock et al., 2005) *(Copyright License No. 5032681321514)*

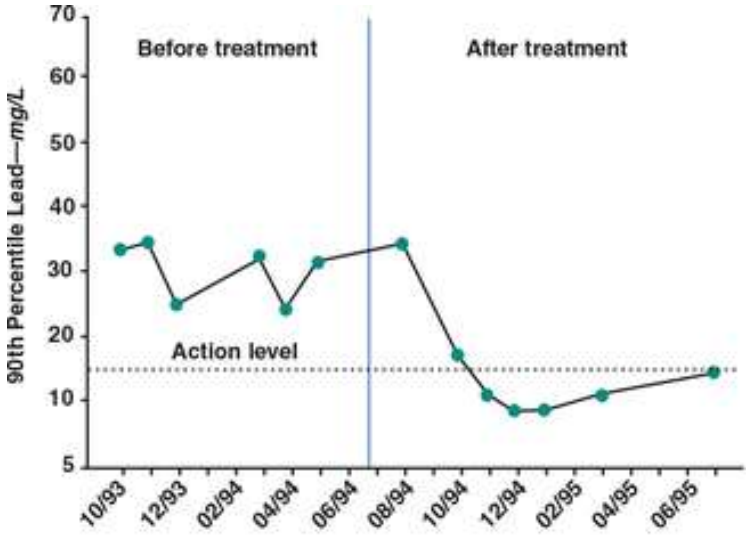


*Figure 3: Change in Lead Level with Silicate Treatment* (Michael R. Schock et al., 2005) *(Copyright License No. 5032681321514)*

Linterer et al.'s 2010 study conducted pilot scale research on silicate doses ranging from 3 to 12 mg/L as $SiO_2$ on lead release. They used samples from a system of copper loops within a pre-existing drinking water distribution system and 50/50 lead-tin coupons. They looked at effects of groundwater, surface water and desalinated water on total and dissolved lead release while also monitoring silicate dose, temperature, alkalinity, chlorides and pH (Lintereur et al., 2010). This study probed the hypothesis of a silica layer forming over lead corrosion scale through an adsorption mechanism, with the film supporting a diffusion barrier that slows the rate at which equilibrium of the system is attained (Lintereur et al., 2010). They were originally planning to dose at 10, 20 and 40 mg/L as $SiO_2$ however dropped the doses during the fourth week of the experiment to 3, 6 and 12 mg/L as $SiO_2$ to prevent precipitation of calcium carbonate that would impede operations. Dissolved lead represented about half of the total lead concentration in the system. Surface characterization of the lead coupons prior to the start of the experiment confirmed the presence of PbO, $Pb(OH)_2$, $PbCO_3$, and $Pb_3(CO_3)_2(OH)_2$ in the scale with hydrocerussite being the dominant phase; these were included to develop an equilibrium model. Equation 2 represents possible reactions with Pb(II) silicate solids, however they were unable to determine any indication that these solids formed, nor thermodynamic evidence that these reactions did occur within the system (Lintereur et al., 2010).

$$PbSiO_{3(s)} + H_2O + 2H^+ \leftrightarrow Pb^{2+} + Si(OH)_4$$
$$Pb_2SiO_{4(s)} + 4H^+ \leftrightarrow 2Pb^{2+} + Si(OH)_4 \qquad \text{Equation 2}$$

Zhou et al. conducted experiments in 2015 on galvanic connections for partial lead service line replacement scenarios to evaluate the impact of various water quality parameters on silicate corrosion control effectiveness. They expected sodium silicates to function as a corrosion inhibitor through one or a combination of two mechanisms: increasing pH of water and decreasing lead release, or formation of insoluble scale (Zhou et al., 2015). The authors evaluated the impact of alkalinity, nitrate, NOM, and disinfectant type on galvanic current and total and dissolved lead release from 24 mg/L as $SiO_2$ sodium-silicate treated partial lead service lines. They found that galvanic current, alkalinity, NOM and disinfectant type had significant positive effects. For both total and dissolved lead, NOM and disinfectant type were significant (Zhou et al., 2015). Differently from previously reported studies, they found that alkalinity had

no effect on lead release in sodium silicate treated water. They presume this is due to the possible benefit of alkalinity promoting a stable pH at the lead surface, outweighing the effect of increased water conductivity and galvanic current. Furthermore, most lead released was in the form of particulate lead rather than dissolved lead. Similar to previously reported studies, the use of monochloramine as a disinfectant resulted in increased total and dissolved lead release (Switzer et al., 2006; Woszczynski, 2011; Xie et al., 2010a; Zhou et al., 2015). The presence of NOM also hindered the effectiveness of sodium silicate. Zhou suggested that for sodium silicate to be an effective corrosion control option for municipal drinking water treatment, chlorine should be used as a secondary disinfectant and minimizing NOM in the water should be prioritized (Zhou et al., 2015). The authors did not present any mechanisms or models by which sodium silicate may function as a corrosion inhibitor for lead.

Li et al. conducted a study investigating the effects of sodium silicates at consistent pH in comparison to orthophosphate and zinc orthophosphate. They used new lead pipes conditioned with 12 mg/L $SiO_2$ for 44 weeks, then 24 mg/L as $SiO_2$ for 28 weeks and 48 mg/L as $SiO_2$ for 12 weeks. The orthophosphate and zinc orthophosphate treated lead pipes were run at 1 mg/L $PO_4^{3-}$ for the entire length of the experiment (Li et al., 2021). Consistent neutral pH levels were maintained through the experiment. Compared to orthophosphate, the authors determined sodium silicate treatment was not an effective corrosion control strategy for their system, however, it should be noted that regardless of treatment method their dissolved lead levels were well above the Canadian MAC of 5 μg/L as well as the USEPA LCR of 15 μg/L. The authors hypothesize the formation of a nanometer thick silicate coating in the silicate-treated system through identification of lead carbonate as the dominant scale phase by XRD analysis, weak Pb 4f, C 1s, and strong Si 2p signal in XPS analysis however they found no evidence that the coating inhibited lead release when comparing levels to those achieved with orthophosphate treatment (Li et al., 2021). They did not observe evidence of layer formation with SEM, but did see increased silicon content in the scale with EDS. They suggest future work should focus on silicate-based barriers that might form due to interaction with other species such as aluminosilicate, quartz or other silicate minerals (Li et al., 2021)

Mishrra et al. recently conducted work studying the effects of silicates at consistent pH on corrosion control of lead service lines. The corrosion scales in the lead service lines consisted of

hydrocerussite, PbO and $SiO_2$ as well as oxides of silicon and aluminum (Mishrra et al., 2021). They observed a decrease in equilibrium dissolved lead concentrations in the pipes treated with 16 and 20 mg/L sodium silicates at pH 7.7, as well as in the pipes with water at pH 8.8 whether or not silicates were present, however the lead release rates did not change with the addition of sodium silicates. The experimental evidence for silica uptake by the scale relied almost entirely on analysis of the silicate content in the aqueous phase; $SiO_2$ concentrations decreased by 7.5 mg/L during the first week of treatment and by 1.5 – 3 mg/L in subsequent weeks with the pipes that took up more silica experiencing greater decreases in dissolved lead concentrations. Analysis of the scale from the treated pipes by SEM-EDS showed only a marginal increase in wt. % silicon (0.7-1.5%) originally present on the scale before treatment (Mishrra et al., 2021). Based on this result, the authors hypothesized uniform uptake of silica throughout the upper portion of the scale as they were unable to identify a discrete silicon rich layer. Furthermore, their XRD and SEM-EDS analysis did not show any silicate solids formed on the pipe scales. The authors hypothesized that in the presence of silicates the system is forming Si- and Al-containing precipitates that are either adsorbing or depositing as an undetectable amorphous solid phase. They also proposed that silicate uptake is a function of the amount of aluminum-rich scale deposited on the surface of the pipes (Mishrra et al., 2021).

The mechanism of lead corrosion control by silicates remains unknown, however, some studies have shown adsorption mechanisms for silicates as corrosion control on other metals. For instance, Yuan et al. used sodium silicates to improve the resistance of hot-dip galvanized (HDG) steels and preventing zinc dissolution. After treating the HDG with silicates and drying the sample, analysis by SEM, XPS, XRD and RA-IR showed a silicon-bearing layer on the HDG metal surface consisting of zinc oxides, zinc silicate and $SiO_2$ (Yuan et al., 2010). A case study conducted in Vancouver, Canada in 1995 looked into using silicates for corrosion control for carbon steel pipes in acidic waters. The work hypothesized that corrosion is inhibited by the formation of a thin metal silicate barrier on top of and interlaced with a metal-hydroxide structure with the deposition of the film depending on the presence of small amounts of corrosion products on the metal surface. It was proposed that the negatively charged silicate ions are attracted to the positive, anodic metallic ions forming a protective film with XRD results confirming the hypothesis and showing a distinct layer adjacent to the water (Katsanis et al., 1986; Macquarrie et al., 1997). Salasi et al. used silicates for corrosion control of carbon steel in

soft water at pH 8. They observed film formation on the metal surface at silicate concentration of 30 ppm and conclude this is the result of a co-inhibitive layer formation between corrosion products. This conclusion also supports the theory regarding the effects of time on silicate inhibitive efficiency, and that silicates need the presence of surface oxidized species to anchor and act as a corrosion inhibitor (Salasi et al., 2007).

## 2.4 Aluminosilicate Formation on Corrosion Scale

The interaction of aqueous aluminum and silica has been studied for many decades. Researchers have theorized that the formation of an aluminosilicate layer in drinking water distribution system pipes may affect the role of corrosion inhibitors and resultant dissolved lead levels. Aluminum is commonly found in distribution systems as alum is a frequently used coagulant in drinking water treatment. Silica is naturally occurring and found in source water.

Studies have identified aluminosilicates as a common phase in corrosion scale characterizations and many researchers have suggested they may have a protective effect on lead dissolution (Guo and Herrera, 2018; Kim and Herrera, 2010; Kvech and Edwards, 2001; Snoeyink et al., 2003). Guo and Herrera observed the outermost scale layer, the layer in contact with water, to be rich in aluminosilicates in their corrosion scale characterization work with four different municipalities in Canada (Guo and Herrera, 2018). Snoeyink et al. conducted a study with corrosion scale from 10 municipalities in the United States and observed aluminum and silica as a major phase in all characterizations where alum was used as a coagulant in the DWDS, and smaller amounts in those municipalities that did not treat their water with alum. They acknowledge some of the aluminum is present as aluminum hydroxide, and some as aluminosilicate (Snoeyink et al., 2003).

Kvech et al. studied the role of aluminosilicate deposits in lead and copper corrosion using water from a system in which aluminosilicate deposits were suspected to be an active agent in corrosion protection. They found that there was no significant difference in lead release in the presence of aluminum with Al concentrations less than 0.01 mg/L. They noted Al sorbed to pipe walls was similar for both lead and copper, however the lead pipes sorbed significantly more silicon. They observed a slight increase in lead and copper release with the formation of aluminosilicate solids. They postulate this is due increased particulates in water causing increased lead release (Kvech and Edwards, 2001).

Li and collaborators studied the effect of aluminum on lead release to drinking water in the presence of the corrosion inhibitor orthophosphate. They found that aluminum accumulation on lead coupons was facilitated by corrosion products, but inhibited by phosphate addition when 200 µg/L Al and 1 mg/L P were used. Dissolved lead levels did not change in the presence of aluminum when phosphate was absent, however, when aluminum was added to the phosphate system dissolved lead levels were 10 – 12 µg/L rather than 1 µg/L which was measured when aluminum was absent. They postulate the increased lead levels were due to the effect of aluminum on the composition and morphology of lead-phosphate compounds forming on coupon surfaces. The pH values used were 6.7, 7.7 and 8.5. Total Al decreased at pH 6.7 and 7.7, revealing Al was adsorbed to the lead surface, however, at pH 8.5 Al accumulation was negligible. They noted that Al was accumulating at an accelerating rate indicating that accumulation was enhanced by the previously formed solids on the coupon surface. No crystalline aluminum solids were visible by XRD – the solids formed were amorphous. Furthermore, no Al-containing solids were visible by SEM suggesting the layer that precipitated was too thin to be visible (Li et al., 2020). They did not discuss the effects that silica might have on their system, nor any information regarding levels of aqueous silica in their system despite mentioning the prevalence of aluminosilicate solids in corrosion scale.

## 2.5 Summary

Lead corrosion control is critical to ensure delivery of safe drinking water to homes, schools and commercial establishments throughout the country. Among corrosion control methodologies, the addition of sodium silicate offers advantages including reduced ecological risk to receiving waters and no build up of calcium along the pipe wall. However, the deployment of a silicate-based corrosion control strategy for drinking water systems requires a better understanding of the associated mechanism of corrosion control and the impacts other common water additives, such as aluminum, might have. This is particularly relevant, given the risks associated with potentially unwanted effects resulting from changes in water quality.

# Chapter 3

# 3 Experimental Methodologies

This chapter presents the methodology and materials used for experimental work and data analysis including experimental set-ups, sampling tools and methods, and characterization specifications. Table 1 presents a summary of experiments.

*Table 1: Experimental Set-Up Summary*

| Experiment | Objective | Batch Reactors |
|---|---|---|
| **Test One** | Impact of silicate on cerussite dissolution at pH 8 | 1A, 1B |
| **Test Two** | Impact of aluminum and silicate on cerussite dissolution at pH 8 | 2A, 2B, 2C, 2D |
| **Test Three** | Impact of aluminum and silicate on cerussite dissolution at pH 7 | 3A, 3B, 3C, 3D |
| **Test Four** | Impact of aluminum and silicate on minimum dissolution | 4A, 4B, 4C, 4D |
| **Test Five** | Impact of solid/aqueous phase ratio on cerussite and plattnerite dissolution | 5A, 5B, 5C |
| **Test Six** | Impact of increasing aluminum on solid/aqueous phase ratio, and cerussite and plattnerite dissolution | 6A, 6B, 6C |

## 3.1 Evaluation of the effect of silicates and aluminum ions in solid phase lead dissolution under drinking water conditions

### 3.1.1 Materials

Cerussite ($PbCO_3$) (Sigma-Aldrich, ACS reagent grade), minium ($Pb_3O_4$) (Alfa Aesar, 97 % metals basis) and plattnerite ($\beta$-$PbO_2$) (Sigma-Aldrich, >97.0 %, ACS reagent grade) were used as sources of lead. Sodium hypochlorite (NaOCl) (Sigma-Aldrich, 10-15 % available chlorine, reagent grade) was used as the source of free chlorine. Sodium sulfate ($Na_2SO_4$) (Sigma-Aldrich, >99.0 %, ACS reagent grade), sodium chloride (NaCl) (Sigma-Aldrich, >99.0 %, ACS reagent

grade), calcium hydroxide (CaOH) (Sigma-Aldrich, >95.0 %, ACS reagent grade), and sodium bicarbonate ($NaHCO_3$) (Sigma-Aldrich, > 99.7%, ACS reagent grade) were used as sources of sulfate, chloride, hardness, and alkalinity, respectively, with megapure water (resistivity of 3 MΩ) to prepare synthetic drinking water. Necessary pH adjustments were performed with nitric acid ($HNO_3$) (Sigma-Aldrich, 70%, purified by redistillation, 99.999 % trace metals basis). Aluminum nitrate nonahydrate ($Al(NO_3)_3 \bullet 9H_2O$) was used as the source of aluminum (Sigma-Aldrich, >98.0 %, ACS reagent grade). N-sodium silicate (National Silicates, Na:Si ratio 3.22) was used as the source of silicates.

Synthetic drinking water was prepared according to the parameters in Table 2 using megapure water. Water was prepared based on the Grand Bend Water Treatment Plant water quality; this is the drinking water supplied to London, Ontario.

*Table 2: Synthetic Drinking Water Parameters*

| **Parameter** | **Grand Bend Water Quality (mg/L)** | **Concentration (mg/L)** | **Chemical Used** |
|---|---|---|---|
| Hardness | 90 | 90 as $CaCO_3$ | Calcium hydroxide |
| Alkalinity | 60 | 60 as $CaCO_3$ | Sodium bicarbonate |
| Chloride | 8 | 8 | Sodium chloride |
| Sulfate | 30 | 30 | Sodium sulfate |
| pH | 8 | 7 – 8 | Nitric acid |
| Free chlorine | 1.2 | 1.2 – 1.8 as $Cl_2$ | Sodium hypochlorite |

### 3.1.2 Experimental Methodology for Tests 1-4

#### *3.1.2.1 Test One – Aluminum-free experiments*

A mother solution of synthetic drinking water was prepared before each experiment. 500 mL was measured using a graduated cylinder and poured into 500 mL high density polyethylene (HDPE) bottles. Test One did not contain aluminum. Batch reactor A (1A) contained 1 g/L of cerussite in synthetic drinking water and batch reactor B (1B) contained 1 g/L cerussite and 20 mg/L silicate in synthetic drinking water. Conditions are summarized in Table 3. Sampling was completed as per the procedure in section 3.1.4. Twice per week 10 mL aliquots were taken, filtered through a

0.2 µm polyethersulfone (PES) filter and preserved in HDPE vials with 1 mL 70% nitric acid. All bottles were placed on a shaker (ThermoScientific MaxQ 2000) at 170 rpm for the 45-day experiment. Following completion of the experiment, vacuum filtration with a 0.45 µm membrane filter was used to separate the solid precipitate for further analysis described in section 3.2. Precipitate was rinsed twice with megapure water prior to drying at room temperature. This experiment was repeated twice to verify results.

*Table 3: Test One – Al-Free Experimental Conditions*

| | **1A** | **1B** |
|---|---|---|
| **Parameter** | **$PbCO_{3(s)}$** | **$PbCO_{3(s)}/SiO_{x(aq)}$** |
| Cerussite (g/L) | 1 | 1 |
| Silicate (mg/L as $SiO_2$) | 0 | 20 |
| Free chlorine (mg/L $Cl_2$) | 1.2 | 1.2 |
| pH | 8 | 8 |
| Experiment length | 45 days | 45 days |

#### *3.1.2.2 Test Two and Three – Aluminum present*

Test Two was designed to determine the combined effect of silicate and aluminum on cerussite. Batch reactor A (2A) contained cerussite, batch reactor B (2B) contained cerussite and aluminum, 2C contained cerussite and silicate and 2D contained cerussite, silicate and aluminum all in synthetic drinking water. 2A and 2C had the same experimental conditions as Test One. Conditions for Test Two are summarized in Table 4. The batch reactors were placed on the shaker at 170 rpm for 45 days and the sampling protocol described in section 3.1.4 was followed. 10 mL aliquots were taken twice per week and preserved with nitric acid for future dissolved lead measurements. After 45 days, vacuum filtration with 0.45 µm membrane filter was completed; solid precipitate was then rinsed twice with megapure water and dried at room temperature for future analysis as described in section 3.2. This experiment was repeated twice to verify results.

*Table 4: Test Two Experimental Conditions – Evaluation of Al Impact with Constant Al Content*

| **Parameter** | **2A** $PbCO_{3(s)}$ | **2B** $PbCO_{3(s)}/Al^{3+}_{(aq)}$ | **2C** $PbCO_{3(s)}/SiO_{x(aq)}$ | **2D** $PbCO_{3(s)}/Al^{3+}_{(aq)}/SiO_{x(aq)}$ |
|---|---|---|---|---|
| Cerussite (g/L) | 1 | 1 | 1 | 1 |
| Silicate (mg/L as $SiO_2$) | 0 | 0 | 20 | 20 |
| Aluminum (mg/L) | 0 | 2 | 0 | 2 |
| Free chlorine (mg/L $Cl_2$) | 1.5 | 1.5 | 1.5 | 1.5 |
| pH | 8 | 8 | 8 | 8 |
| Alkalinity (mg/L as $CaCO_3$) | 60 | 60 | 60 | 60 |
| Experiment Length | 45 days | 45 days | 45 days | 45 days |

Test Three was created as an additional repeat of Test Two but at pH 7 to explore any effect of pH on the uptake of aqueous silicate onto the solid phase. As such, an identical procedure was followed to that described above. The buffering capacity of the water continually brought the pH up to 8 – 8.5; nitric acid was added twice per week to return the pH to the range of 7 – 7.5. Conditions are summarized in Table 5.

*Table 5: Test Three Experimental Conditions – Evaluation of pH Impact*

| **Parameter** | **3A** $PbCO_{3(s)}$ | **3B** $PbCO_{3(s)}/Al^{3+}_{(aq)}$ | **3C** $PbCO_{3(s)}/SiO_{x(aq)}$ | **4C** $PbCO_{3(s)}/Al^{3+}_{(aq)}/SiO_{x(aq)}$ |
|---|---|---|---|---|
| Cerussite (g/L) | 1 | 1 | 1 | 1 |
| Silicate (mg/L as $SiO_2$) | 0 | 0 | 20 | 20 |
| Aluminum (mg/L) | 0 | 2 | 0 | 2 |
| Free chlorine (mg/L $Cl_2$) | 1.5 | 1.5 | 1.5 | 1.5 |
| pH | 7 | 7 | 7 | 7 |
| Alkalinity (mg/L as $CaCO_3$) | 60 | 60 | 60 | 60 |
| Experiment Length | 45 days | 45 days | 45 days | 45 days |

#### *3.1.2.3 Test Four*

Test Four was conducted to analyze any differences between lead oxides and lead carbonates treated with silicates. The experiment was conducted as per the protocol described above. Batch reactor 4A contained minium, 4B contained minium and aluminum, 4C contained minium and silicate and 4D contained minium, aluminum, and silicate all in synthetic drinking water. Conditions are summarized in Table 6. The same sampling protocol was followed as described above. Slightly higher residual chlorine levels were used with average values around 1.8 mg/L. The bottles were on the shaker at 170 rpm for 45 days before vacuum filtration and drying at room temperature for further solid phase characterization.

*Table 6: Test Four Experimental Conditions – Change in Pb-bearing Solid Phase*

| Parameter | 4A $Pb_3O_{4(s)}$ | 4B $Pb_3O_{4(s)}/Al^{3+}_{(aq)}$ | 4C $Pb_3O_{4(s)}/SiO_{x(aq)}$ | 4D $Pb_3O_{4(s)}/Al^{3+}_{(aq)}/SiO_{x(aq)}$ |
|---|---|---|---|---|
| Minium (g/L) | 1 | 1 | 1 | 1 |
| Silicate (mg/L as $SiO_2$) | 0 | 0 | 20 | 20 |
| Aluminum (mg/L) | 0 | 2 | 0 | 2 |
| Free chlorine (mg/L $Cl_2$) | 1.5 | 1.5 | 1.5 | 1.5 |
| pH | 8 | 8 | 8 | 8 |
| Alkalinity (mg/L as $CaCO_3$) | 60 | 60 | 60 | 60 |
| Experiment Length | 45 days | 45 days | 45 days | 45 days |

### 3.1.3 Experimental Methodology for Tests 5-7

#### *3.1.3.1 Test Five*

Test Five was conducted to determine the effect of increased available lead surface area on aqueous silica levels. Experimental conditions are described in Table 7. Batch reactor 5A contained 10 g of cerussite and 10 mg/L of silicate in synthetic drinking water at pH 8. Reactor 5B contained 10 g of cerussite and 10 mg/L of silicate in synthetic drinking water at pH 7. 5C contained 10 g of plattnerite (β-$PbO_2$) and 10 mg/L of silicate in synthetic drinking water at pH 7. 10 mg/L free chlorine was dosed at the start of the experiment to keep the approximate ratio of chlorine to lead as in Tests One – Four. The bottles were placed on a magnetic stirrer for 10 days at mid level stir, then taken off the stirrer for the remainder of the experiment. pH was monitored consistently and adjusted with nitric acid as necessary. Additional chlorine was added when levels dropped below 1 mg/L but only brought back up to approximately 2 mg/L.

*Table 7: Test Five Parameters – Evaluation of Solid/Aqueous Phase Ratio*

| Parameter | 5A $PbCO_{3(s)}/SiO_{x(aq)}$ | 5B $PbCO_{3(s)}/SiO_{x(aq)}$ | 5C $PbO_{2(s)}/SiO_{x(aq)}$ |
|---|---|---|---|
| Cerussite (g/L) | 10 | 10 | 0 |
| Plattnerite (g/L) | 0 | 0 | 10 |
| Silicate (mg/L as $SiO_2$) | 10 | 10 | 10 |
| Aluminum (mg/L) | 0 | 0 | 0 |
| Free chlorine (mg/L $Cl_2$) | 10 | 10 | 10 |
| pH | 8 | 7 | 8 |
| Alkalinity (mg/L as $CaCO_3$) | 60 | 60 | 60 |
| Experiment Length | 100 days | 60 days | 100 days |

Calculations were performed to determine how the aqueous silica concentration would decrease should a monolayer coverage be achieved on the lead surface. The BET surface area of cerussite was measured to be 1.9393 +/- 0.0150 $m^2/g$ using a Micromeritics ASAP 2010 after degassing the sample at 200 °C for two hours. The atomic distance (double layer thickness) of Si – Si in $SiO_2$ has been shown to be 3.02 Å (Kimmel et al., 2009). Using the parameters from Test Five with 10 g/L cerussite and 10 mg/L as $SiO_2$ the following calculations were performed to determine monolayer coverage of $SiO_2$ and resulting change in aqueous phase concentration.

$$Monolayer\ thickness = MT = \frac{1}{2}(SiO_2\ double - layer\ thickness)$$

$$Volume\ SiO_2\ for\ monolayer\ coverage = V_{mono\ SiO_2} = MT * BET\ surface\ area\ of\ PbCO_3$$

$$Mass\ SiO_2\ adsorbed = m = \rho_{SiO_2} * V_{mono\ SiO_2}$$

$$New\ aqueous\ concentration\ SiO_2 = C_{aq\ SiO_2} - \frac{m}{total\ liquid\ volume}$$

#### *3.1.3.2 Test Six*

Tests Six was conducted to determine the effect of adding aluminum to high lead surface area systems. Aluminum was added several times throughout the experiment; 1 mg/L Al was added to batch reactor 6A, 6B and 6C in the first experimental iteration. Chlorine was maintained

between 1 – 2 mg/L. The bottles were placed on a magnetic stirrer for two days at mid level stir, then taken off the stirrer for the remainder of the first iteration. After 21 days for 6A, 14 days for 6B and eight days for 6C, an additional 1 mg/L of $Al^{3+}$ was added to the reactors to determine if spiking the system with additional aluminum would trigger another decrease in aqueous silica levels. The bottles were stirred for two days, then taken off the stirrer for the remainder of the second experimental iteration. After 11 days for 6A, and six days for both 6B and 6C, another 1 mg/L $Al^{3+}$ was dosed. Again, the bottles were stirred for two days and then at rest for the remainder of the third experimental iteration. A fourth iteration was completed on 6A only where an additional 2 mg/L $Al^{3+}$ was added to the system; this final iteration was run for 10 days. Experimental conditions are described in Table 8.

*Table 8: Test Six Parameters – Evaluation of Al Impact – Increasing Al Content*

| | **6A** | **6B** | **6C** |
|---|---|---|---|
| | 4 iterations | 3 iterations | 3 iterations |
| **Parameter** | $PbCO_{3(s)}/Al^{3+}_{(aq)}/SiO_{x(aq)}$ | $PbCO_{3(s)}/Al^{3+}_{(aq)}/SiO_{x(aq)}$ | $PbO_{2(s)}/Al^{3+}_{(aq)}/SiO_{x(aq)}$ |
| Cerussite (g/L) | 10 | 10 | 0 |
| Plattnerite (g/L) | 0 | 0 | 10 |
| Silicate (mg/L as $SiO_2$) | 10 | 10 | 10 |
| Aluminum (mg/L) | 1 → 2 → 3 → 5 | 1 → 2 → 3 | 1 → 2 → 3 |
| Free chlorine (mg/L $Cl_2$) | 2 | 2 | 2 |
| pH | 8 | 7 | 8 |
| Alkalinity (mg/L as $CaCO_3$) | 60 | 60 | 60 |
| Experiment Length (days) | 21 → 11 → 6 → 10 | 14 → 6 → 8 | 8 → 6 → 6 |

### 3.1.4 Sampling Procedure and Analytical Methods

For Tests One through Four, 10 mL sacrificial samples were collected to measure free chlorine using the N,N-diethyl-p-phenylenediamine (DPD) free chlorine Hach colorimetric method 8021. Chlorine was added as necessary to bring levels back up to 1.2 – 1.8 mg/L. 10 mL sacrificial samples were also collected to measure silicate as mg/L $SiO_2$ using the silicomolybdate Hach colorimetric method 8185 once per week. Silica and chlorine measurements were both performed using the Hach DR900 Colorimeter. Twice per week, pH was measured using a Thermo Scientific Orion Star A111 pH meter with a non-glass ISFET probe. The pH meter was calibrated using a 3-point calibration (pH 4, 7 and 10) prior to each set of measurements. The pH probe was cleaned with Deionized Water and a Kimwipe and measurements were taken directly from the reactor. For Tests Two, Three, and Four, 5.6 mL sacrificial samples were taken to measure alkalinity once per two weeks using the Hach drop count titration AL-AP method with sulfuric acid, and aqueous silica levels were measured twice per week rather than once.

For Tests Five and Six, the same equipment as above was used to measure free chlorine, silica, pH and alkalinity. For Test Five, aqueous silica levels were measured twice per day for the first week, twice per week for the next 4 weeks, then once per month for the remainder of the experiment. For Test Six, aqueous silica levels were measured twice per day for the first two days, and once every other day for the remainder of the experiment. The pH was monitored consistently and adjusted with nitric acid as necessary.

Dissolved lead concentrations were measured from the nitric acid preserved 10 mL aliquots taken throughout the experiment via Inductively Coupled Plasma – Mass Spectroscopy (ICP-MS) at Bureau-Veritas Laboratories using US EPA Method 6020B.

## 3.2 Methodology of Characterization

UV-Visible light spectroscopy was performed on the dried solid phase samples using a UV-3600 SHIMADZU spectrophotometer equipped with a Harrick Praying Mantis cell for diffuse reflectance. The wavelength range used was 200 nm to 800 nm with a sampling interval of 1 nm, a *fast* scan speed, and a slit width of 3 nm. The spectra were obtained in diffuse reflectance mode and transformed to absorption using the Kubelka-Munk function in the UVProbe® version 2.41 software. Results were normalized and then smoothed using a 9-point rolling average prior to presentation. UV-Vis spectroscopy was performed in house.

Fourier Transform Infrared spectroscopy was performed using the VERTEX 70 spectrometer equipped with a liquid-nitrogen cooled MCT detector, a Harrick Praying Mantis cell for diffuse reflectance and OPUS® software. Spectra were measured in the mid-range of 400 – 4000 $cm^{-1}$ in absorbance mode at a 4 $cm^{-1}$ resolution and 64 scans per sample. Results were normalized and smoothed using the asymmetric least squares method prior to presentation (Boelens et al., 2005). FTIR spectroscopy was performed in house.

Raman spectroscopy was performed using a ReniShaw micro-Raman 2000 system. The spectra were obtained using a He-Ne laser with a 632.8 nm excitation wavelength, 0 – 2000 $cm^{-1}$ range in micro mode. The acquisition time was 20 s at 2 mW for each spectrum. Four scans were taken at different points for each sample and the average was used as the representative spectra. Results were normalized and smoothed using the asymmetric least squares method prior to presentation (Boelens et al., 2005). Raman spectroscopy was performed by Daiqiang Liu in Dr. Song's laboratory in the Chemistry Department at Western.

Powder XRD (pXRD) was performed using a Rigaku Dmax X-ray diffractometer with radiation type CoKα1 = 1.78897 Å, a power of 40 kV x 35 mA, a beam diameter of 12 mm x 6 mm, a 2-theta step scan with step size 0.02 °/step, step time of 1 s per step and 2Θ range of 5 ° - 90 °. pXRD was performed by Dr. Roberta Flemming at the Powder and Micro X-Ray Diffraction Facility at Western.

X-ray Photoelectron Spectroscopy (XPS) was performed using a Kratos AXIS Supra spectrometer with a monochromatic AI Kα source (15 mA, 15 kV). The instrument work function was calibrated to give a binding energy (BE) of 83.96 eV for the Au 4f7/2 line for metallic gold and the spectrometer dispersion was adjusted to give a BE of 932.62 eV for the Cu 2p3/2 line of metallic copper. The Kratos charge neutralizer system was used on all samples. Samples were mounted on double-sided adhesive tape prior to analysis. Survey scans were carried out with an analysis area of 300 x 700 μm and a pass energy of 160 eV; high resolution analysis was carried out with the same analysis area but a pass energy of 20 eV. Spectra were charge corrected to the main line of the carbon 1s (adventitious carbon) spectrum set to 284.8 eV. Spectra were analysed using the CasaXPS® software version 2.3.14. XPS was performed at Surface Science Western by Dr. Mark Biesinger.

Scanning Electron Microscopy with Energy Dispersive X-ray Spectroscopy (SEM-EDX) was performed with the Zeiss 1540XB Field Emission Scanning Electron Microscope, Oxford Instruments X-Max x-ray detector, and Inca analysis software. EDX analysis was performed at 20 keV beam energy and SEM imaging was performed at 1 keV beam energy. SEM-EDX was performed at the Nanofabrication Facility at Western by Dr. Todd Simpson.

# Chapter 4

# 4 Impact of Aqueous Silicate on Lead Dissolution

## 4.1 Introduction

Elevated lead levels have been observed in tap water across the continent as a result of lead dissolution from corrosion scale in lead service lines and fittings in the drinking water distribution system. Lead service lines and fittings were installed in Canada and the United States until 1986, and several of these lines are still in place today (Government of Canada, 2013). Exposure to even low lead levels poses very serious health threats to humans. Health Canada has set the MAC for lead at 5 ppb to prevent adverse health effects (HealthCanada, 2017). There are, however, numerous municipalities across the continent with homes and schools with lead levels above the MAC.

There are several methods of lead corrosion control including water treatment with orthophosphate, pH adjustment or sodium silicate. In order to develop the most effective corrosion control strategy for a given water quality, a thorough understanding of the mechanisms governing these phenomena is required. There is a knowledge gap specifically surrounding how sodium silicates function as a corrosion control strategy for lead. Many studies have shown the effectiveness of water treatment by sodium silicate, but few, if any, have been able to determine how this water additive interacts with lead to lower exposure in distribution systems (Kogo et al., 2017; Li et al., 2019; Mishrra et al., 2021; Michael R. Schock et al., 2005; Stericker, 1945). Studies have focused on the effectiveness of sodium silicates as a corrosion control strategy for lead at bench, pilot and plant scale by comparing different doses, pre-treatment and conditioning levels and lengths of time, and water qualities with dissolved lead levels (Kogo et al., 2017; Li et al., 2021; Lintereur et al., 2010; Macquarrie et al., 1997; Mishrra et al., 2021; Schock, 1989; Zhou et al., 2015).

Most studies worked with corrosion scale harvested from lead pipes or fabricated through conditioning regimens, however we chose to use pure phase $Pb^{2+}$ carbonates and $Pb^{2+/4+}$ oxides to isolate the effectiveness on scale with well defined lead phase characteristics. Cerussite, minium and plattnerite have all been documented as common major lead phases in lead pipe corrosion scale harvested from DWDS (Guo and Herrera, 2018; Kim and Herrera, 2010; Lytle

and Schock, 2005; Xie et al., 2010b) The dominant phase of lead in the corrosion scale can be predicted based on water quality and disinfectant type. We used batch reactors with various combinations of cerussite, minium, plattnerite, aluminum, and silicates in chlorinated drinking water and analyzed the aqueous chemistry throughout the 45- to 120-day experiments. In addition, the solid phase was harvested, dried and characterized using spectroscopic techniques including UV-Vis, FTIR, Raman, XRD, XPS and SEM-EDX. Both aqueous and solid phase observations provide valuable insight into the mechanisms governing silicates as a corrosion control strategy for lead and confirm the importance of understanding how a corrosion inhibitor works prior to implementation in a DWDS.

## 4.2 Results and Discussion

### 4.2.1 Impact of Aqueous Silicate on Dissolution of Cerussite

#### *4.2.1.1 Analysis of Changes in Aqueous Phase*

Free chlorine measurements and chlorine adjustments were carried every three days. Figure 4 shows the results obtained for the residual levels after periodic adjustment over the span of 45 days. Previous reports indicate that lead carbonates are oxidized in the presence of free ‘ chlorine under typical drinking water conditions (Michael R Schock et al., 2005) and the results depicted in Figure 4 are consistent with these reports. A faster rate of chlorine depletion is observed in the absence of silicates, which could be interpreted as silicate interfering with the oxidation of $Pb^{2+}$ species by free chlorine. These experiments were conducted at consistent pH in order to isolate for the effect of silicates; pH levels with time are depicted graphically in Appendix A Figure 32.

As the experiment progressed, a change in colour of the $PbCO_{3(s)}/Al^{3+}_{(aq)}$ and $PbCO_{3(s)}$ precipitates (reactors 1A, 2A and 2B, 3A and 3B) from white to orange-brown-grey was also observed. Figure 5 depicts a typical example of these changes. This observation hints at a change in lead phase; Pb(II) carbonates are white whereas higher oxidized Pb species, such as Pb(IV) oxides, display color. Indeed, a phase change could be hypothesized, specifically a change from $PbCO_3$ to $Pb_3O_4$ and/or $PbO_2$ through oxidation by free chlorine. $Pb^{2+}$ from lead carbonate is oxidized according to Equation 3 (Xie, 2010). $PbO_2$ occurs as black in colour. The intermediate phase $Pb_3O_4$ (minium), displays a bright orange colour, suggesting that this specific phase may also be present in the precipitate due to the colour change observed. In fact, minium has been

identified as an intermediate phase in the oxidation of $Pb^{2+}$ lead carbonates to $Pb^{4+}$ lead oxides (Guo et al., 2016; Kim and Herrera, 2010). The formation of both phases could explain the colour change that occurred over the course of the experiment in the absence of silicates. In the presence of dissolved silicates, no color change was observed.

Lytle and collaborators reported a similar finding in their study of the effects of orthophosphate on lead phase transformation from hydrocerussite to lead oxides at pH 7.75 – 8.1 with a 3 mg/L free chlorine residual. Throughout their experiment they observed white hydrocerussite darkening in colour to shades of dark red and grey, dependent on pH, as well as a decrease in lead solubility in the absence of orthophosphate (Lytle et al., 2009). Through oxidation-reduction potential (ORP) measurements, they were able to show that the ORP was much higher in the absence of orthophosphate despite the same concentrations of available free chlorine. They proposed that orthophosphate changed the ORP of the water, hence affecting the transformation of the lead carbonate to higher valence lead oxide. Compared to phosphates, silicates have nil redox activity under drinking water conditions. Although ORP was not monitored during these experiments, it is extremely unlikely that the presence of silicates lowered the ORP of the water resulting in slower chlorine consumption and inhibiting the formation of $Pb^{4+}$ oxides. There is, however, a clear impact of chlorine consumption due to the presence of silicates.

To try to obtain a more quantitative description of this effect we carried a simple mass balance, assuming that chlorine was consumed through a direct redox reaction where $Pb^{+2}$ is oxidized to $Pb^{+4}$ in the system. The stoichiometry presented in Equation 3 indicates free chlorine is consumed in a 1:1 mole ratio to form $Pb^{4+}$ species. Using this ratio, we calculated a hypothetical percentage of $Pb^{4+}$ formed (using the total lead present in the system as benchmark). The results obtained from this calculation are presented in Figure 6 as a function of time. First, it is clear that the amount of $Pb^{+4}$ in the system steadily increases over time, however the presence of silicates dramatically slowed the formation of $Pb^{4+}$. There is an approximate 84% difference in final amount of $Pb^{4+}$ formed with and without silicates. Remarkably, the presence of aluminium ions does not impact the observed trend in the case of the silicate-free system (blue vs green data points), however it seems to have a small (though minor) impact for the case where silicate is present in the system.

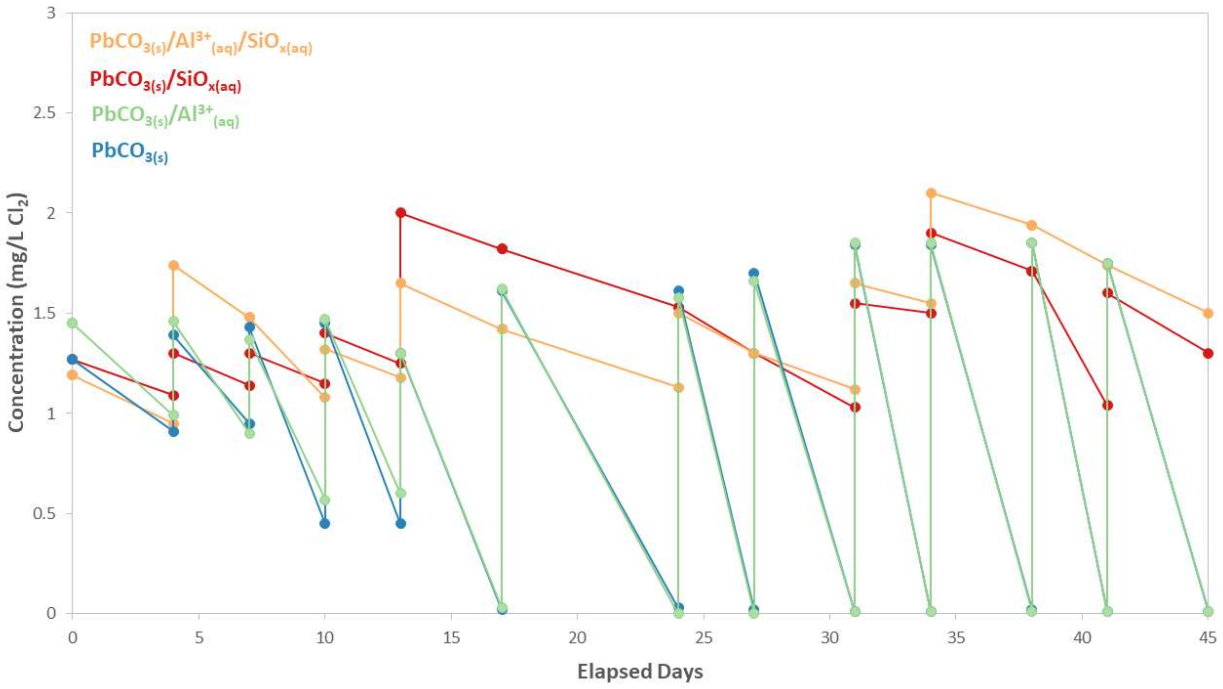


*Figure 4: Change in chlorine concentration with time at pH 8, cerussite solid phase. Chlorine was continually dosed to achieve a 1.5 mg/L residual, and was consumed more slowly in the presence of silicates.*

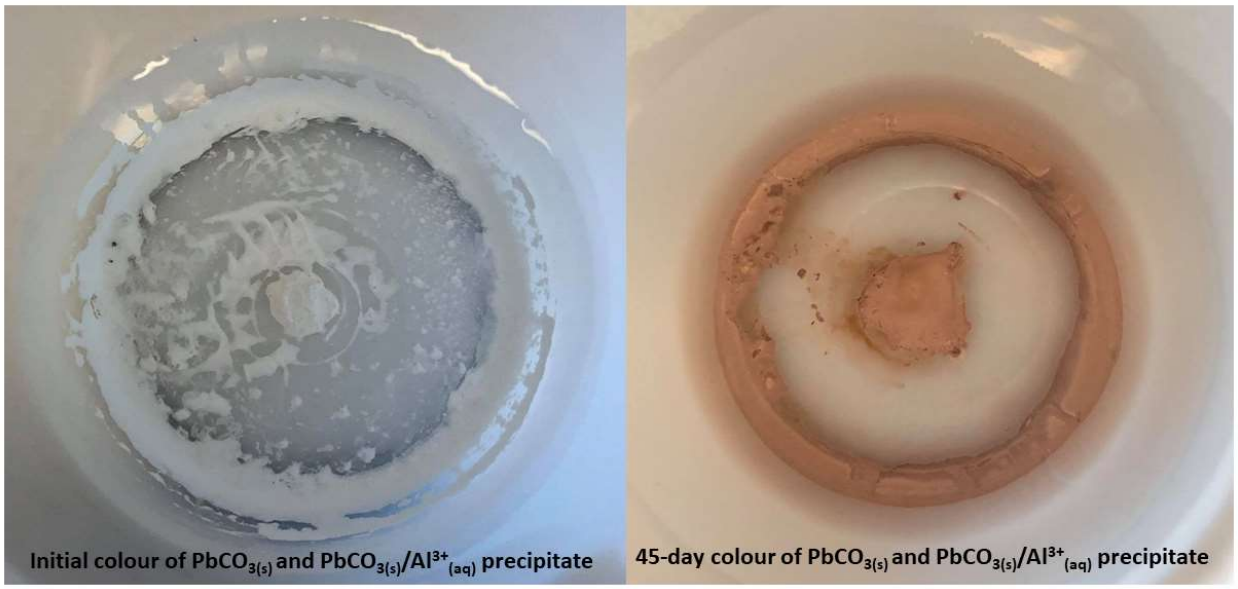


*Figure 5: Colour change of lead carbonate precipitate in the absence of silicate over 45 days of exposure to chlorinated drinking water.*

$$HOCl + Pb^{2+} + H_2O \rightarrow PbO_2 + Cl^- + 3H^+ \qquad \text{Equation 3}$$

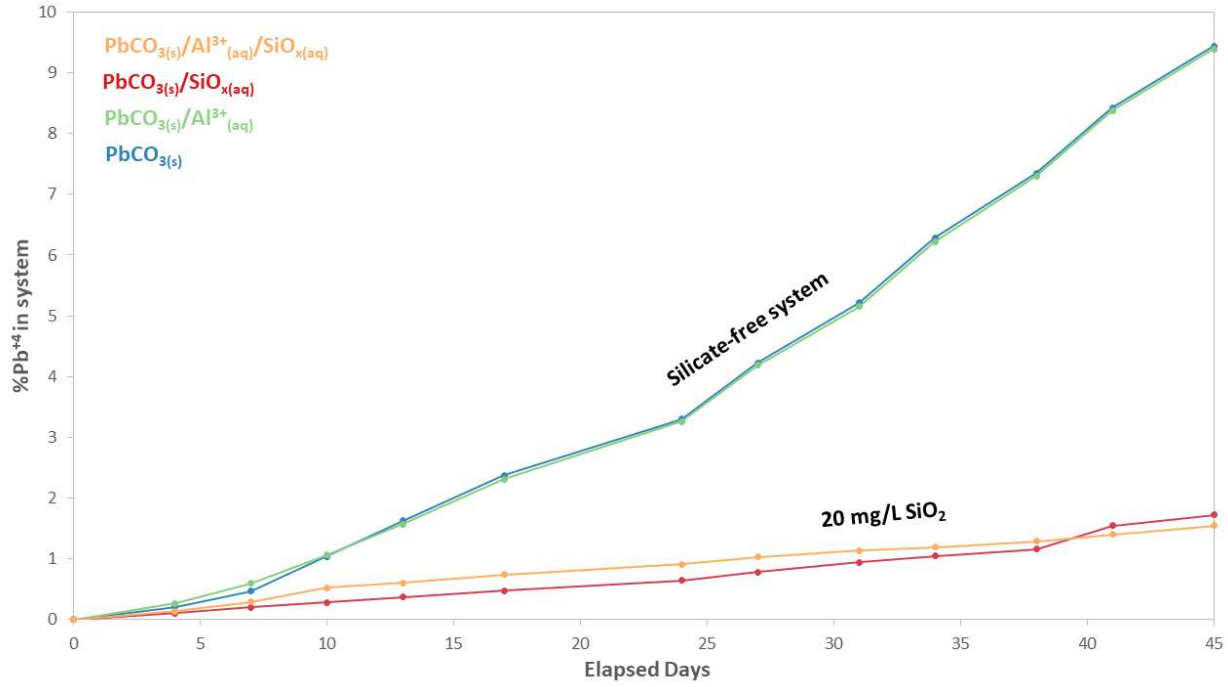


*Figure 6: % Hypothetical amount of $Pb^{+4}$ generated directly from chlorine consumption in cerussite at pH 8*

The results obtained for the ICP chemical analysis of aqueous dissolved lead levels in these experiments are shown in Figure 7. The thermodynamic solubility region for cerussite is shown in the shaded box in the figure (Bilinski and Schindler, 1982; Guo et al., 2016; Xiong, 2015). These results indicate that most measurements were within the region corresponding to the equilibrium concentration of aqueous dissolved lead from cerussite. We can conclude therefore that regardless of the presence of silicates, lead levels are regulated entirely by the thermodynamic solubility of cerussite.

Lead oxides are essentially insoluble in drinking water whereas lead carbonates have a low solubility, but will still dissolve into the water matrix (Lytle et al., 2009; Lytle and Schock, 2005). Plattnerite is found in water distribution systems that have maintained high free chlorine residuals; free chlorine will oxidize Pb to the $Pb^{4+}$ product $PbO_2$ which is insoluble in water (Guo et al., 2014; Xie et al., 2010b, 2010a). Water that has been treated with other disinfectants, such as monochloramine, has a much higher presence of $Pb^{2+}$ in the scale; chloramines are unable to provide the thermodynamic driving force needed to produce or keep $Pb^{4+}$ species, and as a result systems where monochloramine is used as a disinfectant have experienced higher lead dissolution (Lin and Valentine, 2008; Switzer et al., 2006). In fact, a switch of disinfectants in Washington, DC from free chlorine to chloramines caused lead to leach from service lines due to

increased formation of $Pb^{2+}$ and resulted in elevated lead exposure to residents in the municipality (Edwards et al., 2009). The dissolved lead levels measured in these experiments are consistent with previous findings if we assume that, in the absence of silicates, a solid phase change to higher valence lead oxides is taking place. Alternatively, a recent study observed higher dissolved lead in the presence of silicates in a pH-controlled pipe loop study, and attributed it to the formation of colloids containing lead (Aghasadeghi et al., 2021). Figure 7 clearly shows $PbCO_{3(s)}/Al^{3+}_{(aq)}/SiO_{x(aq)}$ has the overall highest dissolved lead levels as the systems move towards equilibrium, which is consistent with the absence of a higher valence lead oxide phase.

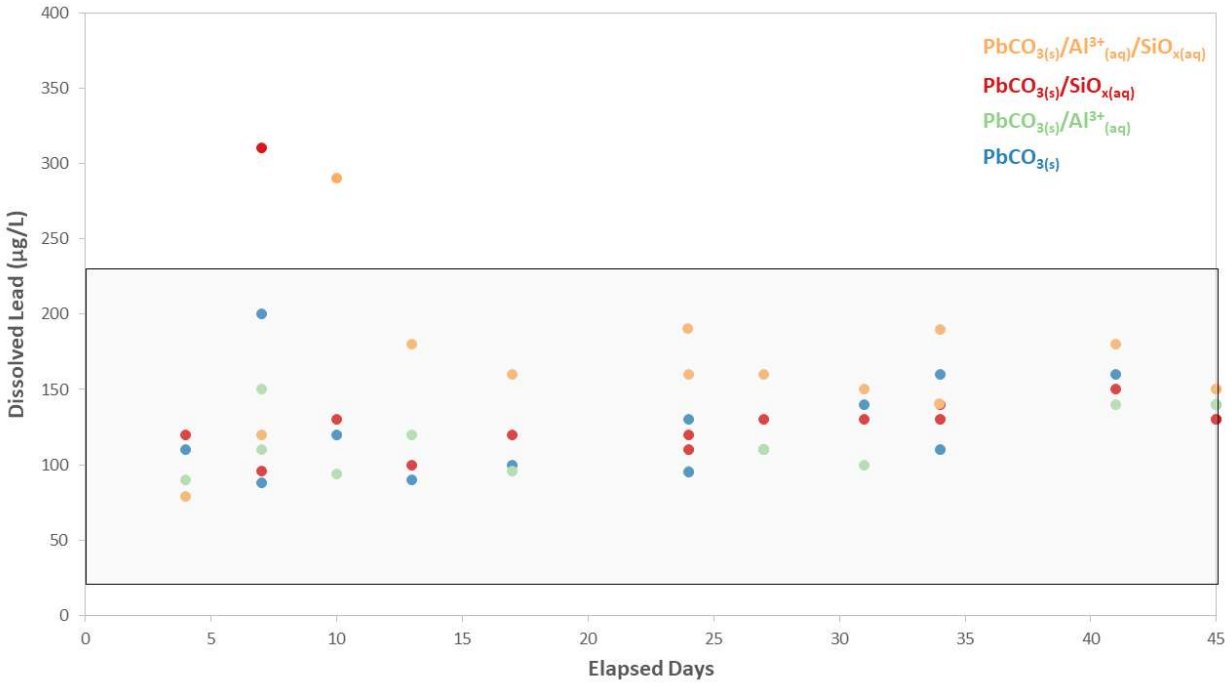


*Figure 7: Dissolved Pb levels from tests two and three with cerussite as lead solid phase over the 45-day experiments.*

#### 4.2.1.2 Analysis of Changes in the Solid Phase

After these dissolution experiments were completed, the samples were sent for SEM analysis to determine any changes in solid phase morphology. Figure 8 shows the results obtained, together with a sample of solid cerussite used as reference. First, the results indicate that the morphology of all samples is different from that of the cerussite reference sample. Cerussite is naturally occurring as thick needles, hydrocerussite as thin plates and lead oxides as clusters (Lui et al., 2008). The crystal morphology obtained in this analysis suggests the presence of both

hydrocerussite and plattnerite on the surface of the solid phase after dissolution. A higher magnification, 1 μm, was used to attempt to determine any further change in the solid phase between the treated samples (Figure 9). At the higher magnification, some hydrocerussite on the reference cerussite sample surface was observed (indicated by a yellow circle) which is attributed to a reaction between the cerussite and moisture in the air. Clusters of $PbO_2$ in the $PbCO_{3(s)}/Al^{3+}_{(aq)}$ sample that are much larger and more prevalent than in the $PbCO_{3(s)}/SiO_{x(aq)}$ or $PbCO_{3(s)}/Al^{3+}_{(aq)}/SiO_{x(aq)}$ samples were observed (shown with red circles), once again suggesting the inhibition of $PbO_2$ formation from $PbCO_3$ in the presence of silicates. A unique fine precipitate appears visible on the $PbCO_{3(s)}/Al^{3+}_{(aq)}/SiO_{x(aq)}$ sample (shown by a blue circle). It is difficult to determine any changes in plate morphology relating to lead phase between the samples exposed to aluminum and/or silicates. The biggest impact appears to be solely from the influence of silicates on $PbO_2$ generation.

To further observe the morphology of the fine precipitate visible on the surface of the $PbCO_{3(s)}/Al^{3+}_{(aq)}/SiO_{x(aq)}$ sample, another round of SEM was performed at a higher magnification (Figure 10). Lead phase and precipitate are identified with the same colours as in Figure 9. The surface of the reference cerussite appears flat and slightly ridged. Some small, smooth pieces of hydrocerussite can be seen on the surface (outlined in yellow). The $PbCO_{3(s)}/Al^{3+}_{(aq)}$ sample shows smooth plates of hydrocerussite, with some clusters of $PbO_2$ (red). There is a small amount of precipitate visible on the smooth surface of the hydrocerussite in the $PbCO_{3(s)}/SiO_{x(aq)}$ sample; this appears visually as impurities on the surface of the smooth hydrocerussite (circled in blue). There is also a cluster of $PbO_2$ in the sample (red). A much larger amount of precipitate is visible on the surface of the $PbCO_{3(s)}/Al^{3+}_{(aq)}/SiO_{x(aq)}$ sample. With this precipitate only visible on the samples exposed to aqueous silicate, we could hypothesize that silicates are depositing on the sample surfaces and more silicate is precipitating out in the presence of aluminum, perhaps suggesting the formation of an aluminosilicate phase. This scenario will be further explored in section 4.2.3.

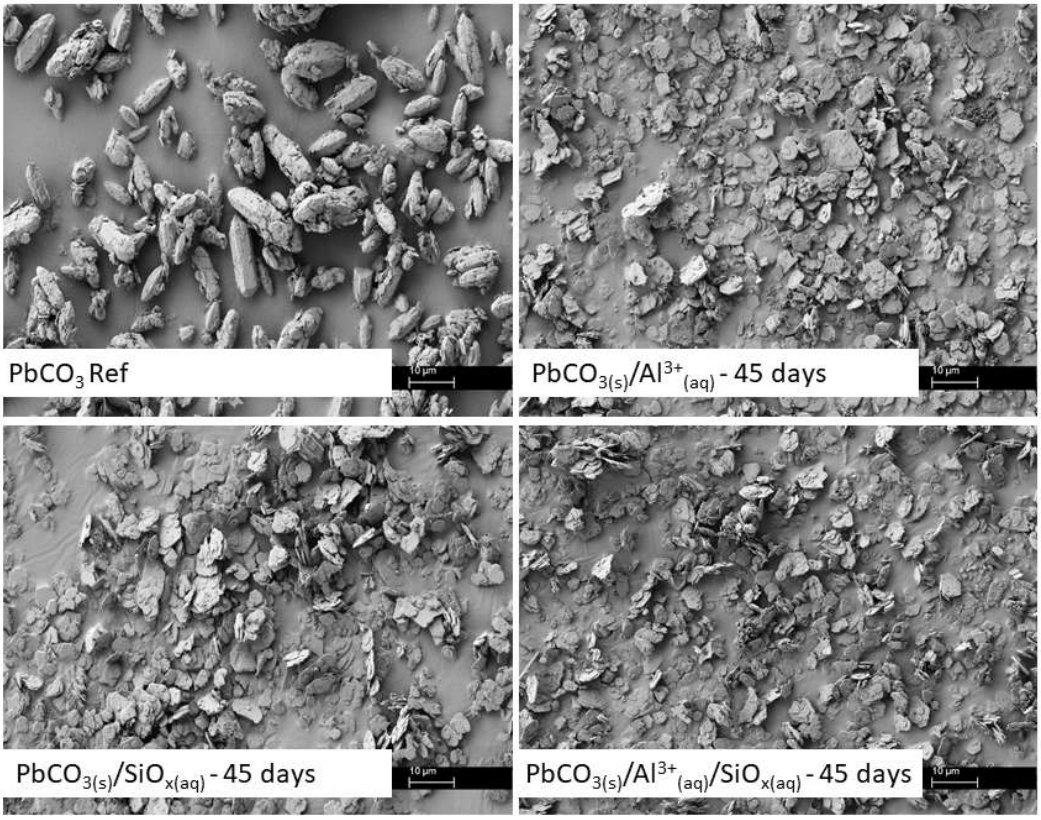


*Figure 8: SEM images of cerussite precipitate harvested from chlorinated synthetic drinking water at pH 8, with and without exposure to Si and Al, at 10 µm scale. Change in morphology of lead phase is visible when compared to reference cerussite.*

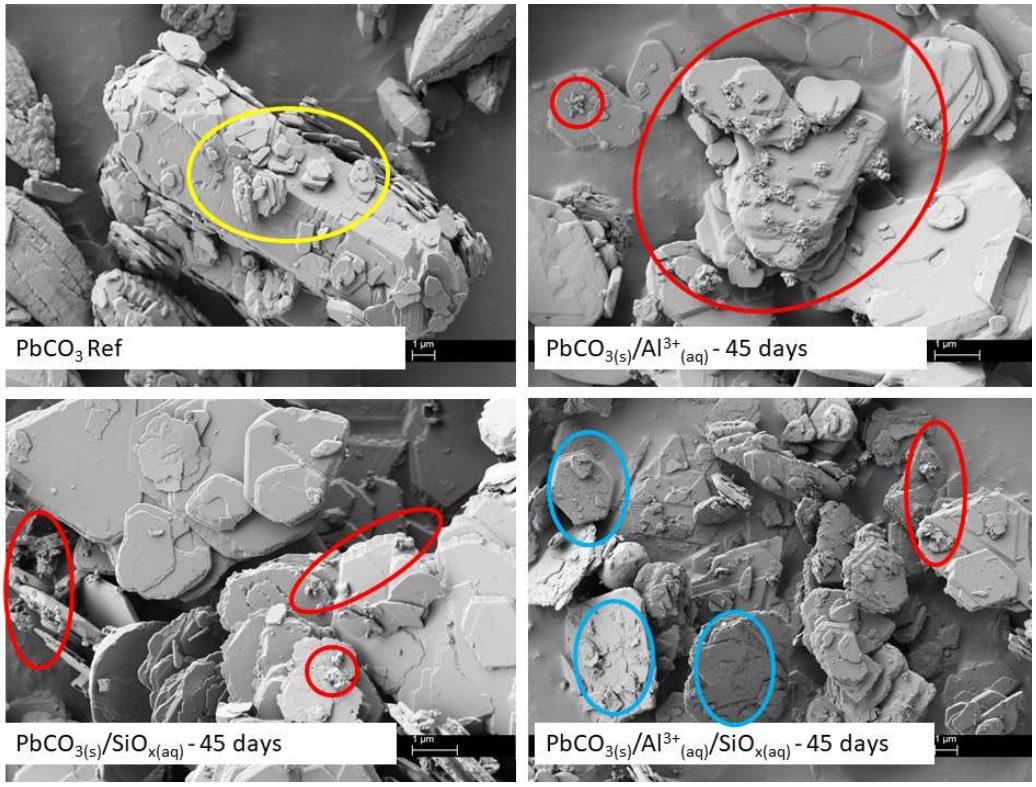


*Figure 9: SEM images of cerussite precipitate harvested from chlorinated synthetic drinking water at pH 8, with and without exposure to Si and Al, at 1 µm scale. Clusters of $PbO_2$ can be seen primarily in the sample not exposed to silicates. A fine precipitate on the sample exposed to Al and Si is visible.*

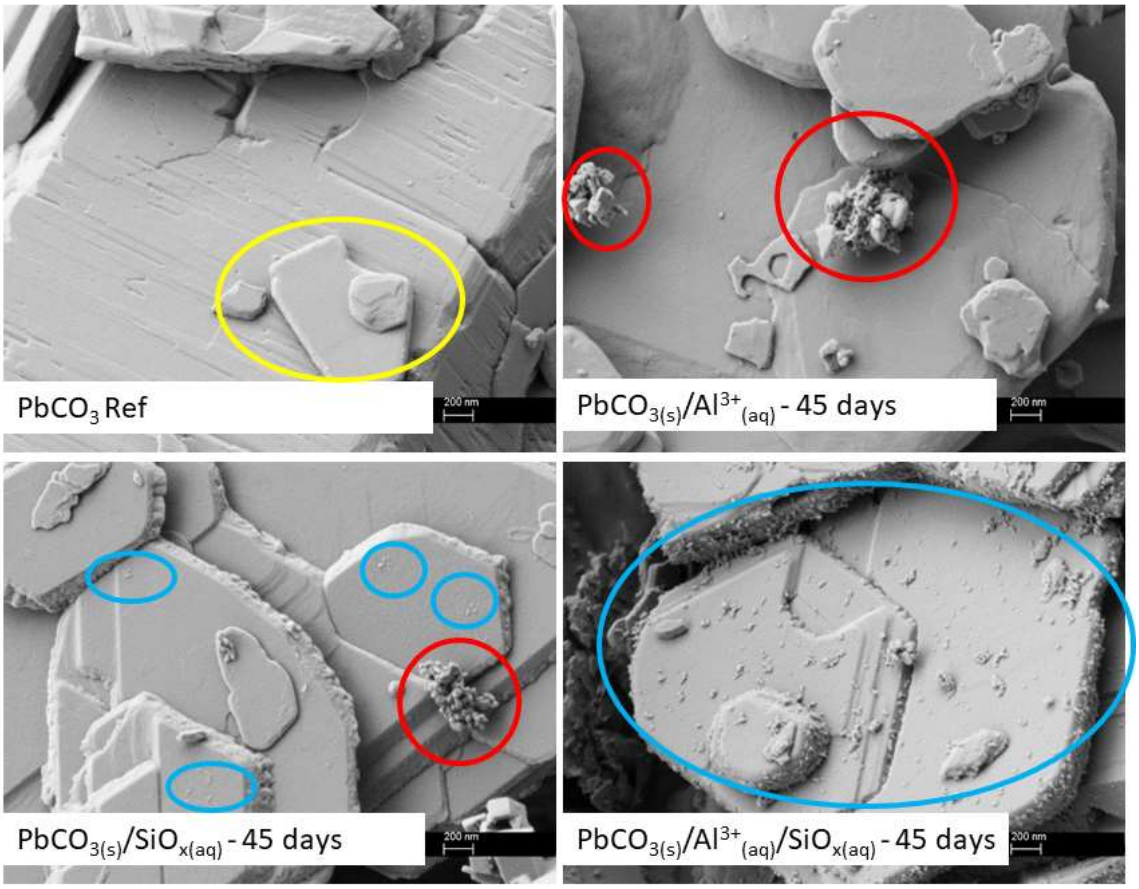


*Figure 10: SEM images of cerussite precipitate harvested from chlorinated synthetic drinking water at pH 8, with and without exposure to Si and Al, at 200 nm scale. Clusters of $PbO_2$ can be seen primarily in the sample not exposed to silicates. A fine precipitate on the samples exposed to Si is visible.*

EDX was performed on the above samples to determine bulk phase composition, Table 9 shows the results for each sample by atomic percentage. The results clearly indicate the composition of all the samples is different from that of reference cerussite. All samples contain similar amounts of Pb, but the contents of C and O significantly change among them. This variation is likely due to phase variation during the dissolution experiments, specifically cerussite to hydrocerussite and higher valence Pb oxides. Al is observed for the case of the samples exposed to aqueous aluminum, and Si is present in the samples exposed to aqueous silicates. The highest amount of Si is observed in the sample that was exposed to both aqueous silicate and aluminum ions ($PbCO_{3(s)}/Al^{3+}_{(aq)}/SiO_{x(aq)}$, 0.98 at% of solid Si content in the sample) whereas only a small amount is present in $PbCO_{3(s)}/SiO_{x(aq)}$ at 0.16 at%. This result is consistent with the observation of the fine precipitate visible at 200 nm in the SEM images where a small amount of precipitate was observed on $PbCO_{3(s)}/SiO_{x(aq)}$ and a much larger amount on $PbCO_{3(s)}/Al^{3+}_{(aq)}/SiO_{x(aq)}$. It

should be noted that there is a background carbon signal included in EDX measurements; the at% does not portray accurate percentage of the sample makeup and is most useful for comparing the ratio of Pb:Si:Al. With that being the case, we can see that the atomic ratio of **Si:Pb is five times higher when aqueous Al is also present**. This observation is consistent once again with the presence of aluminum playing a role in the interaction between the aqueous silicate and the solid lead phase. Specifically, the presence of aluminium ions may contribute to the precipitation of silicates from aqueous phase in drinking water.

*Table 9: Bulk atomic composition of cerussite with and without silicate treatment following 45 days exposure to chlorinated drinking water, measured by EDX*

| | **Atomic %** | | | |
|---|---|---|---|---|
| **Element** | **$PbCO_3$ Ref** | **$PbCO_{3(s)}/Al^{3+}_{(aq)}$ – 45 days** | **$PbCO_{3(s)}/SiO_{x(aq)}$ – 45 days** | **$PbCO_{3(s)}/Al^{3+}_{(aq)}/SiO_{x(aq)}$ – 45 days** |
| Pb | 8.53 | 9.41 | 8.09 | 9.37 |
| C | 43.19 | 49.36 | 55.6 | 44.43 |
| O | 48.28 | 39.53 | 36.15 | 44.79 |
| **Al** | **0** | **1.7** | **0** | **0.41** |
| **Si** | **0** | **0** | **0.16** | **0.98** |
| **Si:Pb atomic ratio** | **-** | **-** | **0.02** | **0.1** |

EDX is a bulk phase measurement. Because Si was detected in the bulk and differences in morphology were observed with SEM, XPS surface measurements were used to determine surface composition and attempt to clearly identify the chemical state of the lead phases present in the outer layers of the solids. XPS is a surface characterization technique; it probes the surface to a depth of 5 – 10 nm only. Since any changes in the solid phase resulting from interaction with the aqueous phase should be localized at the sample surface, XPS is the most adequate technique to evaluate these changes.

The average Pb binding energy (4f7/2) of $PbCO_3$ is 138.3 eV. The range for the lead oxides is wider, with $Pb_3O_4$ typically displaying a 4f 7/2 binding energy between 137.4 – 137.7 eV and $PbO_2$ between 136.8 – 137.6 eV (National Institute of Standards and Technology, 2012; Thomas

and Tricker, 1974). Because the lead oxide binding energies are so similar it is not possible to differentiate between them, however it is technically possible to differentiate between oxides and carbonates which can give an indication as to whether the top sample layers are in the +2 or +4 state. Figure 11 shows the intensity normalized survey scan obtained in the Pb 4f region for two samples exposed to synthetic drinking water for 45 days. One sample was exposed to aqueous silicate, while the other was not. As indicated by the arrow, we observe a shoulder on the 4f peak for $PbCO_{3(s)}/Al^{3+}_{(aq)}$ at a binding energy around 137.5 which is indicative of the presence of two lead phases, $Pb^{2+}$ from $PbCO_3$ at the higher binding energy of 138.5 eV and $Pb^{4+}$ from either $Pb_3O_4$ or $PbO_2$ at 137.5 eV.

A high resolution Pb 4f scan was conducted on the samples in an attempt to quantify the results from the survey scan and confirm the two peaks under the Pb 4f envelope for $PbCO_{3(s)}/Al^{3+}_{(aq)}$ belonged to $Pb^{2+}$ and $Pb^{4+}$. Unfortunately, when the samples were run at high resolution the contribution of the $Pb^{4+}$ seems to be enveloped within the $Pb^{2+}$ 4f peak and only a single peak is visible. Figure 12 shows the envelope with a dotted line, and Pb 4f fitting with solid lines. The peak for $PbCO_{3(s)}/Al^{3+}_{(aq)}$ is centered at 138.3 eV and the peak for $PbCO_{3(s)}/Al^{3+}_{(aq)}/SiO_{x(aq)}$ is centered at 138.4 eV. A fitting performed on this spectrum showed only the $Pb^{2+}$ peak, any contribution from $Pb^{4+}$ species could be masked in the envelope of the $Pb^{2+}$ peak.

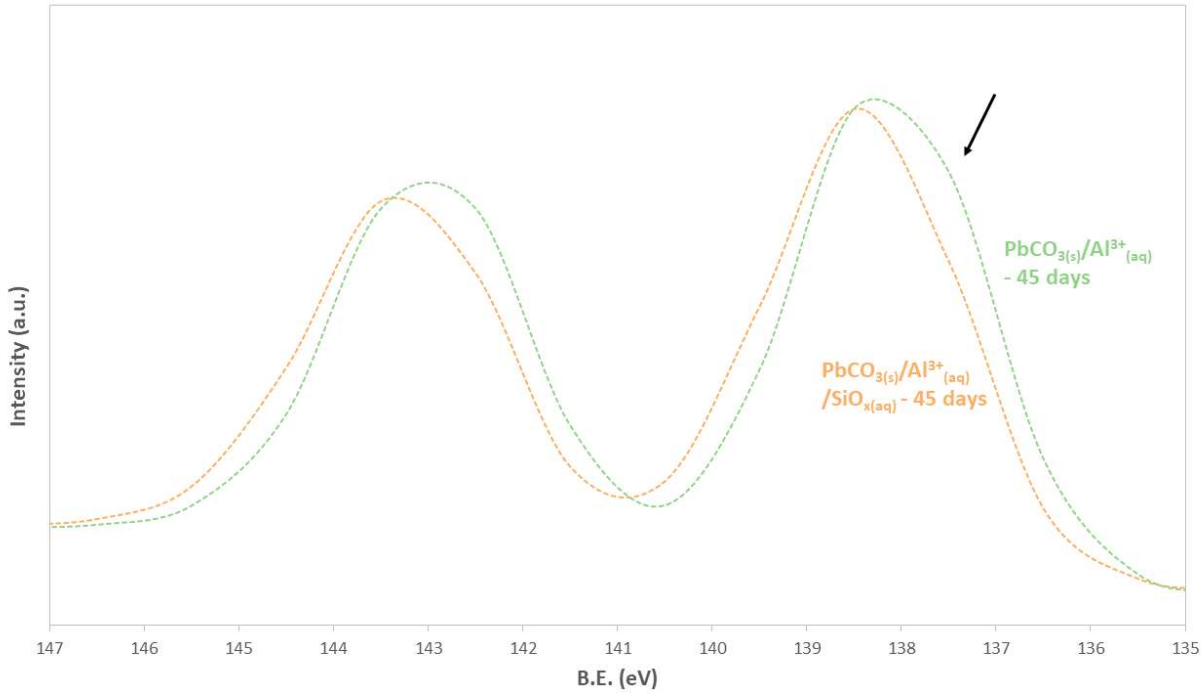


*Figure 11: XPS survey scan of cerussite harvested from synthetic drinking water with and without aqueous silicate exposure; shoulder indicates $Pb^{+4}$ phase in absence of Si.*

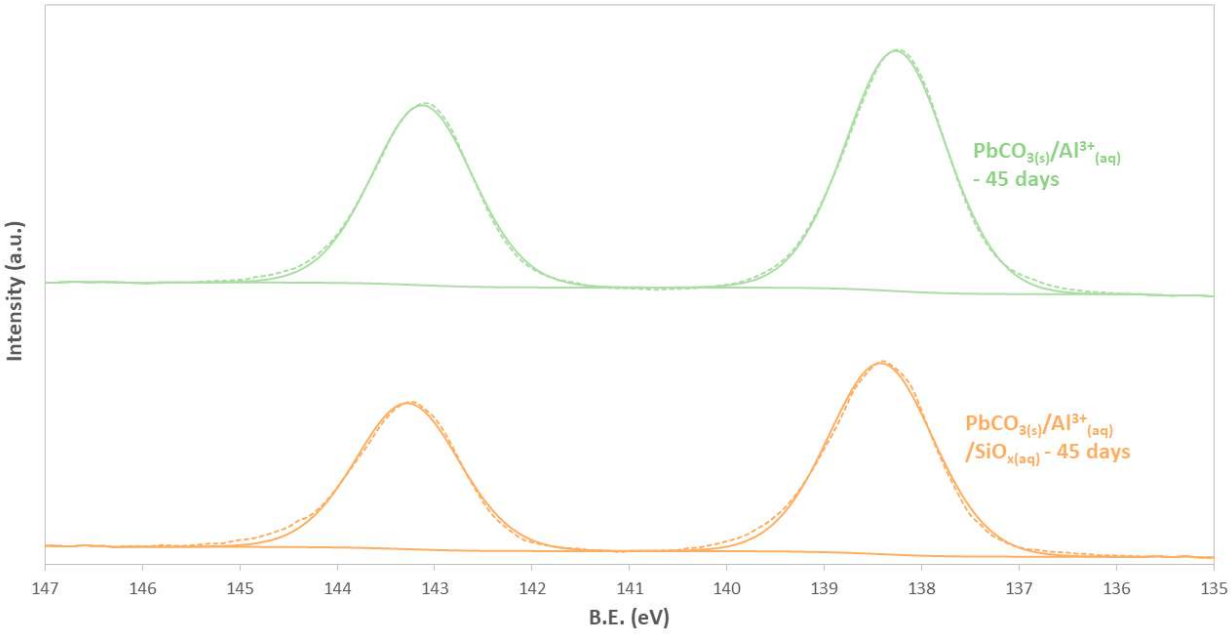


*Figure 12: High resolution Pb 4f XPS scan and fitting of cerussite precipitate harvested from synthetic drinking water with and without exposure to aqueous silicate, showing no shoulder or indication of $Pb^{+4}$*

The XPS results were further used to obtain the samples' surface composition in atomic percentage. The surface analysis obtained is shown in Table 10. This specific analysis probes a

different sample region compared to EDX which is a bulk analysis. The survey scan identified the presence of O, Ca, C, Pb, Si, and Al in both the $PbCO_{3(s)}/Al^{3+}_{(aq)}/SiO_{x(aq)}$ and $PbCO_{3(s)}/Al^{3+}_{(aq)}$ samples, however the relative amounts of each element vary. A higher amount of oxygen is observed in the silicate-treated sample, whereas a higher amount of carbon and lead is observed in the silicate-free system. There is also a significant difference between the amount of Si and Al in both samples. The differing amounts of O, C and Pb between the two samples is likely linked to the dominant lead phase and differing amounts of cerussite, hydrocerussite and lead oxides in the sample surface. In order to contrast these result with those obtained using EDX, the Si:Pb and Si:Al ratios obtained using both EDX and XPS were calculated and plotted in Figures 13 and 14. As expected, a higher Si:Pb ratio is observed in the surface (XPS) than in the bulk of the samples (EDX), indicating additional Si is found in the surface. The Si:Al ratios obtained, however, were similar in both the surface and bulk phases. This result suggests the silica-alumina precipitate formed extends well into the bulk phase with a similar atomic ratio of that in surface layers. This result is consistent with two recent reports by Mishrra, Aghasadeghi and coworkers, where SEM-EDX indicated an increase of 0.7 – 1.5 wt% in pipe loop scale Si concentration following sodium silicate treatment for up to 48 weeks and their hypothesis of silicate migrating into the bulk of the corrosion layer (Aghasadeghi et al., 2021; Mishrra et al., 2021). The results portrayed in Figures 13 and 14 together with the SEM micrographs shown before clearly indicate that after aqueous silicate exposure the sample is heterogeneous with a silica-alumina rich outer layer.

*Table 10: Surface atomic composition of cerussite with and without aqueous silicate treatment following 45 days exposure to chlorinated drinking water, measured by XPS*

| | **Atomic %** | |
|---|---|---|
| **Element** | **$PbCO_{3(s)}/Al^{3+}_{(aq)}/SiO_{x(aq)}$ – 45 days** | **$PbCO_{3(s)}/Al^{3+}_{(aq)}$ – 45 days** |
| O 1s | 52.4 | 47 |
| Ca 2p | 1.3 | 1.6 |
| C 1s | 23.1 | 32.5 |
| Pb 4f | 13.1 | 17.8 |
| Si 2p | 6.6 | Below detection limit |
| Al 2p | 3.5 | 0.8 |

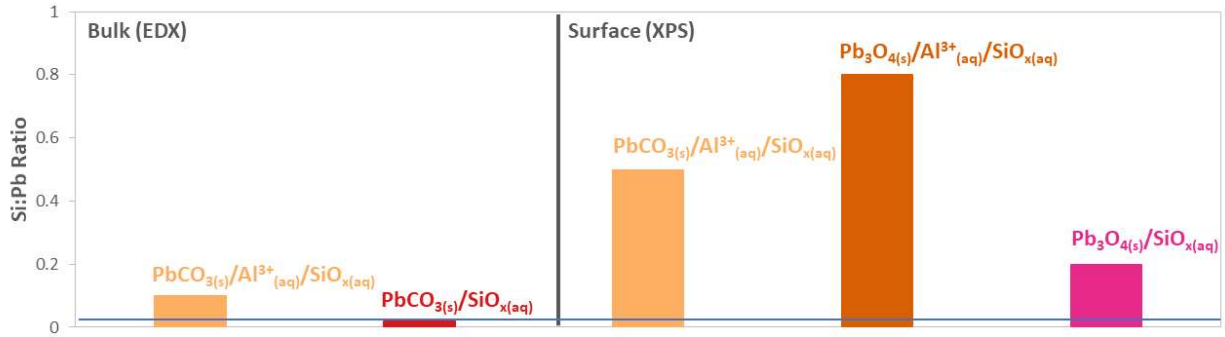


*Figure 13: Si:Pb atomic ratio comparison of XPS and EDX results for cerussite and minium samples following treatment in synthetic drinking water, showing surface and bulk silicate enrichment. Blue line represents total system ratio (value 0.02)*

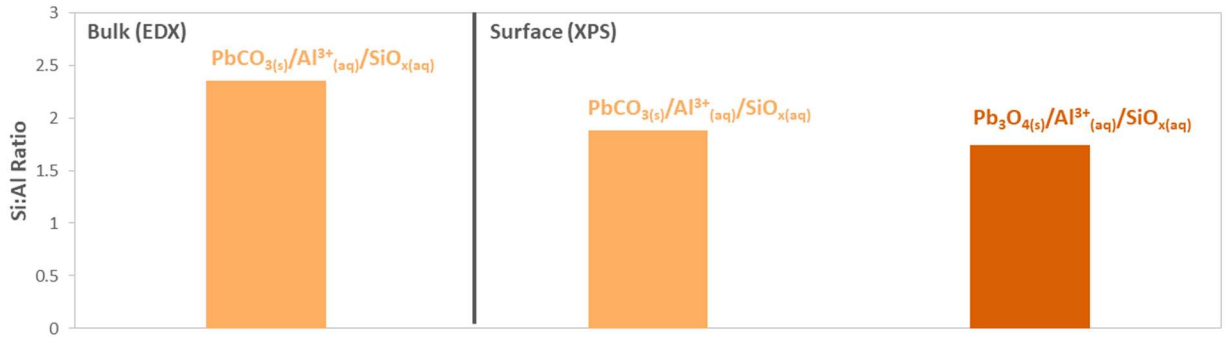


*Figure 14: Si:Al atomic ratio comparison of XPS and EDX for cerussite and minium samples following treatment in synthetic drinking water. Total aqueous phase system ratio is approximately 10.*

Given the presence of Si in the sample surface, a high-resolution XPS Si 2p scan was completed; the results obtained are depicted graphically in Appendix B Figure 34. The Si 2p binding energy for $PbCO_{3(s)}/Al^{3+}_{(aq)}/SiO_{x(aq)}$ was identified as 102.2 eV. Silicates typically have a 2p binding energy in the range of 103.8 – 101.6 eV depending on other cations present, including $Al^{3+}$ and/or the degree of silicate oligomerization (Biesinger, n.d.; Childs et al., 1997; Li et al., 2012). The result is further confirming the presence of silicates precipitating onto the solid phase under our experimental conditions.

Since the result of the high resolution Pb 4f peak (Figure 12) was inconclusive at identifying a new Pb-bearing surface phase on the cerussite formed from the interaction of aqueous and solid phase, we pursued further surface analysis using UV-Vis spectroscopy. The spectra obtained are presented in Figure 15. The general shape of all four samples is similar with a main peak centered in the 200 – 300 nm range. There is however a difference between the samples in the 300 – 600 nm region; the samples exposed to silicates do not have any further peaks or bands,

but the samples exposed to the aqueous phase in the absence of silicates have an additional broad band that tails down around 600 nm.

To interpret these observed differences, analyses of reference cerussite, minium and plattnerite samples were also performed; the lower portion of Figure 15 shows the reference spectra. Using this information, we can proceed to assign the features observed in the samples. The band centered around 200 – 300 nm present in all samples is attributed to cerussite and/or hydrocerussite as the main peak for both lead carbonate species occurs between 200 – 270 nm (Guo et al., 2016). This also matches the reference spectrum obtained for cerussite. This result indicates that the dominant lead phase remains lead carbonate in all cases, regardless of the exposure to aqueous silicates. The broad band and long tail from 300 – 600 nm clearly observed in the spectra obtained of the samples that were not exposed to aqueous silicate, $PbCO_{3(s)}$ and $PbCO_{3(s)}/Al^{3+}_{(aq)}$, suggests the presence of a lead oxide phase; lead oxides exhibit a broader range of absorption under UV light. Minium exhibits a sharp decrease around 550 nm; plattnerite does not exhibit an intensity decrease until 750 nm. The lead oxide phase present in both silicate-free samples is therefore expected to be a combination of minium and plattnerite due to the gradual decrease between 500 – 700 nm. These results are consistent with the colour change observed over the course of the 45-day experiment, as well as presence of possible $Pb^{4+}$ oxide clusters seen in the SEM images, and the XPS shoulder attributed to $Pb^{+4}$ surface phase observed in Figure 11. When combined, these results clearly show that after exposure to drinking water conditions in the absence of silicate ions, a lead oxide phase is formed on the cerussite surface (likely the result of the interaction of chlorine residual with the lead bearing solid surface, section 4.2.1.1). In contrast, if silicate is present in the aqueous phase, this process does not take place and a lead oxide phase is not observed.

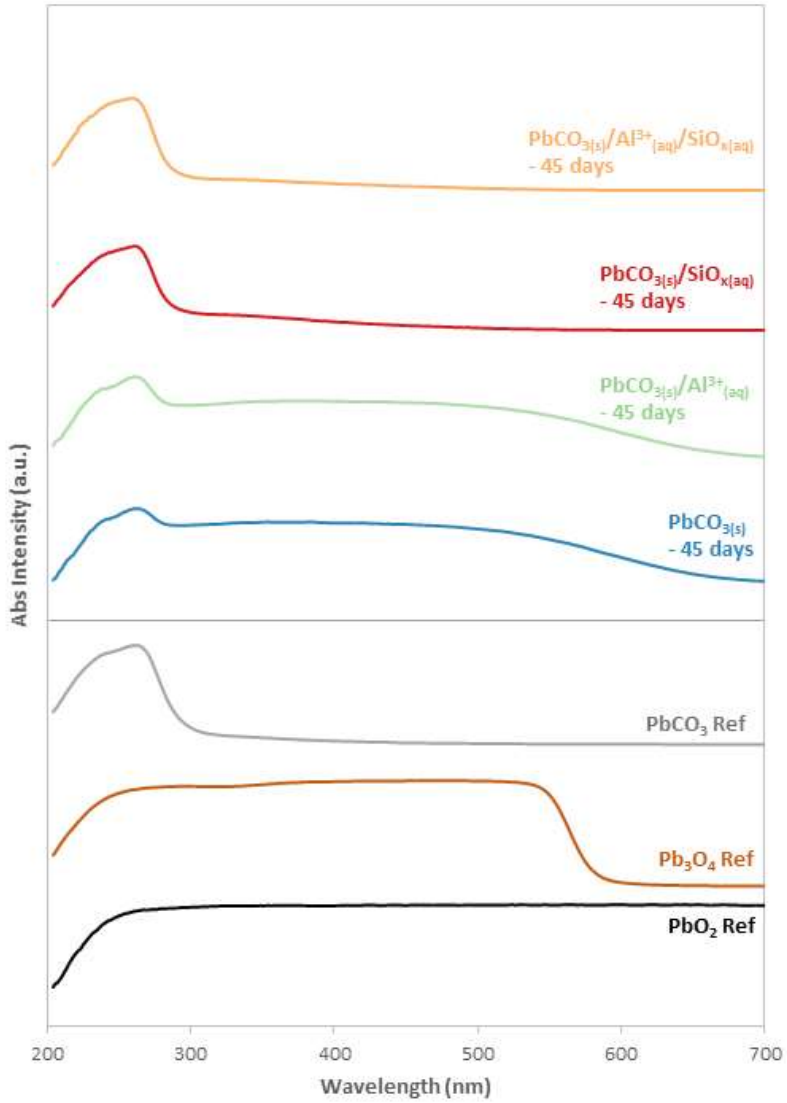


*Figure 15: UV-Vis reference spectra for lead carbonate and lead oxides, and spectra for cerussite samples harvested from synthetic drinking water with and without exposure to Si and Al. Broad band indicating presence of lead oxides is visible in the absence of Si.*

To further explore this phenomenon, analysis of the four samples was performed using FTIR spectroscopy. Results are presented in Figure 16, together with reference spectra for cerussite, minium and plattnerite. The spectra for the four samples appear quite similar. There are no additional peaks present in any samples, however there are some distinct differences in intensity of peaks in the 900 – 600 $cm^{-1}$, and 2800 – 2400 $cm^{-1}$ region. The characteristic bands for cerussite occur at 1045, 850 and 680 $cm^{-1}$. The major carbonate band occurs at 1450 $cm^{-1}$, and bicarbonate band at 1600 $cm^{-1}$ (Guo and Herrera, 2018; RRUFF Database, n.d.). The reference spectrum for cerussite also displays adsorbed water peaks at 3450 and 1640 $cm^{-1}$; the lead oxide

reference spectra do not display adsorbed water peaks. Finally, the spectrum for minium shows a carbonate peak that can be attributed to adsorbed carbonates on the lead surface.

The cerussite and carbonate bands are visible in all sample spectra, however the signals have a lower intensity in the absence of silicates. The broad band in the 650 – 500 $cm^{-1}$ range is attributed to metal oxides, however there is significant overlap with the cerussite peak around 680 $cm^{-1}$ and it is difficult to separate the contributions of both lead carbonates and lead oxides (Senvaitiene et al., 2007). A characteristic peak for cerussite located at 850 $cm^{-1}$ is not visible in any of the samples. This could be attributed to the presence of the previously identified hydrocerussite, as this peak does not occur in both forms of the $Pb^{2+}$ carbonate. Equation 4 shows how hydrocerussite forms spontaneously from cerussite in the presence of hydroxide ions (Guo et al., 2016). The carbonate and bicarbonate peaks (shown with a black arrow) have a higher intensity for the samples exposed to aqueous silicates, indicating a higher amount of lead carbonate in the solid phase. Furthermore, the water peaks also display a higher intensity (shown with a black arrow), suggesting the $Pb^{2+}$ carbonate present is likely hydrocerussite. The $PbCO_{3(s)}/Al^{3+}_{(aq)}/SiO_{x(aq)}$ and $PbCO_{3(s)}/SiO_{x(aq)}$ spectra suggests the dominant phase remains $Pb^{2+}$ carbonate with only a small contribution from lead oxides. The spectra for $PbCO_{3(s)}/Al^{3+}_{(aq)}$ and $PbCO_{3(s)}$ indicate $Pb^{2+}$ carbonate remains the dominant phase, but the lower intensity of carbonate peaks indirectly suggests a higher contribution from lead oxides in the samples.

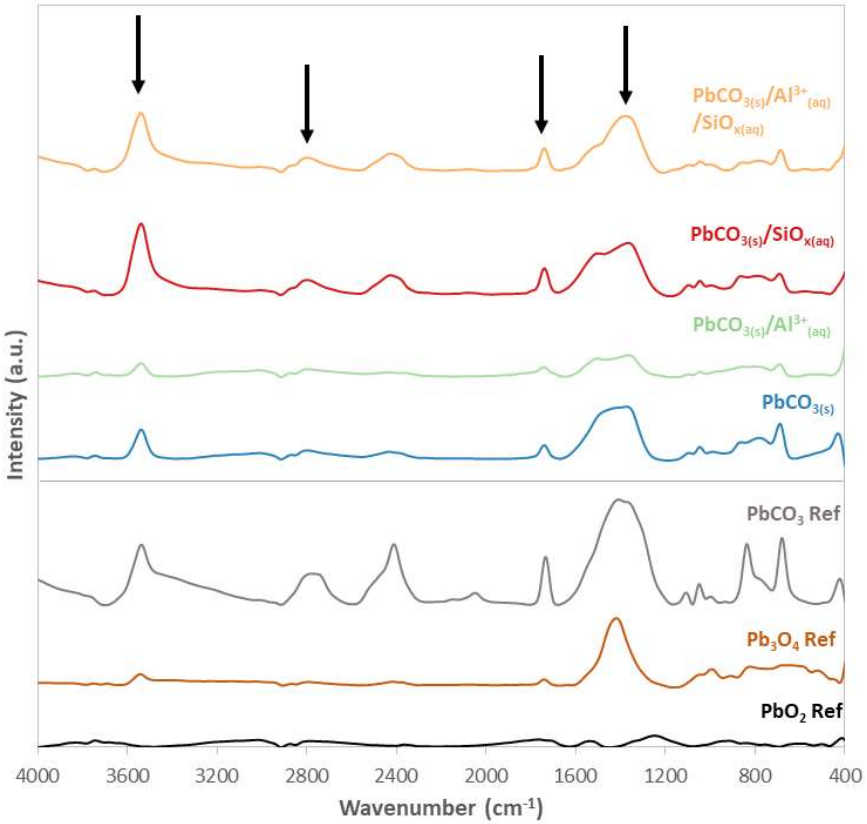


*Figure 16: FTIR reference spectra for lead carbonate and oxides, and spectra for cerussite samples harvested from synthetic drinking water with and without exposure to aqueous Si and Al. Changes in peak intensity based on exposure to Si and Al are visible.*

$$3PbCO_{3(s)} + 2OH^{-}_{aq} \leftrightarrow Pb_3(CO_3)_2(OH)_{2(s)} + CO^{2-}_{3(aq)} \qquad \text{Equation 4}$$

Raman spectroscopy was performed to determine any signals that may be present with a different form of IR spectroscopy. All four samples were analyzed, and results are presented in Figure 17. It is evident that the silicate-treated samples exhibit different spectra than those obtained in the absence of aqueous silicate. Both $PbCO_{3(s)}/Al^{3+}_{(aq)}/SiO_{x(aq)}$ and $PbCO_{3(s)}/SiO_{x(aq)}$ show a sharp peak at 1045 $cm^{-1}$, as well as other distinct peaks at 1355, 410 and 110 $cm^{-1}$. $PbCO_{3(s)}$ and $PbCO_{3(s)}/Al^{3+}_{(aq)}$ show main distinct peaks only at 515, 260 and 130 $cm^{-1}$. The main peak for cerussite occurs at 1050 $cm^{-1}$, and for hydrocerussite at 1040 $cm^{-1}$. Similar to the FTIR results, there was no main cerussite peak present in the Raman spectra for $PbCO_{3(s)}$ and $PbCO_{3(s)}/Al^{3+}_{(aq)}$, whereas this peak is very distinctive for the silicate treated samples, once again indicating the dominant presence of lead carbonate in the sample surface when silicates are present in the aqueous phase. The peaks from 600 – 100 $cm^{-1}$ for $PbCO_{3(s)}$ and $PbCO_{3(s)}/Al^{3+}_{(aq)}$ can be

attributed to lead oxides; the main peaks for $PbO_2$ are at 200 $cm^{-1}$ and 139 $cm^{-1}$ and for $Pb_3O_4$ are at 550 $cm^{-1}$, 391 $cm^{-1}$, and 151 $cm^{-1}$. The peaks at 1355 $cm^{-1}$ and 600 – 100 $cm^{-1}$ for $PbCO_{3(s)}/SiO_{2(aq)}$ and $PbCO_{3(s)}/Al^{3+}{}_{(aq)}/SiO_{2(aq)}$ can be attributed to cerussite and hydrocerussite (Kim and Herrera, 2010; RRUFF Database, n.d.). The results from this analysis align with the results obtained by SEM, EDX, XPS, UV/Vis and FTIR showing that silicates inhibited the formation of $Pb^{4+}$ oxides.

Two small peaks are present in the spectra for $PbCO_{3(s)}/Al^{3+}{}_{(aq)}/SiO_{x(aq)}$ and $PbCO_{3(s)}/SiO_{x(aq)}$ that are not present in reference spectra for cerussite; these are located at 1076 and 960 $cm^{-1}$ and shown in Figure 17 with black arrows. Si-O-Si peaks are typically located at 1070 and 950 $cm^{-1}$ (Creton et al., 2008), thus this result aligns with the XPS and EDX data (Figures 13 and 14) indicating the presence of silicates in the solid surface. It is postulated that the additional peaks on the spectra are likely Si-O-Si or Si-OH peaks, although it is possible that a peak for Si-O-Al also occurs and is not visible due to overlap with other major phases present (for example, the Raman peak for allophane occurs at 1050 $cm^{-1}$ and would be within the main cerussite peak). Another study confirmed the three main bands in all $SiO_2$ spectra are due to bridged oxygen atom vibrations and occur at 1100 $cm^{-1}$ (stretching), 800 $cm^{-1}$ (bending) and 480 $cm^{-1}$ (rocking) (Handke and Mozgawa, 1993). Peaks are observed in these areas for both silicate-treated samples, thus further indicating the presence of silicates in the solid phase.

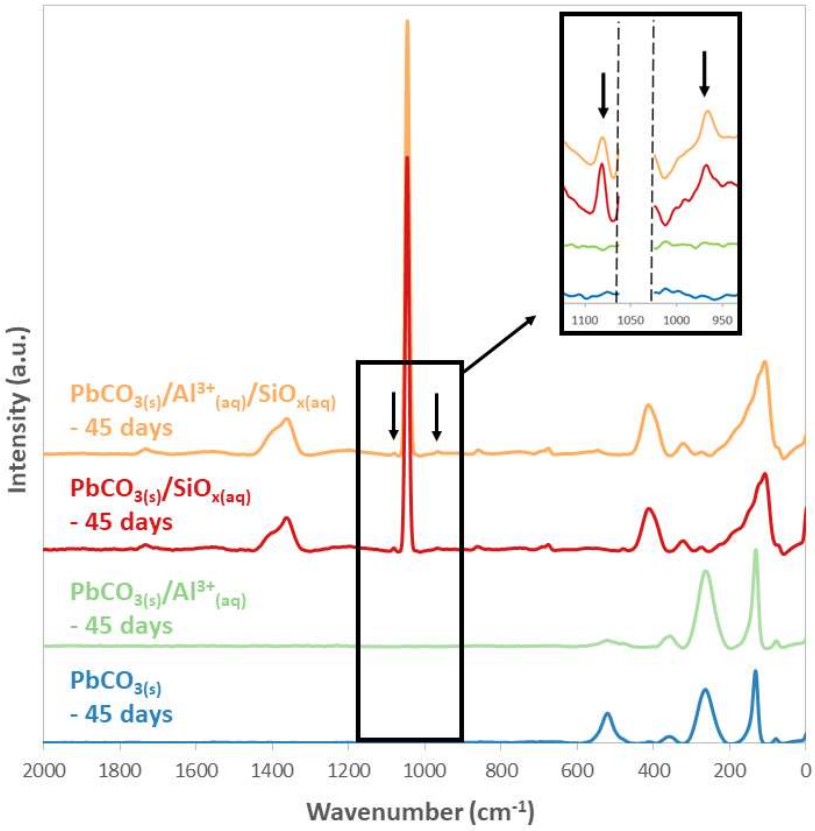


*Figure 17: Raman spectra for cerussite samples harvested from synthetic drinking water with and without exposure to Si and Al; characteristic lead carbonate peaks are absent in absence of silicates. Inset shows additional Si-O peaks in silicate-treated samples.*

XRD was performed to observe any differences in crystal phase between the samples. Figure 18 shows the diffractograms obtained for the four samples, which appear almost identical. The main peaks are located at 40 °, 31.7 ° and 28.8 ° with many other small peaks located in the 75 – 25 ° region. There is one additional peak visible in the $PbCO_{3(s)}/Al^{3+}_{(aq)}/SiO_{x(aq)}$ diffractogram at an angle of 31 °, indicated by the black arrow. This appears to be the only different peak between all four samples.

Analysis of results was performed using Jade software. All samples show the main peaks for cerussite, located at 28.8 ° and 42.1 °, and hydrocerussite, located at 2Θ angles of 31.5 ° and 40 ° (RRUFF Database, n.d.). Based on the highest intensity peak occurring at 40 °, hydrocerussite is the dominant crystal phase in each sample with contributions from cerussite. The small peaks located throughout the diffractograms are also present in both $Pb^{2+}$ carbonate phases. Because Si was detected in the bulk phase in EDX measurements, the main peaks for silica were verified with the additional peak identified in the $PbCO_{3(s)}/Al^{3+}_{(aq)}/SiO_{x(aq)}$ sample. The main peaks for

silica are located at 30.6 ° and 70 °; the additional peak at 31 ° could be attributed to silica as there is already a small peak at 70 ° in all diffractograms. Silicates and aluminosilicates are amorphous and would not be detected with XRD. Furthermore, XRD is sensitive to heavy metals which could make it even more difficult to detect other phases such as silica or silicates, which could explain why only one very small peak is visible (Guo and Herrera, 2018). No evidence of lead oxide was visible in the diffractograms for $PbCO_{3(s)}$ and $PbCO_{3(s)}/Al^{3+}_{(aq)}$ samples.

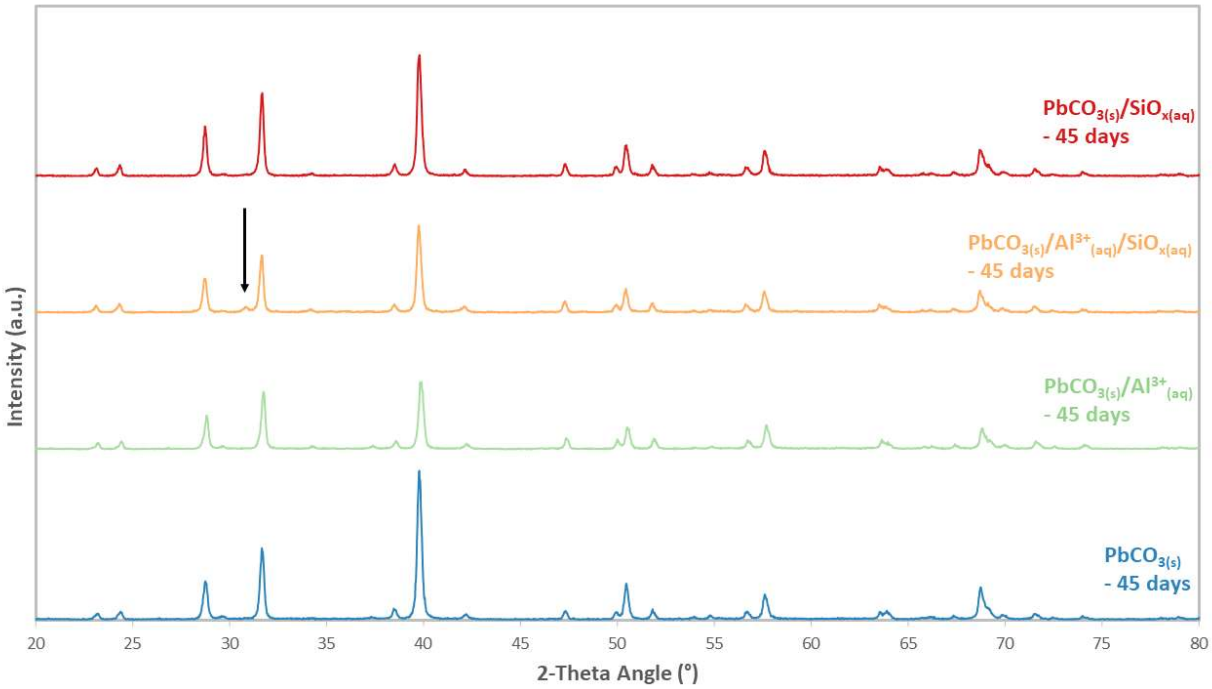


*Figure 18: XRD diffractogram for cerussite samples harvested from synthetic drinking water with and without exposure to Si and Al.*

## 4.2.2 Impact of Aqueous Silicate on Dissolution of Minium

### *4.2.2.1 Analysis of Changes in Aqueous phase*

The previous experiments were also completed using minium, instead of cerussite, as the lead solid phase, as described in Test Four. Minium is a mixed phase lead oxide; it has lead in both the +2 and +4 oxidation states and occurs as an intermediate in the oxidation of lead corrosion scale (Guo et al., 2016). Chlorine was measured and dosed as required every three days to maintain the chlorine residual around 1.5 mg/L $Cl_2$; experiments were conducted at consistent pH levels as depicted in Appendix A Figure 33. Figure 19 shows chlorine levels throughout the 45-day experiment. Similar to observations made with cerussite, the batch reactors in the absence

of silicates consumed chlorine significantly faster and required additional chlorine dosages to maintain the residual.

Throughout the experiments, the bright orange colour of minium changed in the $Pb_3O_{4(s)}$ and $Pb_3O_{4(s)}/Al^{3+}_{(aq)}$ system to a darker orange shade, shown in Figure 20. Minium oxidation by free chlorine has been proposed by Guo et al. according to Equation 5. The darkening of the bright orange minium suggests formation of some black $Pb^{4+}$ oxides. Once again, assuming a stoichiometric direct oxidation by chlorine of Pb species present in $Pb_3O_4$, a graph of additional $Pb^{4+}$ generation over time was prepared and is presented in Figure 21. Actual $PbO_2$ levels are expected to be higher; minium reacts with H+ in water to form both $Pb^{2+}$ and $PbO_2$ (Equation 5), however, only $PbO_2$ generated directly from minium oxidation by free chlorine is presented in Figure 21. A similar trend to that of cerussite is observed with less $Pb^{4+}$ generated in the presence of silicates, indicating the presence of silicates inhibits the interaction of aqueous chlorine with the solid phase and resulting in formation of less $Pb^{4+}$ species.

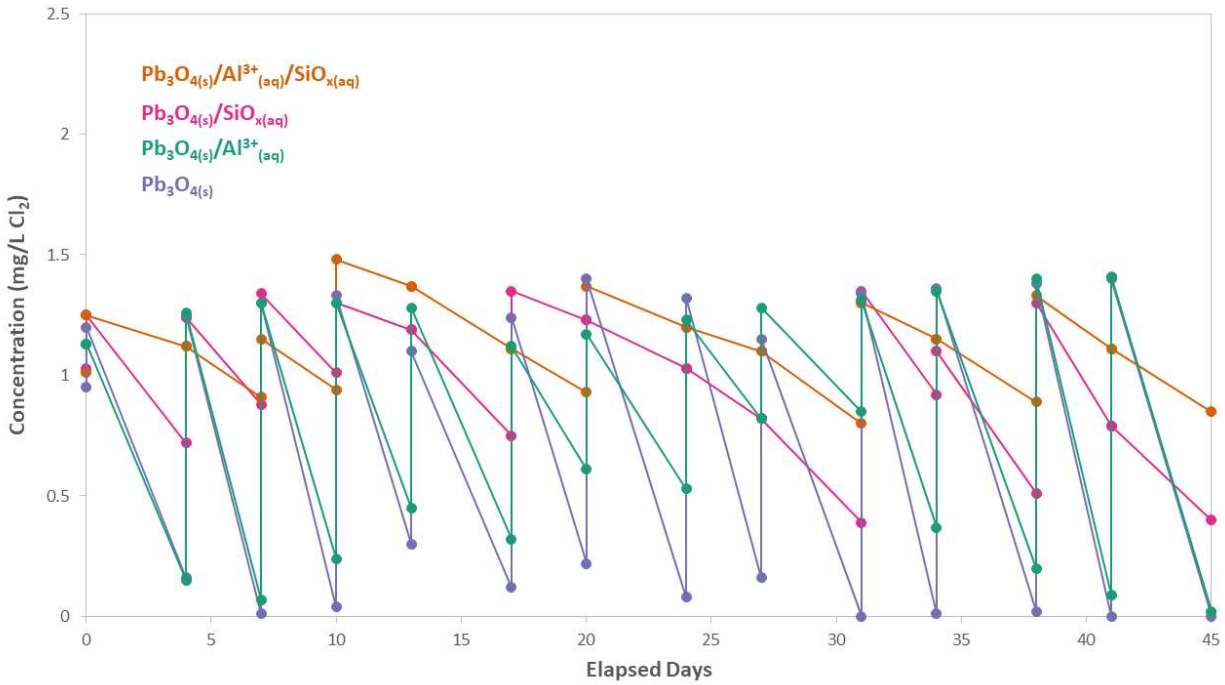


*Figure 19: Change in chlorine concentration with time at pH 8, minium solid phase. Chlorine was continually dosed to achieve a 1.5 mg/L residual, and was consumed more slowly in the presence of silicates.*

$$Pb_3O_{4(s)} + 4H^+_{aq} \leftrightarrow 2Pb^{2+}_{aq} + PbO_{2(s)} + 2H_2O$$
$$Pb^{2+}_{aq} + OCl^-_{aq} + H_2O_l \leftrightarrow Cl^-_{aq} + PbO_{2(s)} + 2H^+_{aq}$$

Equation 5

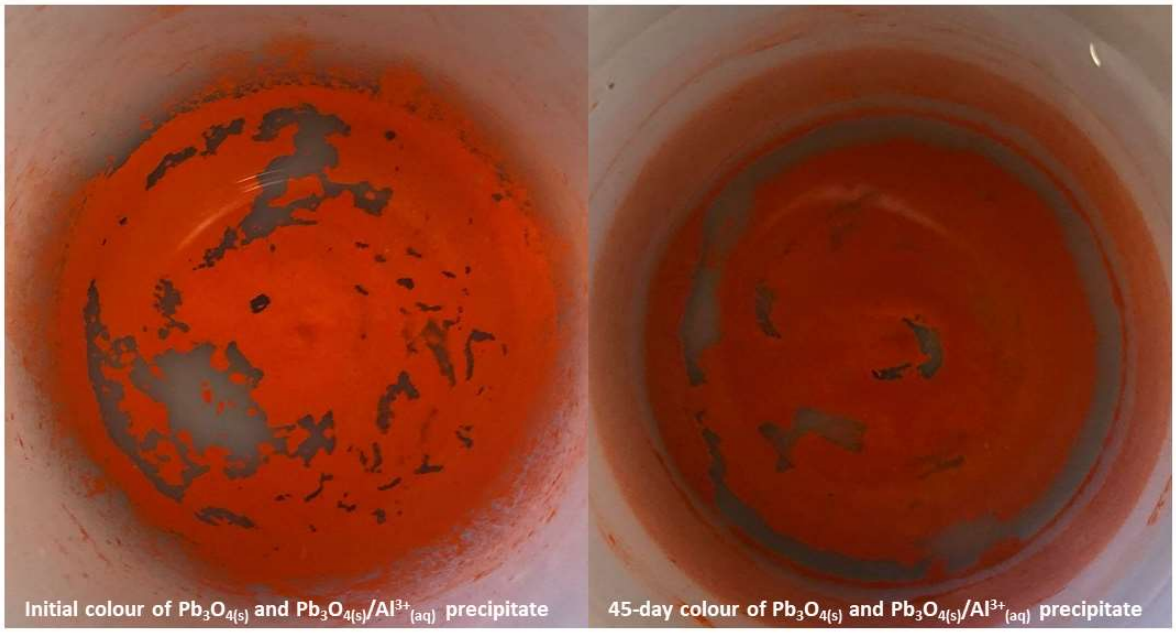


*Figure 20: Colour change of minium precipitate in the absence of silicate over 45 days exposure to chlorinated drinking water*

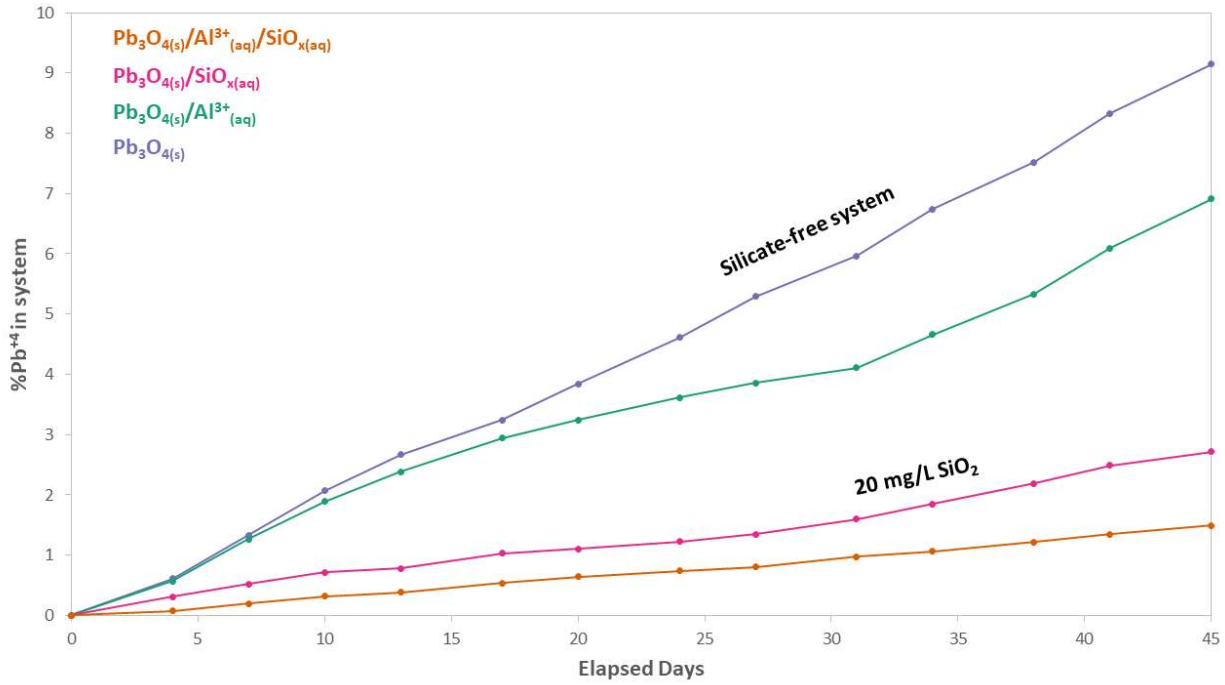


*Figure 21: % Hypothetical amount of $Pb^{+4}$ generated from direct chlorine consumption in minium at pH 8 over 45 days exposure to chlorinated drinking water*

The dissolved lead levels measured throughout Test Four are shown in Figure 22. The levels appear to rapidly decrease at the start of the experiment and then slowly increase to equilibrium levels determined by minium thermodynamic solubility. Unlike cerussite,

$Pb_3O_{4(s)}/Al^{3+}_{(aq)}/SiO_{x(aq)}$ does not appear to have the highest dissolved lead levels consistently throughout the experiment. Rather, both $Pb_3O_{4(s)}/Al^{3+}_{(aq)}/SiO_{x(aq)}$ and $Pb_3O_{4(s)}/SiO_{x(aq)}$ have the highest levels until the final measurement at which point $Pb_3O_{4(s)}$ increases sharply. All samples follow the trend of starting with a high measurement, sharply decreasing and then slowly increasing to stabilize around solubility equilibrium. Reports of minium solubility are extremely variable, and this contrasting behaviour to that of cerussite is likely linked to the kinetics of the dissolution process playing a larger role for the case of lead oxides. Fraser and Fairhall reported minium solubility in distilled water to be 553 ug/L at room temperature, however McKinley and collaborators reported $Pb_3O_4$ to have a water solubility of 6.9 ng/L, and Guo et al. reported 140 ug/L (Brokbartold et al., 2013; Fraser and Fairhall, 1959; Guo et al., 2014; McKinley et al., 2002). The average solubility region is shown with the shaded box in Figure 22. Lytle et al. observed a similar trend with dissolved lead rapidly decreasing at the start of their experiment using lead carbonates and orthophosphate, leveling off, and then increasing to solubility equilibrium levels towards the end of the experiment. They attribute this trend to the conversion of $Pb^{2+}$ to relatively insoluble $Pb^{4+}$ occurring more rapidly at the beginning of the experiment (Lytle et al., 2009). Furthermore, the free chlorine levels were slightly lower towards the end of the Test Four experiment (Figure 19), which could have triggered some conversion from $Pb^{4+}$ back to $Pb^{2+}$. This could explain the increase in dissolved lead levels in the final measurements on day 45. These results are in agreement with previous reports suggesting the dissolution of minium is a kinetically controlled process. Overall, a similar trend is observed with the silicate-treated minium samples experiencing higher dissolved lead levels throughout the experiment as was observed with silicate-treated cerussite.

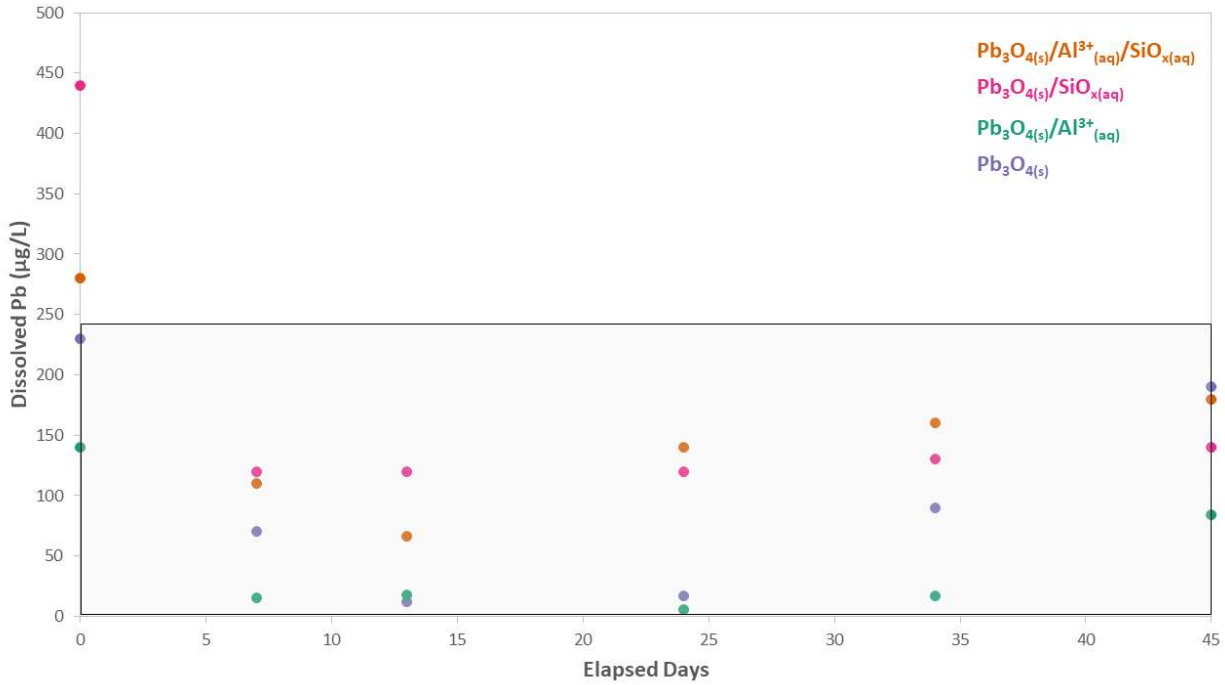


*Figure 22: Dissolved Pb levels from test four at pH 8 with and without silicate exposure in chlorinated drinking water, with minium as lead solid phase*

#### 4.2.2.2 Solid Phase Changes

XPS was performed on the minium samples for a solid phase characterization. A Pb 4f high resolution scan and fitting is presented in Figure 23, where the dotted line represents the envelope and the solid lines represent the 4f7/2 and 4f5/2 fittings. Significant differences can be seen in the shape of the envelopes, as well as the size of the peak fittings, based sample exposure to aqueous silicates. The high resolution Pb 4f signal for $Pb_3O_{4(s)}/Al^{3+}_{(aq)}$ displays a much larger secondary peak around 139 eV compared to that of $Pb_3O_{4(s)}/Al^{3+}_{(aq)}/SiO_{x(aq)}$. Indeed, for the sample obtained in the presence of silicate the fitting shows 21.2% of the area at 139 eV and 78.8% of the area at 137.8 eV. For $Pb_3O_{4(s)}/Al^{3+}_{(aq)}$, the fitting shows 9.6% of the area at 138.7 eV and 90.4% of the area at 137.7 eV. It should be noted that the $Pb_3O_{4(s)}/SiO_{x(aq)}$ sample was also analyzed via XPS high resolution Pb 4f and displayed a very similar phase breakdown as $Pb_3O_{4(s)}/Al^{3+}_{(aq)}/SiO_{x(aq)}$, (19.7% of the area at 138.7 eV and 80.3% at 137.7 eV) therefore the results for this sample were not shown in Figure 23. This clearly indicates a difference in the surface composition of the lead oxide phase in each sample. The $Pb^{2+}$ peak for $Pb_3O_4$ is reported to occur at 138.6 eV, and the $Pb^{4+}$ peak at 137.6 (Thomas and Tricker, 1974). Furthermore, the 4f peak for $PbO_2$ occurs at a lower binding energy (137.5 +/- 0.4 eV) than those obtained in lead phases in a lower valence (+2) state (138.3 – 139 eV) (National Institute of Standards and

Technology, 2012). Using these reports, we can thus confirm that the peak located around 139 eV is linked to $Pb^{2+}$ species whereas the peak located around 137.7 eV can be assigned to $Pb^{4+}$. The surface of the sample in the absence of silicates exhibits 11.6% more $Pb^{4+}$ than the sample exposed to aqueous silicates. This is further confirmation of the inhibitive effect of silicates on the generation of $Pb^{4+}$ by aqueous phase interaction.

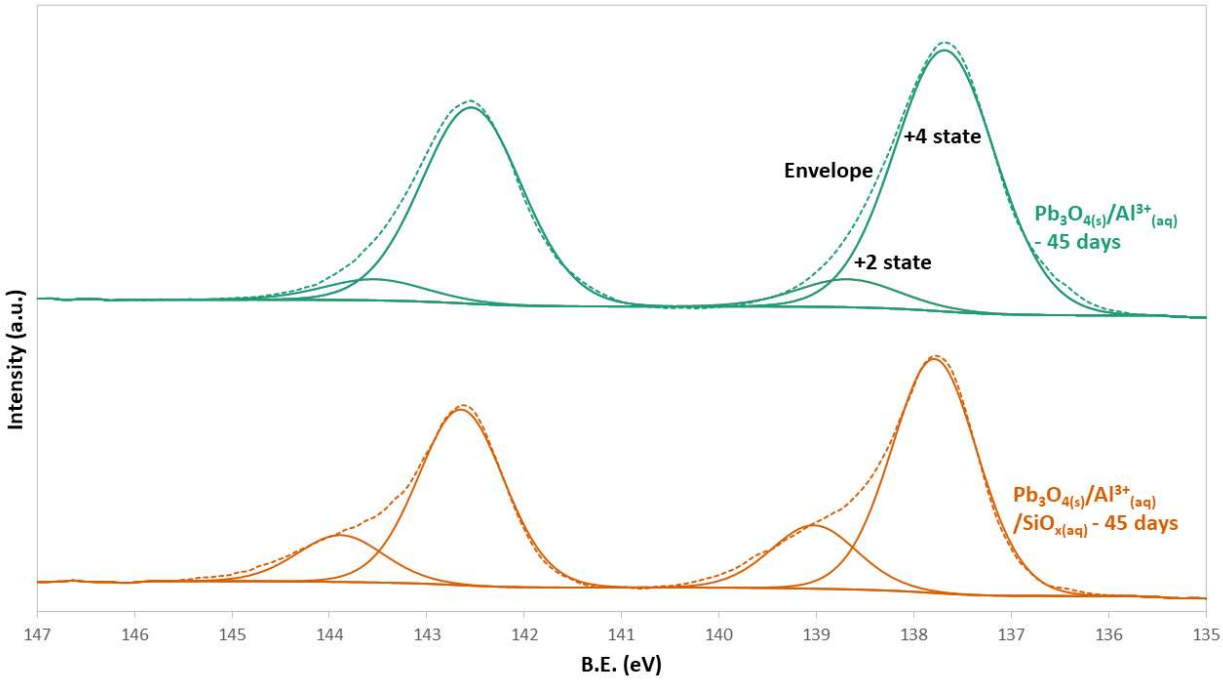


*Figure 23: Pb 4f high resolution XPS fitting of minium following 45 days exposure to chlorinated drinking water with and without silicates, showing higher $Pb^{+4}$ in absence of silicate treatment*

The surface composition in atomic percentage was also determined by XPS survey scan (Table 11). The survey scan identified the presence of O, Ca, C, Pb, Si, and Al in the $Pb_3O_{4(s)}/Al^{3+}_{(aq)}/SiO_{x(aq)}$, $Pb_3O_{4(s)}/Al^{3+}_{(aq)}$ and $Pb_3O_{4(s)}/SiO_{x(aq)}$ samples, however the relative amounts of each element vary. There is a significant difference between the amount of Si and Al in the samples. In order to compare with previous results presented in this thesis, the Si:Pb and Si:Al ratios (Figures 13 and 14) will be discussed. There was four times more Si in the surface of the $Pb_3O_{4(s)}/Al^{3+}_{(aq)}/SiO_{x(aq)}$ sample compared to $Pb_3O_{4(s)}/SiO_{x(aq)}$. The silicon content in the $Pb_3O_{4(s)}/Al^{3+}_{(aq)}$ sample was below detection limit. Once again, this confirms the critical role of aluminum ions in the surface precipitation of silicate species on the solid sample. Furthermore, the Si:Al ratio in the $Pb_3O_{4(s)}/Al^{3+}_{(aq)}/SiO_{x(aq)}$ sample is quite similar to the surface ratio observed

for the previously discussed $PbCO_{3(s)}/Al^{3+}_{(aq)}/SiO_{x(aq)}$, suggesting the precipitation of silicate is regulated mostly by aqueous aluminum and is likely independent of lead phase morphology.

*Table 11: Surface composition of minium samples following 45 days exposure to chlorinated drinking water with and without silicates, measured by XPS*

| | Atomic % | | |
|---|---|---|---|
| **Element** | **$Pb_3O_{4(s)}/ Al^{3+}_{(aq)}/SiO_{x(aq)}$ – 45 days** | **$Pb_3O_{4(s)}/Al^{3+}_{(aq)}$ – 45 days** | **$Pb_3O_{4(s)}/SiO_{x(aq)}$ – 45 days** |
| O 1s | 53.2 | 38.2 | 42.3 |
| Ca 2p | 2.9 | 1.4 | 2 |
| C 1s | 18.8 | 33 | 31.2 |
| Pb 4f | 11 | 25.9 | 20.2 |
| **Si 2p** | **8.9** | **Below detection limit** | **3.7** |
| Al 2p | 5.1 | 1.2 | Below detection limit |

Given the presence of Si in the sample surface, a high-resolution Si 2p scan was completed. The Si 2p binding energy for $Pb_3O_{4(s)}/Al^{3+}_{(aq)}/SiO_{x(aq)}$ was identified at 102.2 eV, and for $Pb_3O_{4(s)}/SiO_{x(aq)}$ at 101.8 eV (fittings shown in Appendix B Figure 35). Silicates typically have a 2p binding energy in the range of 103.8 – 101.6 eV depending on cations present, and silicates in the presence of aluminum have been shown to have an Si 2p binding energy in the range of 102.9 – 101.8 eV depending on degree of polymerization (Biesinger, n.d.; Li et al., 2012). Because both measurements for the silicate-treated samples fall within the range for silicates, it is likely that the Si phase present is silicate. This further confirms the presence of silicates precipitating onto the solid phase under drinking water conditions regardless of the morphology of the lead solid phase.

### 4.2.3 Role of Aluminum in Silicate Precipitation and Lead in Drinking Water

The results portrayed clearly indicate that the presence of silicates inhibits the interaction between the Pb-bearing solid and the aqueous phase containing chlorine residual. However, they also suggest that aluminum ions also play a role in this inhibitory effect as the solids precipitating in the presence of aqueous silicate also contain aluminum. Aluminum, iron, manganese and other metals are often identified in lead corrosion scale characterizations;

aluminosilicates have been consistently identified as a major phase in lead bearing corrosion scales harvested from drinking water distributions systems (Guo and Herrera, 2018; Kim and Herrera, 2010; Snoeyink et al., 2003). Iron and manganese have been reported to increase lead release from corrosion scale by accelerating lead oxidation, however the effects of aluminum are still relatively unknown (Li et al., 2020). Aluminum is found in most drinking water distribution systems either naturally occurring or from water treatment with alum. Silica is also naturally occurring in water (Kvech and Edwards, 2001; Snoeyink et al., 2003). Some studies have proposed aluminosilicate formation on pipe surface may have a protective effect on metal ion dissolution, and many have investigated the prevalence of aluminosilicates in corrosion scale harvested from municipalities across North America (Snoeyink et al., 2003). An early study in 1973 noted the solubility of silica at pH 8.0 decreased with increasing aluminum concentration; the authors hypothesized the formation of an aluminosilicate solid that results in a reduction of both aluminum and silica levels (Iler, 1973; Snoeyink et al., 2003). A more recent study conducted in 2020 assessed the effect of aluminum on dissolved lead levels in phosphate treated water. They found that in phosphate treated systems, the presence of aluminum increased dissolved lead levels due to interference with formation of protective lead-phosphate compounds on the pipe surface (Li et al., 2020).

Allophane and imogolite are poorly crystalline aluminosilicate solids commonly found in soils. They have Si:Al ratios between 0.5 and 4; imogolite is typically Al-rich whereas allophane is Si-rich however ratios are pH dependent. The formation of both aluminosilicates is kinetically favoured when dissolved silica and aluminum concentrations are between 0.1 – 4 mmol/L and can form in any environment where there is a sufficient supply of silica and aluminum (Harsh et al., 2018). Both allophane and imogolite have been prepared synthetically in a lab environment by adjusting ratios of aqueous aluminum, silica, pH and temperature (Wada and Kubo, 1975; Wada et al., 1979). Wada and Kubo were able to show that the $SiO_2/Al_2O_3$ ratio of amorphous aluminosilicate precipitation from solution is in the range of 1.0 – 3.0 when precipitation takes place at a weakly acid to alkaline pH (Wada and Kubo, 1975). Allophane can be found with $SiO_2/Al_2O_3$ ratios typically between 0.9 – 2.1 depending on parent solution conditions and temperature; these specific experiments were completed at temperatures ranging from 60 – 90 °C however temperature is not limiting as both aluminosilicates have been known to form in volcanic ash in Iceland (Harsh et al., 2018; Wada et al., 1979). $Pb^{2+}$ has been shown to sorb

selectively to allophane and imogolite in soils. Furthermore, Al-rich allophanes tend to be unstable and Si-rich allophanes are most likely to occur in natural waters (Harsh et al., 2018). Studies have found that allophane is the most common phase formed under drinking water conditions with the Si/Al ratio affected by pH (Arai et al., 2005; Guo and Herrera, 2018; Opiso et al., 2009). Other work, however, indicates that this not might be always the case. A kinetic study performed at 25 °C determined that imogolite could be formed in drinking water distribution systems with alum coagulated waters (resultant Al concentration around 200 µg/L) and silica concentrations as low as 2 mg/L  although pH was not discussed; a further comment by the same author indicated the formation of imogolite occurs most easily at pH 4.5 (Farmer and Lumsdon, 1994; Snoeyink et al., 2003).

The aim of this section is to determine how silicates and aluminum interact under drinking water conditions to precipitate aluminosilicate solids onto lead. Batch reactor experiments with varying concentrations and phases of silicates, aluminum and lead were conducted. Aqueous silica levels were monitored consistently; experiments lasted 45 – 120 days followed by surface and bulk solid phase characterization performed via UV-Vis, FTIR, Raman, XRD, XPS, and/or SEM-EDX.

#### *4.2.3.1 Analysis of Changes in Aqueous Phase*

Throughout the experiments conducted to isolate the effects of silicates, observations were made regarding the effect of aluminum on silicate precipitation. Aqueous silica measurements were taken every three to seven days throughout Tests Two, Three and Four with minium and cerussite as the solid phase. These results are seen in Figures 24 and 25. Consistently, the aqueous silica levels decreased in the presence of aluminum regardless of lead solid phase or pH.

The decrease in silica levels in the presence of aluminum may be due to the formation and precipitation of an aluminosilicate phase on the lead surface, similar to that which is found on the outermost scale layers harvested from lead service lines. Another recent study monitored the aqueous alumina levels in a phosphate treated system and saw levels decrease over the course of the experiment. They hypothesize the formation of aluminum hydroxide depositing on the lead surface as aluminum hydroxide particles are positively charged and the surface of cerussite and lead oxides are negatively charged (Li et al., 2020). They did not, however, detect the presence of any alumina-containing species through XRD or SEM analysis of the Pb coupons used in their

experiments. Furthermore, they determined that in the presence of orthophosphate, aluminum uptake to scale was inhibited due to change in surface charge from positive to negative (Li et al., 2020). In our water quality regime, some of the aluminum complexes are expected to remain positive, suggesting precipitation of aluminum and silicate is in the form of aluminosilicates that are attracted to the negative surface of the lead carbonates or oxides.

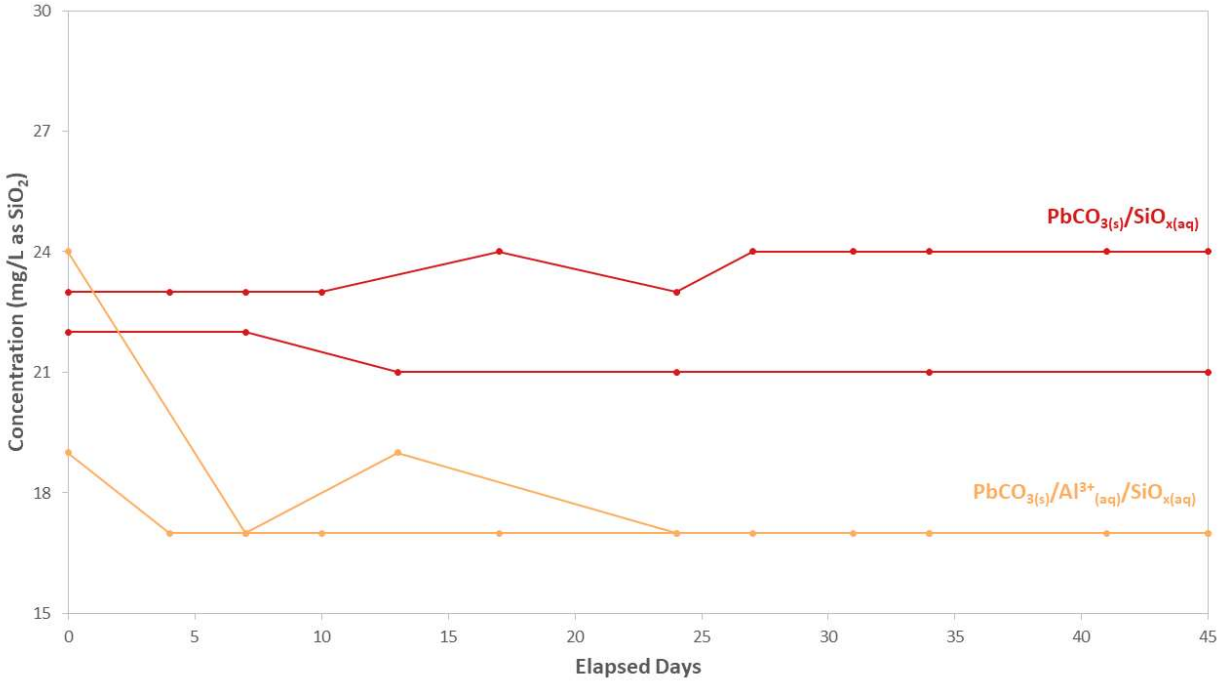


*Figure 24: Aqueous silicate concentration variations with time in tests two and three over 45 days exposure to chlorinated drinking water, cerussite as lead solid phase*

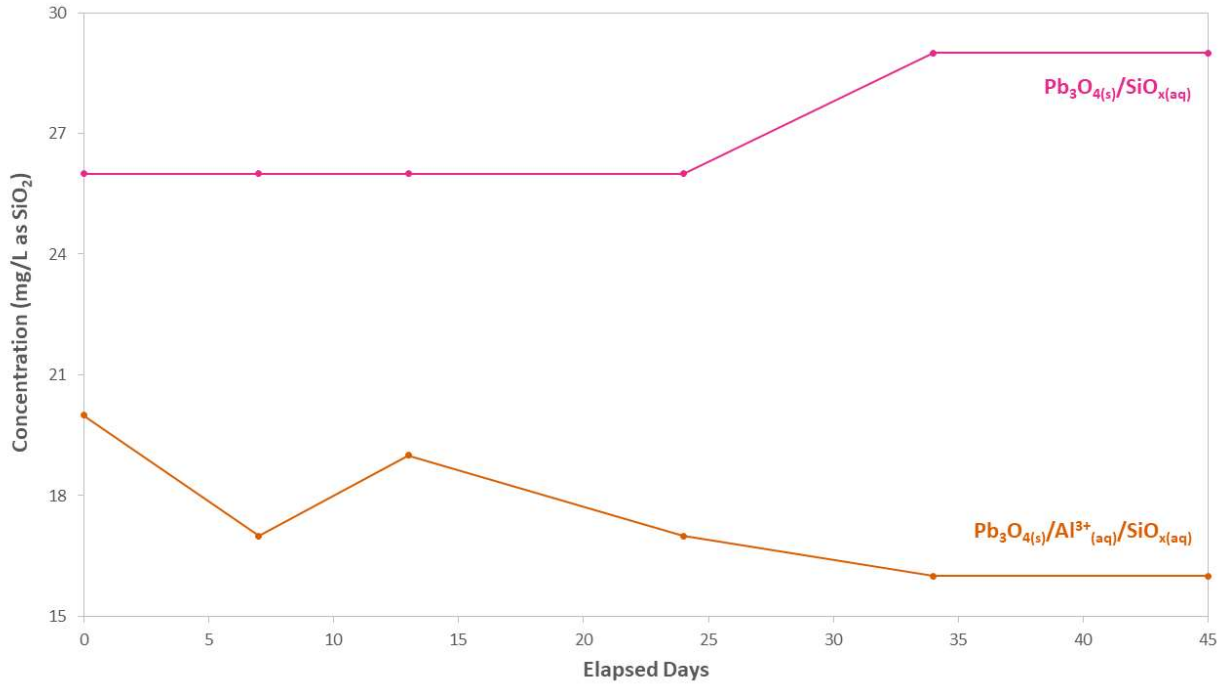


*Figure 25: Aqueous silicate concentration variations with time in test four over 45 days exposure to chlorinated drinking water, minium as lead solid phase*

Allophane and imogolite are two commonly found aluminosilicates. Previous studies have suggested that both could form under drinking water conditions, but based on pH, allophane is most likely to form given most drinking water parameters and neutral to slightly basic pH (Farmer and Lumsdon, 1994; Kim and Herrera, 2010; Snoeyink et al., 2003). Allophane typically has the composition $Al_2O_3(SiO_2)_{1.3\text{-}2}\bullet(H_2O)_{2.5\text{-}3}$ and has a positive surface charge ("Allophane Mineral Data," n.d.; Guo and Herrera, 2018). The Al/Si ratio depends on pH and affects its surface properties (Guo and Herrera, 2018; Harsh et al., 2018). Si-rich allophanes, typical Al/Si ratio of 0.6, form naturally at pH above 5 to near neutral, and a pH above 4.7 is needed for precipitation (Guo and Herrera, 2018; Parfitt and Kimble, 1989). Previous studies have shown that the surface of cerussite and hydrocerussite under drinking water conditions have negative zeta potentials, indicating that the positively charged aluminosilicates could adsorb to the surface of the solid lead carbonate (Guo and Herrera, 2018; Harsh et al., 2018). Another study found that the zeta potential of sodium silicate treated iron oxide was substantially more negative than untreated iron oxides, and this is expected for other transition metals as well (Li et al., 2019). That being considered, sodium silicate treated lead carbonate or oxide could have a more negative surface charge which would result in enhanced deposition of aluminosilicates to the

lead surface. Furthermore, synthetic allophanes have been prepared in solutions with pH between 6.0 to 8.0 and $SiO_2/Al_2O_3$ ratios between 1 and 3 at room temperature (Wada et al., 1979).

We tested the possibility that an aluminosilicate phase is forming on the solid lead precipitate by designing a set of experiments with a higher amount of solid phase under the hypothesis that a higher amount of solid surface area would increase the number of available sites for precipitation. It is important to emphasize that the underlaying hypothesis assumes that aluminosilicate precipitation is occurring at the surface of the solid lead phase, thus Pb-phase mediated, and not freely in the aqueous phase through direct interaction of silicate and aluminum ions reaching the thermodynamic solubility product. In some of these experiments, the aluminum dosage was consistently spiked with 1 mg/L over time to attempt to trigger decreases in aqueous silica levels (Tests Five and Six) using both cerussite and plattnerite at both pH 7 and 8.

The results obtained for aqueous silica levels in this set of experiments are shown in Figures 26 – 28. Consistently, after each aluminum spike of 1 mg/L, a decrease in aqueous silicate levels is observed. The amount of silicate precipitating, however, depends on the system pH. For the case of the experiment run at pH 8, a consistent decrease of 2 mg/L as $SiO_2$ (Figure 26) is observed after a 1mg/L Al spike is introduced to the system. At pH 7, each aluminum spike of 1 mg/L led to a decrease in aqueous silica levels of 1 mg/L. This 1 mg/L decrease was observed for both $PbCO_3$ and $PbO_2$ (Figure 27 and Figure 28). When aluminum was not present, varying levels of aqueous $SiO_2$ were observed with no consistent decrease over time. Overall, the aqueous $SiO_2$ levels were more consistent and predictable in the presence of aluminum. There are several conclusions that can be drawn from this experiment. First, it appears the lead solid phase does not impact precipitation; at pH 7 the aluminosilicate formation and precipitation rates were the same for both $PbCO_3$ and $PbO_2$. As discussed above, at this pH the surface of both lead carbonates and oxides is negative, therefore both would attract the positively charged aluminosilicates towards surface precipitation.

It is well stablished that in aqueous solutions at neutral pH, aluminum ions are forming hexa-aqueous complexes of the form $[Al(OH_2)_x(OH)_y]^{+3-y}$ (Rudolph et al., 2000). At pH 7, the main species present are $[Al(OH_2)_4(OH)_2]^{+1}$, $[Al(OH_2)_3(OH)_3]^0$ and $[Al(OH_2)_2(OH)_4]^{-1}$ (Bertsch and Parker, 1996). We could propose that the positively charged aluminum species act as a bridge between the negative solid surface and the negatively charged silicate ions. Given the similar

atomic weights of Si (28 g/mol) and Al (27 g/mol), it is remarkable that these results demonstrate that per each atom of aluminum introduced to the system, one atom of silicate is lost from the aqueous phase into the solid surface and, moreover, this stoichiometry is pH dependent. Indeed, when the pH is raised to 8, twice as much (2 mg/L as $SiO_2$) aqueous silicate is lost to the solid phase after each 1 mg/L Al spike to the system. We could rationalize this observation once again assuming the positively charged aqueous aluminum complex is acting as an interface between the negatively charged solid lead surface and the aqueous silicate ions. At higher pH, three effects take place: the surface of the solid lead bearing phase would become more negatively charged (if no total charge saturation has taken place), the coordination sphere around the silicate ions might also become more negative, and the speciation of the aqueous aluminum complexes changes due to hydroxyl ligand substitution in the inner coordination sphere (Huang et al., 2018), resulting in a larger amount of $[Al(OH_2)_2(OH)_4]^{-1}$ species at the expense of the positively charged and neutral aluminum complexes. Hence, the effectiveness of this "interface" effect would be very sensitive to aqueous pH levels.

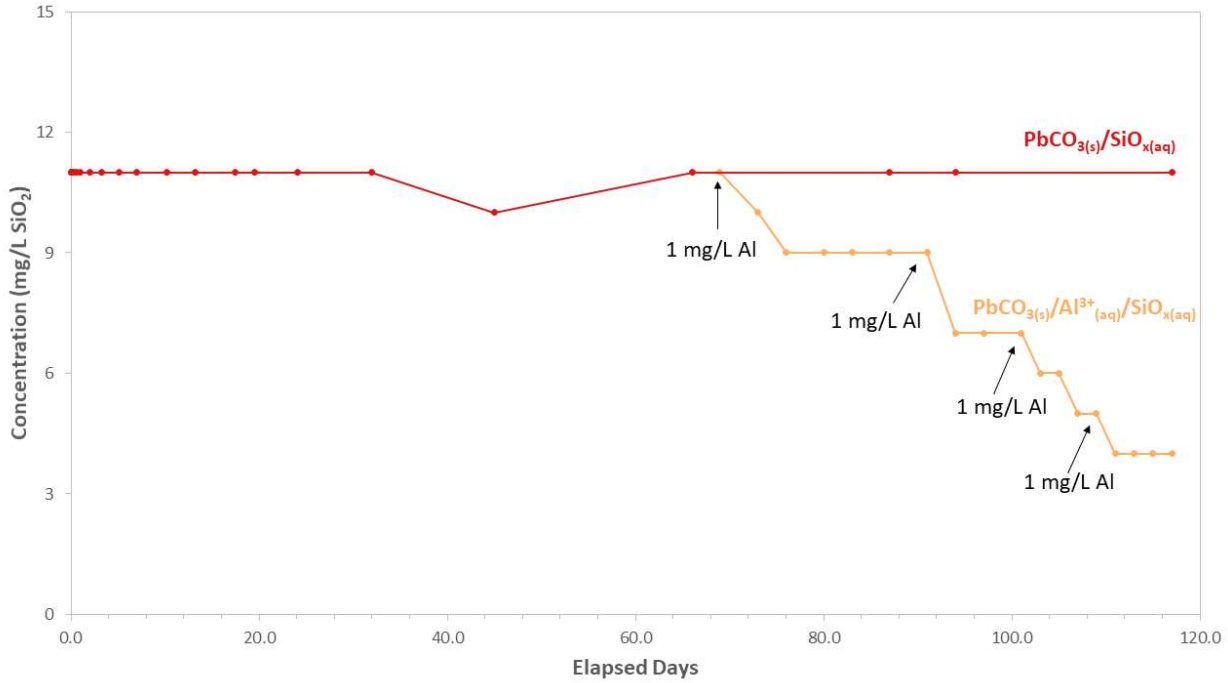


*Figure 26: Aqueous silicate concentration variations with time for high available surface area, with cerussite as lead solid phase, over 45 days exposure to chlorinated drinking water at pH 8 with increasing aqueous aluminum content. Silicate concentration decreases with each dose of 1 mg/L Al.*

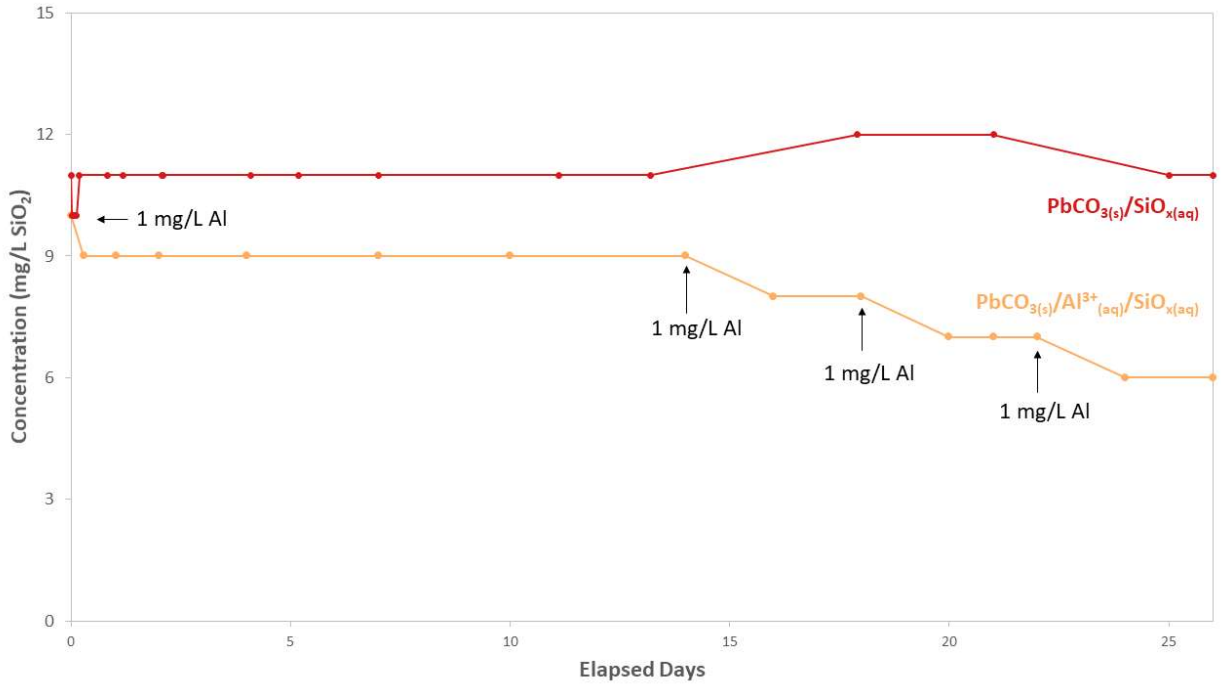


*Figure 27: Aqueous silicate concentration variations with time for high available surface area, with cerussite as lead solid phase, over 45 days exposure to chlorinated drinking water at pH 7 with increasing aqueous aluminum content. Silicate concentration decreases with each dose of 1 mg/L Al.*

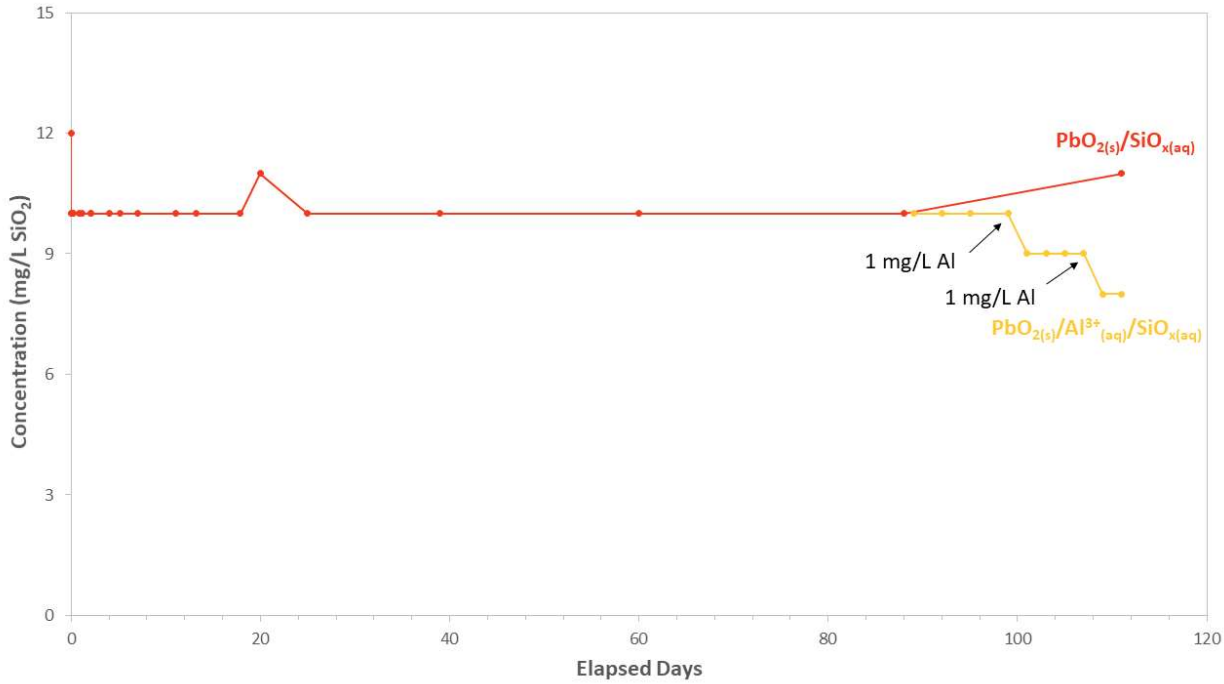


*Figure 28: Aqueous silicate concentration variations with time for high available surface area, with plattnerite as lead solid phase, over 45 days exposure to chlorinated drinking water at pH 7 with increasing aqueous aluminum content. Silicate concentration decreases with each dose of 1 mg/L Al.*

#### 4.2.3.2 Analysis of Changes in Solid Phase

XPS was conducted on the solid phase harvested from Tests Five and Six after 117 days of aqueous experimental work. It should be noted that the $PbCO_{3(s)}/Al^{3+}_{(aq)}/SiO_{x(aq)}$ sample was only exposed to aluminum for 48 days out of the total 117-day experiment; prior to aluminum addition it had an identical makeup to the $PbCO_{3(s)}/SiO_{x(aq)}$ sample. The XPS analysis provided a high resolution Pb 4f spectrum (Figure 29), as well as the atomic makeup of the sample surface through a survey scan (Table 12). The Pb 4f fittings are shown with solid lines, and the spectra envelopes are shown with dotted lines. The high-resolution spectrum shows lead in three phases with binding energies centered at 139.8 eV, 138.5 eV and 136.8 eV. Pb metal has been shown to have a binding energy between 136.4 – 137 eV, and $PbO_2$ between 136.8 – 137.7 eV (Chang and He, 2004; National Institute of Standards and Technology, 2012; Wang and Zheng, 1996), however, given the oxidizing environment to which these samples were exposed, it is extremely unlikely that this peak is Pb metal. The binding energy of 136.8 eV is likely attributed to $PbO_2$. From the 4f fittings, both samples had similar amounts of $PbO_2$ at 4.1 area% for $PbCO_{3(s)}/Al^{3+}_{(aq)}/SiO_{x(aq)}$ and 4.9 area% for $PbCO_{3(s)}/SiO_{x(aq)}$. The majority of the phase present for both samples is centered around 138.5 eV; $PbCO_{3(s)}/Al^{3+}_{(aq)}/SiO_{x(aq)}$ had 87.5 area% and $PbCO_{3(s)}/SiO_{x(aq)}$ had 93.3 area%. As previously discussed, this peak is assigned to lead carbonate (National Institute of Standards and Technology, 2012). The presence of aluminum may have resulted in additional lead phase transformation; more lead remained as $PbCO_3$ in the absence of aluminum. Finally, the third peak at 139.8 eV was difficult to match. $PbCO_{3(s)}/Al^{3+}_{(aq)}/SiO_{x(aq)}$ had 8.4 area% and $PbCO_{3(s)}/SiO_{x(aq)}$ had 1.8 area%. Lead is a difficult metal to characterize with XPS due to a similar range of binding energies for many compounds. It is likely that this peak belongs to a $Pb^{2+}$ compound as most $Pb^{2+}$ compounds have a Pb 4f7/2 binding energy in the range of 138 – 139.5 eV, whereas $Pb^{4+}$ or $Pb^0$ are in the range of 136.5 – 137.5 eV (National Institute of Standards and Technology, 2012; Thomas and Tricker, 1974).

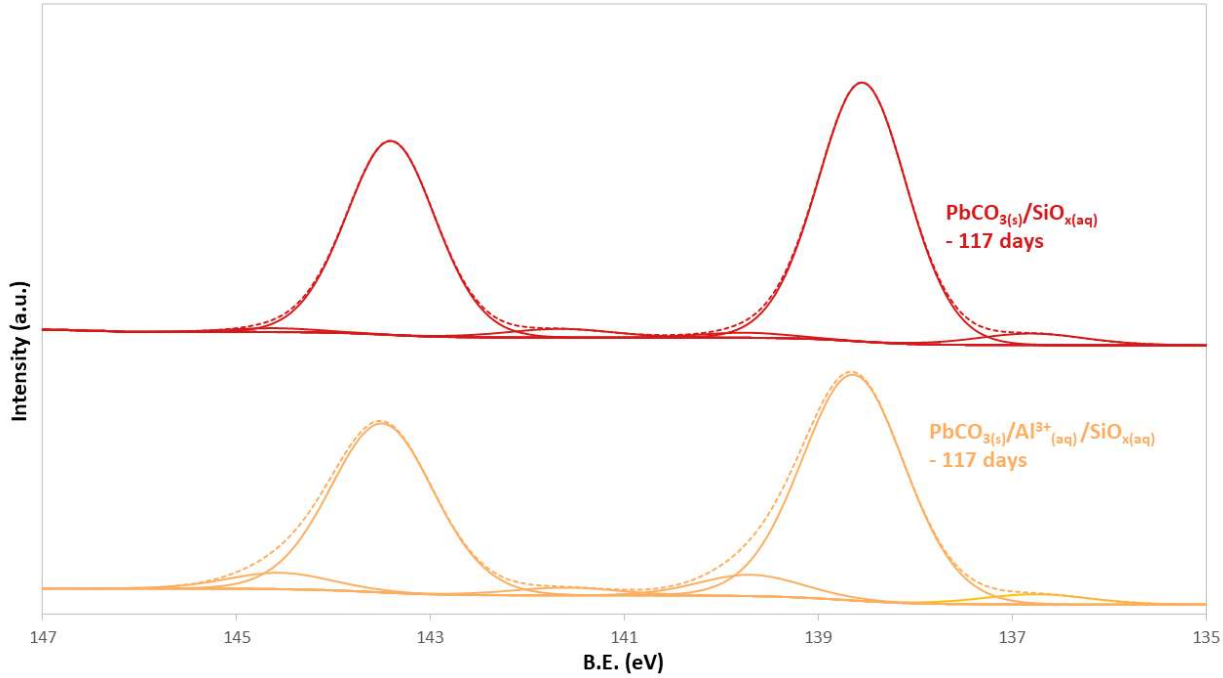


*Figure 29: High resolution Pb 4f XPS fitting for cerussite exposed to aqueous silicate in chlorinated drinking water at pH 8 for 117 days, with and without aqueous aluminum.*

The survey scan results for the above two samples are presented in Table 12. The composition of the two samples is similar except for the presence of Si and Al. The sample spiked with aqueous aluminum ions ($PbCO_{3(s)}/Al^{3+}_{(aq)}/SiO_{x(aq)}$) contained 2.2 at% Si whereas the amount of Si in control sample ($PbCO_{3(s)}/SiO_{x(aq)}$ no aluminum spiked) was below detection limit. A value of 3.6 at% Al was also observed in the surface of the $PbCO_{3(s)}/Al^{3+}_{(aq)}/SiO_{x(aq)}$ samples whereas no aluminum, as expected, was observed in the control $PbCO_{3(s)}/SiO_{x(aq)}$ sample. The ratios of Si:Pb (0.27) obtained are smaller in this experiment compared to that observed on the sample obtained after 45-days (Figure 30), likely due to experimental conditions used in the 117 days experiment: half the aqueous silicate concentration and a tenfold increase of lead in the solid phase. Although the observed surface aluminum content is similar in both cases (3.5 at%, Table 10 – 45 day experiment vs 3.6 at%, Table 12 – 117 day experiment), the Si:Al ratios are different. For the longer experiment (117 days), the Si:Al ratio in the surface layer is 0.6 (Table 12, Figure 30) whereas for the 45-day tests this value is 1.9 (Table 10, Figure 30). These values indicate not only that an aluminosilicate phase has formed and precipitated onto the solid but also suggest, once again, that once precipitated, Si migrates into the bulk. Indeed, the surface ratio of Si/Al obtained at 45 days is almost 4 times larger than that obtained after 117 days. Finally, a larger amount of silicon is observed in the $PbCO_{3(s)}/Al^{3+}_{(aq)}/SiO_{x(aq)}$ sample compared to

$PbCO_{3(s)}/SiO_{x(aq)}$, as expected, due to the observed decrease in aqueous silicate concentration in the presence of aluminum.

*Table 12: Surface composition of cerussite exposed to aqueous silicate for 117 days in chlorinated drinking water, with and without aluminum, obtained by XPS*

| | Atomic % | |
|---|---|---|
| **Element** | **$PbCO_{3(s)}/SiO_{x(aq)}$ – 117 days** | **$PbCO_{3(s)}/Al^{3+}_{(aq)}/SiO_{x(aq)}$ – 117 days** |
| O 1s | 44.4 | 50.9 |
| Ca 2p | 0.9 | 0.2 |
| C 1s | 41.7 | 33.8 |
| Pb 4f | 12.8 | 8.2 |
| **Si 2p** | **Below detection limit** | **2.2** |
| Al 2p | 0 | 3.6 |

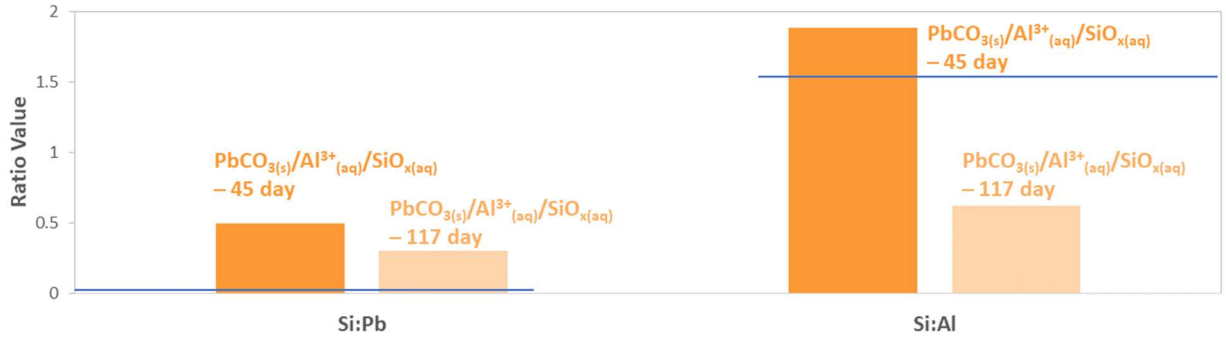


*Figure 30: Comparison of surface ratio for Si:Pb and Si:Al with experiment length, blue line represents total system ratio. Higher ratios are observed in shorter-term experiments, indicating silicate migration into the bulk.*

High resolution Si 2p and Al 2p scans were also performed. The Si 2p binding energy was 101.7 eV for $PbCO_{3(s)}/SiO_{x(aq)}$, and the Al 2p and Si 2p binding energies were 74.4 eV and 102.1 eV, respectively, for $PbCO_{3(s)}/Al^{3+}_{(aq)}/SiO_{x(aq)}$ (Appendix B Figures 36 and 37). As previously mentioned in this thesis, the binding energy for silicates is typically in the range of 101.6 – 103.8 eV depending on the presence of other cations, such as $Al^{3+}$ (Biesinger, n.d.). The Si 2p measurements suggest silicates are present in the solid phase for both samples. A study on the XPS characteristics of allophane found the Al 2p peak (for an Al/Si ratio 1-2.2) at 74.3 eV (Childs et al., 1997). As the Al 2p peak for this sample is located at 74.4 eV, and in light of previously reported work (Guo and Herrera, 2018; Li et al., 2020; Wada et al., 1979), the presence of allophane in the sample is likely. These results indicate the formation of a high Al:Si

ratio allophane forming under drinking water conditions on the lead solid phase upon introduction of aluminum ions to the aqueous silicate system.

Allophane was identified in the solid phase of the 117-day experiments based on XPS (Tables 10 and 11); Al 2p analysis was also performed on the 45-day samples (Appendix B Figure 38) to verify results were consistent. The peaks from the high-resolution Al scan located binding energies at 73.8 – 73.95 eV in the absence of silicates. In the presence of silicates, the Al 2p peaks are located at 74.1 – 74.2 eV. The presence of silicates appears to change the Al 2p binding energy, suggesting the chemical morphology of Al in the solid phase is dependent on exposure to aqueous silicates. The binding energy for gibbsite ($Al(OH)_3$) is 73.9 +/- 0.1 eV (Biesinger, n.d.). Furthermore, gibbsite has been hypothesized to form in aluminum rich drinking water systems (Li et al., 2020; Opiso et al., 2009). Therefore, it is likely that in the absence of silicates, gibbsite forms on the lead surface. Allophane exhibits an Al 2p peak (Al/Si ratio 1-2.2) at 74.3 eV (Childs et al., 1997). Assuming the assignments in these previous works are correct, we can hypothesize that gibbsite is present in the silicate-free samples, while in the presence of silicates, allophane is the main phase.

The results from previous characterizations performed with the 45-day experiments were analyzed for any indication of presence of allophane or other aluminum-bearing phase in the solid. Based on the Al 2p XPS feature attributed to allophane in the solid phase of the $PbCO_{3(s)}/Al^{3+}_{(aq)}/SiO_{x(aq)}$ – 45 day sample, it is expected that the chemical state of the precipitate visible by SEM in Figure 10 is allophane. In terms of IR spectroscopy (Figures 16 and 17), there were no peaks indicating any presence of aluminum in the solid phase for $PbCO_{3(s)}/Al^{3+}_{(aq)}$. In a Raman spectrum, Al-OH and Al-O-Al peaks appear between 970 – 940 $cm^{-1}$ and an aluminum hydroxide mineral species such as bayerite or gibbsite would appear with peaks in the 3600 – 3400 $cm^{-1}$ range (Phambu, 2003). UV-Vis cannot identify allophane with lead carbonate as the solid phase as the dominant peak occurs at 270 nm, which is in the same region as cerussite and hydrocerussite (Figure 15) (Guo and Herrera, 2018). Allophane is amorphous and would not be expected to show through XRD (Figure 18). This is consistent with the expected amorphism of the aluminosilicate phase in harvested corrosion scale (Li et al., 2020).

The EDX results in Table 9 do present additional information regarding the state of aluminum in the solid. The Si:Al ratio for $PbCO_{3(s)}/Al^{3+}_{(aq)}/SiO_{x(aq)}$ – 45 day is 1.9. The results also indicate a

high amount of Al in the $PbCO_{3(s)}/Al^{3+}_{(aq)}$ – 45 day sample (1.7 at%) compared to the $PbCO_{3(s)}/Al^{3+}_{(aq)}/SiO_{x(aq)}$ – 45 day sample (0.41 at%). Both samples were in aqueous phase at pH 8 with 2 mg/L $Al^{3+}$ but the bulk atomic percentage of **Al in the solid phase is over four times higher in the absence of silicates**. This could be due to aluminum precipitating out of solution as an aluminum hydroxide, similar to what was observed with decreasing aqueous aluminum concentrations by Li and collaborators. They did not detect any Al-containing crystalline solids by XRD or visually observe anything on the lead surface by SEM. They did not conduct XPS or EDX measurements on their samples but from the reported decrease in aqueous concentrations of Al they inferred a significant amount of aluminum lost from the aqueous into the solid phase. This did not, however, impact dissolved lead concentrations. Furthermore, they observed less uptake of aluminum by the solid lead phase in the presence of orthophosphate, similar to what was observed in our experiments in the presence of silicate (Li et al., 2020).

The XPS results in Table 10 and 11 also present information regarding aluminum and the formation of an aluminosilicate phase on the sample surfaces. XPS showed more aluminum in $PbCO_{3(s)}/Al^{3+}_{(aq)}/SiO_{x(aq)}$ – 45 day (3.5 at%) than $PbCO_{3(s)}/Al^{3+}_{(aq)}$ – 45 day (0.8 at%). The same trend was observed with the minium samples from Test Four; significantly more Al is present in the sample exposed to aqueous silicates. The Si:Al ratio however stayed similar to that observed in the bulk phase (EDX) and matched hypothesized values based on the precipitation 2:1 ratio of Si:Al from aqueous phase. This strongly suggests the formation of allophane with a ratio of approximately 2-2.5 which is well within the ratio theorized for a drinking water matrix and further confirms that the precipitate extends into the bulk phase with a similar atomic ratio of Si:Al.

## 4.3 Proposed model for the role of Si and Al on lead dissolution.

All observations and discussion described above can be incorporated into a simple model that describes the role of silicates and aluminum ions with the interaction of solid lead and the aqueous phase. This model is shown in Figure 31. In the presence of free chlorine, $Pb^{2+}$ is oxidized to $Pb^{4+}$, and $OCl^-$ is reduced to $Cl^-$. In the presence of the chlorine residual, the dominant form of lead in the solid phase will eventually become $Pb^{4+}$, and lower dissolved lead levels will be observed. When silicates are present, the redox reaction between the lead carbonate phase and chlorine does not take place and $Pb^{2+}$ remains the dominant lead phase in the solid.

Silicates inhibit the oxidation of lead, and higher dissolved lead levels are observed as lead levels are now controlled by the highly soluble lead carbonate phase. When aluminum ions are present in aqueous phase along with silicates, lead oxidation remains inhibited and an aluminosilicate passivation layer forms on the lead surface extending into the bulk phase. Again, higher dissolved lead levels are observed when the dominant lead phase is a $Pb^{2+}$ carbonate.

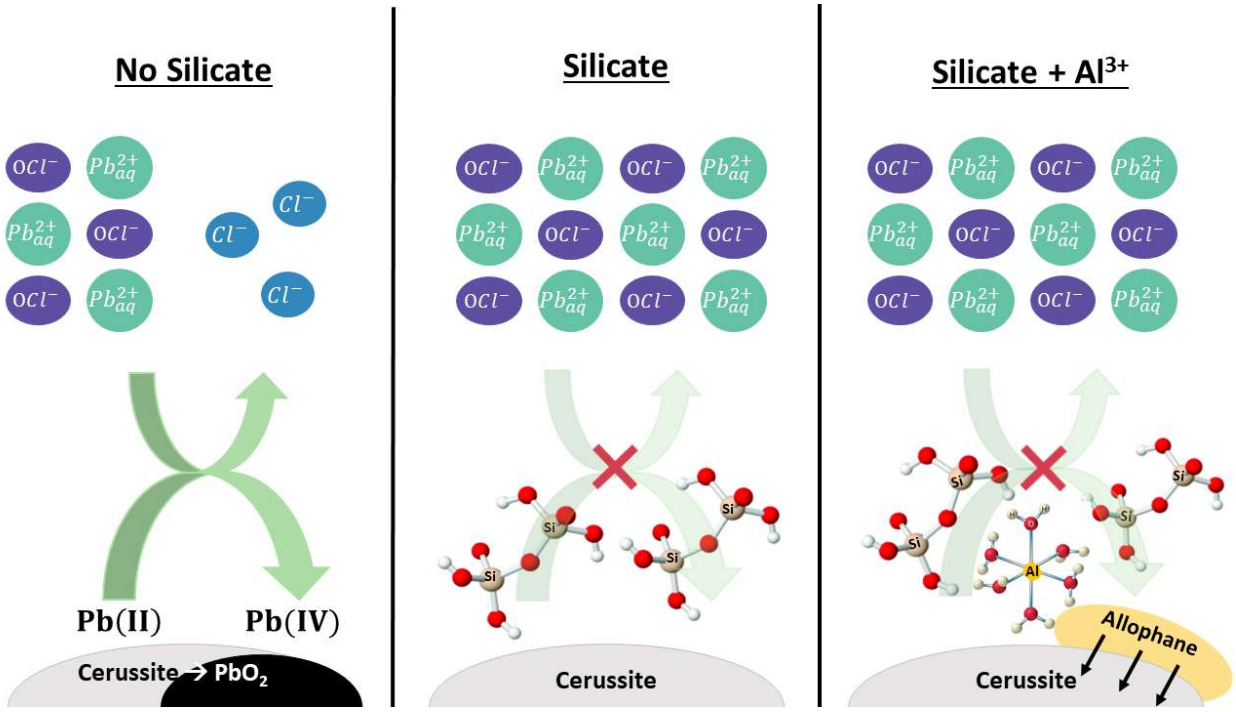


*Figure 31: Graphical depiction of thesis results. In absence of silicates, lead carbonate is oxidized to less soluble $PbO_2$. In the presence of silicates, the oxidation is inhibited, and dominant lead phase remains as lead carbonate. In the presence of silicates and aluminum, the oxidation is inhibited and allophane forms on the lead surface extending into the bulk.*

## 4.4 Environmental Implications

The environmental implications of these results are significant and reinforce the importance of developing a thorough fundamental understanding of the various corrosion control strategies to mitigate lead dissolution in drinking water systems. Our results indicate that the presence of aqueous silicates inhibited oxidation of lead carbonate by free chlorine, resulting in higher amounts of more soluble $Pb^{2+}$ in the solid phase. Since the silicate is interfering in the interaction of the lead carbonate phase with the chlorine in the aqueous phase, the transformation of cerussite/hydrocerussite into less soluble $PbO_2$ bearing phases will significantly slow down, and hence could result in serious consequences for municipalities considering the use of silicates as a

corrosion inhibitor where the lead bearing plumbing is rich in lead carbonates. Similar results were observed in a recent pipe-loop study with a scale rich in carbonates; Aghasadeghi and collaborators observed higher aqueous lead levels in the presence of sodium silicates compared to treatment by orthophosphate or pH adjustment alone (Aghasadeghi et al., 2021). On the other hand, the effect of silicates in $PbO_2$ dissolution needs to be explored. It is well established now that under certain conditions passivation of lead scale by chlorine ensures that dissolved lead levels remain below action levels. In any case, the results of this work suggest that silicates should not be used as a corrosion inhibitor in water systems that have higher amounts of $Pb^{2+}$ solids in the corrosion scale or where the interaction of chlorine residual is solely responsible for passivation of lead bearing plumbing. Silicates should investigated further for systems that have maintained a high chlorine residual and have plattnerite as the main lead phase in the corrosion scale. Further long-term studies are required to investigate whether the aluminosilicate solids forming on the lead surface function as a passivation layer and provide protection against lead dissolution.

# Chapter 5

# 5 Conclusions and Future Work

## 5.1 Conclusions

Silicates have been identified as a corrosion control option for lead, however, additional research is required to develop an understanding of how silicates work and might best be implemented to achieve lower dissolved lead levels in drinking water distribution systems. The mechanisms governing the interaction of silicates with lead and other metals found in DWDS have not been studied in detail, are not well understood, and the complex aqueous chemistry of silicates exacerbates this knowledge gap. Though several studies have investigated the use of silicates with lead service lines in terms of conditioning requirements and dosages to achieve levels below MACs, few have focused on understanding the chemical processes behind their effectiveness or lack thereof. Many studies have identified the presence of aluminosilicates in harvested corrosion scale from LSLs and hypothesized the formation of a passivation layer, however to our knowledge, no work has been able to show the formation of this layer in a simulated drinking water environment, nor how it interacts with lead and water.

In this thesis, silicates were studied under representative drinking water conditions. It was found that the presence of silicates inhibited oxidation of lead carbonates by free chlorine. As a result, the dominant lead phase remained $Pb^{2+}$ and dissolved lead levels increased. In the absence of silicates, lead carbonates were oxidized into less soluble lead oxides and as a result, batch reactors experienced lower dissolved lead levels. Aqueous samples were analyzed for free chlorine, alkalinity, silica, and dissolved lead throughout each experiment. Solid phase characterization was performed following harvesting and drying of lead precipitate; spectroscopic and microscopic techniques including UV-Vis, FTIR, Raman, XPS, XRD and SEM-EDX were used to identify elements and oxidation states in the solid phase. The presence of $Pb^{4+}$ oxides was found in larger quantities in the absence of silicates compared to samples which had been exposed to aqueous silicates. From previous works, it is known that it is preferable to have $PbO_2$ in a lead pipe corrosion scale as plattnerite is insoluble in a drinking water matrix and leads to lower dissolved lead levels. Environmental implications are significant; silicates should not be used to treat water in which the expected main phase of the

corrosion scale is $Pb^{2+}$, such as water systems that have previously or currently use monochloramine as a secondary disinfectant. We expect use of silicates under these conditions will result in elevated lead dissolution and subsequent human exposure.

Further experiments were completed to determine the role of aluminum in silicate precipitation and resultant formation of an aluminosilicate layer on the lead solid phase. Aluminosilicates have been identified as a major corrosion scale component, however the underlying mechanisms of formation remained relatively unknown. Through our experimental work, we found silicates precipitate out of aqueous solution in the presence of aluminum and accumulate as an aluminosilicate on the solid phase. Silicates do not precipitate or form a passivation layer in the absence of aluminum. The aluminosilicate precipitate was identifiable through spectroscopic and microscopic techniques including Raman, XPS and SEM-EDX. At 200 nm scale, it was possible to observe the deposits on the lead surface. EDX confirmed the aluminosilicate extends into the bulk phase and is not solely a surface phenomenon. This work confirmed that an aluminosilicate passivation layer will form on the solid phase in the presence of aqueous aluminum and silicate. In the short term, presence of aluminum and silicates in the aqueous phase resulted in increased dissolved lead levels due to inhibition of $Pb^{2+}$ oxidation. The degree to which this layer protects against lead dissolution over the long term remains undetermined.

## 5.2 Future Work

In this thesis, we found that the oxidation of lead carbonates is inhibited by the presence of silicates, resulting in lead remaining primarily in the +2 oxidation state. However, our experiments were completed in the range of 45 – 120 days. It is recommended to conduct long term studies with lead carbonates as the solid phase and treatment with both aluminum and silicates to determine the effect on dissolved lead levels over time as a passivation layer develops more fully on the lead surface. Moreover, we recommend testing this passivation layer in both free chlorine and monochloramine treated systems as we hypothesize use of silicates will increase dissolved lead for monochloramine treated water systems in which the dominant lead phase is $Pb^{2+}$. We further recommend long term experiments using $PbO_2$ as the lead solid phase to determine how dissolved lead levels would be affected should an aluminosilicate passivation layer form on the plattnerite surface. Specifically, this would answer questions such as: would plattnerite undergo a reverse redox reaction if the passivation layer prevents lead from remaining

in the $Pb^{4+}$ state due to chlorine oxidation, or would dissolved lead levels decrease with time and continual build up of the passivation layer?

Furthermore, we suggest conducting experiments using harvested corrosion scale for aluminosilicate passivation layer experiments, rather than pure phase lead compounds that have been identified as major phases in corrosion scale. Actual corrosion scales contain many compounds and have a complex chemistry that could alter formation of the aluminosilicate layer or react differently in the presence of chlorine.

Finally, we recommend experiments using lower aqueous aluminum levels; we used the MAC in order to make it easier to detect the precipitate on the lead surface however most drinking waters contains 10 – 20 times less aqueous phase aluminum. Experiments should be conducted to determine how long would it take the layer to form under these conditions, how effective it is at controlling lead release (if at all), and how a higher aqueous ratio of Si:Al ratio impacts layer formation. These questions need to be answered in order to fully understand the use of silicates as corrosion inhibitors in municipal DWDS, as well as the overall effectiveness of long-term corrosion control strategies for lead.

# References


Aghasadeghi, K., Peldszus, S., Trueman, B.F., Mishrra, A., Cooke, M.G., Slawson, R.M., Giammar, D.E., Gagnon, G.A., Huck, P.M., 2021. Pilot-scale comparison of sodium silicates, orthophosphate and pH adjustment to reduce lead release from lead service lines. Water Res. 195, 116955. https://doi.org/10.1016/j.watres.2021.116955

Allophane Mineral Data [WWW Document], n.d. URL http://webmineral.com/data/Allophane.shtml#.YD54EOhKiUk (accessed 3.2.21).

Arai, Y., Sparks, D.L., Davis, J.A., 2005. Arsenate adsorption mechanisms at the allophane - Water interface. Environ. Sci. Technol. 39, 2537–2544. https://doi.org/10.1021/es0486770

Bertsch, P.M., Parker, D.R., 1996. The Environmental Chemistry of Aluminum, Second. ed. CRC/Lewis Publ., Boca Raton, FL.

Biesinger, M., n.d. X-ray Photoelectron Spectroscopy (XPS) Reference Pages: Silicon [WWW Document]. URL http://www.xpsfitting.com/search/label/Silicon (accessed 3.8.21a).

Biesinger, M., n.d. X-ray Photoelectron Spectroscopy (XPS) Reference Pages: Aluminum [WWW Document]. URL http://www.xpsfitting.com/search/label/Aluminum (accessed 3.8.21b).

Bilinski, H., Schindler, P., 1982. Solubility and equilibrium constants of lead in carbonate solutions (25°C, I = 0.3 mol dm-3). Geochim. Cosmochim. Acta 46, 921–928. https://doi.org/10.1016/0016-7037(82)90048-5

Boelens, H.F.M., Eilers, P.H.C., Hankemeier, T., 2005. Sign constraints improve the detection of differences between complex spectral data sets: LC-IR as an example. Anal. Chem. 77, 7998–8007. https://doi.org/10.1021/ac051370e

Brokbartold, M., Temminghoff, E.J.M., Weng, L., Marschner, B., 2013. Unique Characteristics of Pb in Soil Contaminated by Red Lead Anti-Corrosion Paint. Soil Sediment Contam. An Int. J. 22, 839–855. https://doi.org/10.1080/15320383.2013.770443

CDC, 2018. Lead: Health Problems Caused by Lead [WWW Document]. URL https://www.cdc.gov/niosh/topics/lead/health.html (accessed 4.20.20).

Chang, W.L., He, J.L., 2004. XPS studies of PZT films deposited by metallic lead and ceramic PZT dual target co-sputtering, in: Journal of Electroceramics. pp. 47–50. https://doi.org/10.1007/s10832-004-5074-2

Childs, C.W., Inoue, K., Seyama, H., Soma, M., Theng, B.K.G., Yuan, G., 1997. X-ray photoelectron spectroscopic characterization of Silica Springs allophane. Clay Miner. 32, 565–572. https://doi.org/10.1180/claymin.1997.032.4.07

Creton, B., Bougeard, D., Smirnov, K.S., Guilment, J., Poncelet, O., 2008. Structural model and computer modeling study of allophane. J. Phys. Chem. C 112, 358–364. https://doi.org/10.1021/jp0738412

Edwards, M., Dudi, A., 2004. role of chlorine and chloramine in corrosion of lead-bearing plumbing materials. J. Am. Water Works Assoc. 96, 69–81. https://doi.org/10.1002/j.1551-8833.2004.tb10724.x

Edwards, M., Triantafyllidou, S., Best, D., 2009. Elevated Blood Lead in Young Children Due to Lead-Contaminated Drinking Water: Washington, DC, 2001-2004. Environ. Sci. Technol. 43, 1618–1623. https://doi.org/10.1021/es802789w

Farmer, V.C., Lumsdon, D.G., 1994. An assessment of complex formation between aluminium and silicic acid in acidic solutions. Geochim. Cosmochim. Acta 58, 3331–3334. https://doi.org/10.1016/0016-7037(94)90088-4

Fraser, D.A., Fairhall, L.T., 1959. The newer phenolic and vinyl base paints present less of Laboratory Study of the Solubility of Red Lead Paint in Water. Public Health Rep. 74, 501–510.

Gilbert, P.M., Seitzinger, S., Heil, C.A., Burkholder, J.M., Parrow, M.W., Codispoti, L.A., Kelly, V., 2005. Eutrophication The Role of in the Global Proliferation of Harmful Algal Blooms. Oceanography 18.

Government of Canada, 2013. Final Human Health State of the Science Report on Lead - Canada.ca [WWW Document]. URL https://www.canada.ca/en/health-canada/services/environmental-workplace-health/reports-publications/environmental-contaminants/final-human-health-state-science-report-lead.html#a8 (accessed 6.16.20).

Guo, D., Herrera, J.E., 2018. Corrosion Scale Characteristics and Lead Oxide Dissolution in Chloraminated Water. University of Western Ontario.

Guo, D., Robinson, C., Herrera, J.E., 2016. Mechanism of dissolution of minium (Pb3O4) in water under depleting chlorine conditions. Corros. Sci. 103, 42–49. https://doi.org/10.1016/j.corsci.2015.10.042

Guo, D., Robinson, C., Herrera, J.E., 2014. Role of Pb(II) defects in the mechanism of dissolution of plattnerite (β-PbO2) in water under depleting chlorine conditions. Environ. Sci. Technol. 48, 12525–12532. https://doi.org/10.1021/es502133k

Handke, M., Mozgawa, W., 1993. Vibrational spectroscopy of the amorphous silicates. Vib. Spectrosc. 5, 75–84. https://doi.org/10.1016/0924-2031(93)87057-Z

Hanna-Attisha, M., LaChance, J., Sadler, R.C., Champney Schnepp, A., 2016. Elevated Blood Lead Levels in Children Associated With the Flint Drinking Water Crisis: A Spatial Analysis of Risk and Public Health Response. Am. J. Public Health 106, 283–90. https://doi.org/10.2105/AJPH.2015.303003

Harsh, J., Chorover, J., Nizeyimana, E., 2018. Allophane and Imogolite, in: Soil Mineralogy with Environmental Applications. SSSA Book Series. John Wiley & Sons, Ltd, pp. 291–322. https://doi.org/10.2136/sssabookser7.c9

HealthCanada, 2017. Health Canada Sets New Guideline for Lead in Drinking Water.

Huang, P.M., Wang, M.K., Kämpf, N., Schulze, D.G., 2018. Aluminum Hydroxides. John Wiley & Sons, Ltd, pp. 261–289. https://doi.org/10.2136/sssabookser7.c8

Iler, R.K., 1973. Effect of adsorbed alumina on the solubility of amorphous silica in water. J. Colloid Interface Sci. 43, 399–408. https://doi.org/10.1016/0021-9797(73)90386-X

Katsanis, E.., Esmonde, W.D., Spencer, R.W., 1986. Soluble Silicate Corrosion Inhibitors in Water Systems. Mater. Perform. 25, 19–25.

Kim, E.J., Herrera, J.E., 2010. Characteristics of lead corrosion scales formed during drinking water distribution and their potential influence on the release of lead and other contaminants. Environ. Sci. Technol. 44, 6054–6061. https://doi.org/10.1021/es101328u

Kim, E.J., Herrera, J.E., Huggins, D., Braam, J., Koshowski, S., 2011. Effect of pH on the concentrations of lead and trace contaminants in drinking water: A combined batch, pipe loop and sentinel home study. Water Res. 45, 2763–2774. https://doi.org/10.1016/j.watres.2011.02.023

Kimmel, A., Sushko, P., Shluger, A., Bersuker, G., 2009. Positive and Negative Oxygen Vacancies in Amorphous Silica. ECS Trans. 19, 3–17. https://doi.org/10.1149/1.3122083

Kitman, J.L., 2000. The Secret History of Lead.

Kogo, A., Payne, S.J., Andrews, R.C., 2017. Comparison of three corrosion inhibitors in simulated partial lead service line replacements. J. Hazard. Mater. 329, 211–221. https://doi.org/10.1016/j.jhazmat.2017.01.039

Kvech, S., Edwards, M., 2001. Role of Aluminosilicate deposits in Lead and Copper Corrosion. J. Am. Water Works Assoc. 93, 104–112. https://doi.org/10.1002/j.1551-8833.2001.tb09339.x

LaRose Thompson, J., Scheetz, B.E., Schock, M.R., Lytle, D.A., Delaney, P.J., 1997. Sodium Silicate Corrosion Inhibitors: Issues of Effectiveness and Mechanism, in: Water Quality Technology Conference. PQ Corporation, Denver, CO.

Lehrman, L., Shuldener, H.L., 1952. Action of Sodium Silicate as a Corrosion Inhibitor in Water Piping. Ind. Eng. Chem. 44, 1765–1769.

Li, B., Trueman, B.F., Munoz, S., Locsin, J.M., Gagnon, G.A., 2021. Impact of sodium silicate on lead release and colloid size distributions in drinking water. Water Res. 190, 116709. https://doi.org/10.1016/j.watres.2020.116709

Li, B., Trueman, B.F., Rahman, M.S., Gao, Y., Park, Y., Gagnon, G.A., 2019. Understanding the impacts of sodium silicate on water quality and iron oxide particles. Environ. Sci. Water Res. Technol. 5, 1360–1370. https://doi.org/10.1039/c9ew00257j

Li, G., Bae, Y., Mishrra, A., Shi, B., Giammar, D.E., 2020. Effect of Aluminum on Lead Release to Drinking Water from Scales of Corrosion Products. Environ. Sci. Technol. 54, 6142–6151. https://doi.org/10.1021/acs.est.0c00738

Li, T., Liu, H., Fan, Y., Yuan, P., Shi, G., Bi, X.T., Bao, X., 2012. Synthesis of zeolite y from natural aluminosilicate minerals for fluid catalytic cracking application. Green Chem. 14, 3255–3259. https://doi.org/10.1039/c2gc36101a

Lin, Y.P., Valentine, R.L., 2008. Release of Pb(II) from monochloramine-mediated reduction of lead oxide (PbO2). Environ. Sci. Technol. 42, 9137–9143. https://doi.org/10.1021/es801037n

Lintereur, P.A., Duranceau, S.J., Taylor, J.S., Stone, E.D., 2010. Sodium silicate impacts on lead release in a blended potable water distribution system. Desalin. Water Treat. 16, 427–438. https://doi.org/10.5004/dwt.2010.1477

Lui, H., Korshin, G. V., Ferguson, J.F., 2008. Investigation of the kinetics and mechanisms of the oxidation of cerussite and hydrocerussite by chlorine. Environ. Sci. Technol. 42, 3241–3247. https://doi.org/10.1021/es7024406

Lytle, D.A., Schock, M.R., 2005. Formation of Pb(IV) oxides in chlorinated water. J. Am. Water Works Assoc. 97, 102–114. https://doi.org/10.1002/j.1551-8833.2005.tb07523.x

Lytle, D.A., Schock, M.R., Scheckel, K., 2009. The inhibition of Pb(IV) oxide formation in chlorinated water by orthophosphate. Environ. Sci. Technol. 43, 6624–6631. https://doi.org/10.1021/es900399m

Macquarrie, D.M., Mavinic, D.S., Neden, D.G., 1997. Greater Vancouver Water District drinking water corrosion inhibitor testing. Can. J. Civ. Eng. 24, 34–52.

McKinley, J.P., Dlaska, M.K., Batson, R., 2002. Red lead: Understanding red lead in lead-acid batteries, in: Journal of Power Sources. Elsevier, pp. 180–186. https://doi.org/10.1016/S0378-7753(01)01003-5

Mishrra, A., Wang, Z., Sidorkiewicz, V., Giammar, D.E., 2021. Effect of sodium silicate on lead release from lead service lines. Water Res. 188, 116485. https://doi.org/10.1016/j.watres.2020.116485

National Institute of Standards and Technology, 2012. NIST X-ray Photoelectron Spectroscopy Database [WWW Document]. https://doi.org/10.18434/T4T88K

Ng, D.-Q., Strathmann, T.J., Lin, Y.-P., 2012. Role of Orthophosphate As a Corrosion Inhibitor in Chloraminated Solutions Containing Tetravalent Lead Corrosion Product PbO 2. Environ. Sci. Technol. 46, 11062–11069. https://doi.org/10.1021/es302220t

Noel, J.D., Wang, Y., Giammar, D.E., 2014. Effect of water chemistry on the dissolution rate ofthe lead corrosion product hydrocerussite. Water Res. 54, 237–246. https://doi.org/10.1016/j.watres.2014.02.004

O'Connor, D., Hou, D., Ye, J., Zhang, Y., Ok, Y.S., Song, Y., Coulon, F., Peng, T., Tian, L., 2018. Lead-based paint remains a major public health concern: A critical review of global production, trade, use, exposure, health risk, and implications. Environ. Int. https://doi.org/10.1016/j.envint.2018.08.052

Opiso, E., Sato, T., Yoneda, T., 2009. Adsorption and co-precipitation behavior of arsenate, chromate, selenate and boric acid with synthetic allophane-like materials. J. Hazard. Mater. 170, 79–86. https://doi.org/10.1016/j.jhazmat.2009.05.001

Parfitt, R.L., Kimble, J.M., 1989. Conditions for Formation of Allophane in Soils. Soil Sci. Soc. Am. J. 53, 971–977. https://doi.org/10.2136/sssaj1989.03615995005300030057x

Phambu, N., 2003. Characterization of aluminum hydroxide thin film on metallic aluminum powder. Mater. Lett. 57, 2907–2913. https://doi.org/10.1016/S0167-577X(02)01395-2

RRUFF Database, n.d. Hydrocerussite R160062 [WWW Document]. URL https://rruff.info/hydrocerussite/display=default/R160062 (accessed 3.18.21).

Rudolph, W.W., Mason, R., Pye, C.C., 2000. Aluminium(III) hydration in aqueous solution. A Raman spectroscopic investigation and an ab initio molecular orbital study of aluminium(III) water clusters. Phys. Chem. Chem. Phys. 2, 5030–5040. https://doi.org/10.1039/b003764h

Salasi, M., Shahrabi, T., Roayaei, E., Aliofkhazraei, M., 2007. The electrochemical behaviour of environment-friendly inhibitors of silicate and phosphonate in corrosion control of carbon steel in soft water media. Mater. Chem. Phys. 104, 183–190. https://doi.org/10.1016/J.MATCHEMPHYS.2007.03.008

Scheetz, B.E., LaRosa Thompson, J., Delaney, P.J., 1997. XPS Characterization of Films

Formed on Distribution Systems Using Additives to Control Pb/Cu Levels in Drinking Water, in: Water Quality Technology Conference. PQ Corporation, Denver, CO.

Schock, M.R., 1989. Understanding corrosion control strategies for lead. J. Am. Water Work. Assoc. 81, 88–100. https://doi.org/10.1002/j.1551-8833.1989.tb03244.x

Schock, M.R., Celement, J.A., 1998. Lead and copper control with non-zinc orthophosphate. Artic. J. New Engl. Water Work. Assoc. 20–43.

Schock, Michael R., Lytle, D.A., Sandvig, A.M., Clement, J., Harmon, S.M., 2005. Replacing polyphosphate with silicate to solve lead, copper, and source water iron problems. J. Am. Water Works Assoc. 97, 84–93. https://doi.org/10.1002/j.1551-8833.2005.tb07521.x

Schock, Michael R, Scheckel, K.G., DeSantis, M.K., Gerke, T., 2005. Mode of Occurrence, Treatment and Monitoring Significance of Tetravalent Lead, in: AWWA Water Quality Technology Conference.

Senvaitiene, J., Smirnova, J., Beganskiene, A., Kareiva, A., 2007. XRD and FTIR Characteristics of Lead Oxide-Based Pigments and Glazes. Acta Chim. Slov. 185–193.

Sgro, J., 2017. Committee Report No. 21 - TRAN (42-1).

Snoeyink, V.L., Schock, M.R., Sarin, P., Wang, L., Chen, A.S.C., Harmon, S.M., 2003. Aluminium-containing scales in water distribution systems: Prevalence and composition. J. Water Supply Res. Technol. - AQUA 52, 455–474. https://doi.org/10.2166/aqua.2003.0042

Steffen, M.M., Belisle, B.S., Watson, S.B., Boyer, G.L., Wilhelm, S.W., 2014. Status, causes and controls of cyanobacterial blooms in Lake Erie. J. Great Lakes Res. https://doi.org/10.1016/j.jglr.2013.12.012

Stericker, W., 1945. Protection of Small Water Systems from Corrosion. Ind. Eng. Chem. 37, 716–720.

Stericker, W., 1938. Sodium Silicates in Water to Prevent Corrosion. Ind. Eng. Chem. 30, 348–351. https://doi.org/10.1021/ie50339a029

Switzer, J.A., Rajasekharan, V. V., Boonsalee, S., Kulp, E.A., Bohannan, E.W., 2006. Evidence that monochloramine disinfectant could lead to elevated Pb levels in drinking water.

Environ. Sci. Technol. 40, 3384–3387. https://doi.org/10.1021/es052411r

Tam, Y.S., Elefsiniotis, P., 2009. Corrosion control in water supply systems: Effect of pH, alkalinity, and orthophosphate on lead and copper leaching from brass plumbing. J. Environ. Sci. Heal. - Part A Toxic/Hazardous Subst. Environ. Eng. 44, 1251–1260. https://doi.org/10.1080/10934520903140009

Thomas, J.M., Tricker, M.J., 1974. Electronic Structure of the Oxides of Lead Part 2.I-An XPS Study of Bulk Rhombic PbO, Tetragonal PbO, /?-PbO, and Pb304. J. Chem. Soc., Faraday Trans. 2 329–336.

USEPA, 2020. Basic Information about Lead in Drinking Water [WWW Document]. URL https://www.epa.gov/ground-water-and-drinking-water/basic-information-about-lead-drinking-water (accessed 11.13.20).

Van Der Leer, D., Weatherill, N.P., Sharp, R.J., Hayes, C.R., 2002. Modelling the diffusion of lead into drinking water. Appl. Math. Model. 26, 681–699. https://doi.org/10.1016/S0307-904X(01)00077-4

Wada, K., Kubo, H., 1975. Precipitation of amorphous aluminosilicates from solutions containing monomeric silica and aluminum ions. J. Soil Sci. 26, 100–111. https://doi.org/10.1111/j.1365-2389.1975.tb01935.x

Wada, S.I., Eto, A., Wada, K., 1979. Synthetic Allophane and Imogolite. J. Soil Sci. 30, 347–355. https://doi.org/10.1111/j.1365-2389.1979.tb00991.x

Wang, P.W., Zheng, L., 1996. Structural Role of Lead in Lead Silicate Glasses Derived from XPS Spectra. J. Non-Crystalline Solids 129–134.

Wang, Y., Wu, J., Wang, Z., Terenyi, A., Giammar, D.E., 2013. Kinetics of lead(IV) oxide (PbO2) reductive dissolution: Role of lead(II) adsorption and surface speciation. J. Colloid Interface Sci. 389, 236–243. https://doi.org/10.1016/j.jcis.2012.09.022

Woszczynski, M.B., 2011. Controlling Lead Release from Premise Plumbing: A Pilot Scale Comparison of Sodium Silicates and Phosphate. Dalhousie University.

Xie, Y., 2010. Dissolution, Formation, and Transformation of the Lead Corrosion Product PbO

2 : Rates and Mechanisms of Reactions that Control Lead Release in Drinking Water Distribution Systems. Washington University.

Xie, Y., Giammar, D.E., 2011. Effects of flow and water chemistry on lead release rates from pipe scales. Water Res. 45, 6525–6534. https://doi.org/10.1016/j.watres.2011.09.050

Xie, Y., Wang, Y., Giammar, D.E., 2010a. Impact of chlorine disinfectants on dissolution of the lead corrosion product PbO2. Environ. Sci. Technol. 44, 7082–7088. https://doi.org/10.1021/es1016763

Xie, Y., Wang, Y., Singhal, V., Giammar, D.E., 2010b. Effects of pH and carbonate concentration on dissolution rates of the lead corrosion product PbO2. Environ. Sci. Technol. 44, 1093–1099. https://doi.org/10.1021/es9026198

Xiong, Y., 2015. Experimental Determination of Lead Carbonate Solubility at High Ionic Strengths: A Pitzer Model Description. Carlsbad, NM, USA.

Yuan, M. rong, Lu, J. tang, Kong, G., 2010. Effect of SiO2:Na2O molar ratio of sodium silicate on the corrosion resistance of silicate conversion coatings. Surf. Coatings Technol. 204, 1229–1235. https://doi.org/10.1016/j.surfcoat.2009.10.024

Zhou, E., Payne, S.J.O., Hofmann, R., Andrews, R.C., 2015. Factors affecting lead release in sodium silicate-treated partial lead service line replacements. J. Environ. Sci. Heal. - Part A Toxic/Hazardous Subst. Environ. Eng. 50, 922–930. https://doi.org/10.1080/10934529.2015.1030283

# Appendices

## Appendix A: pH Levels

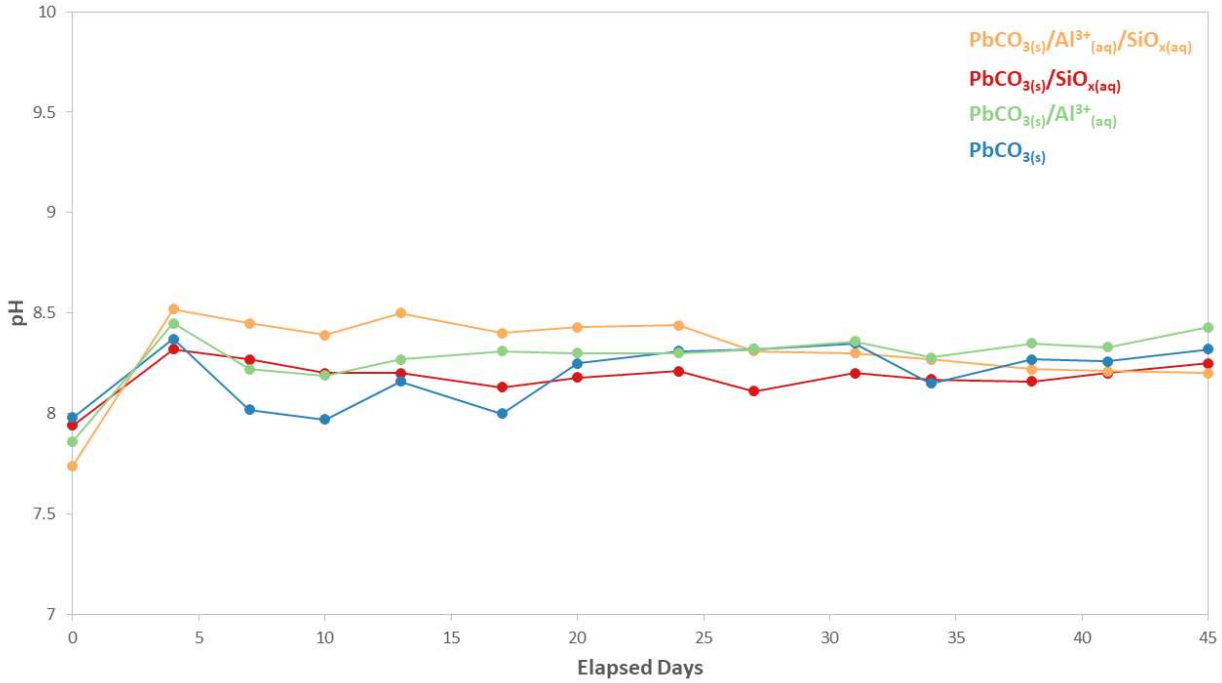


*Figure 32: pH levels over time for cerussite system exposed to chlorinated drinking water with and without silicates over 45 days (test two)*

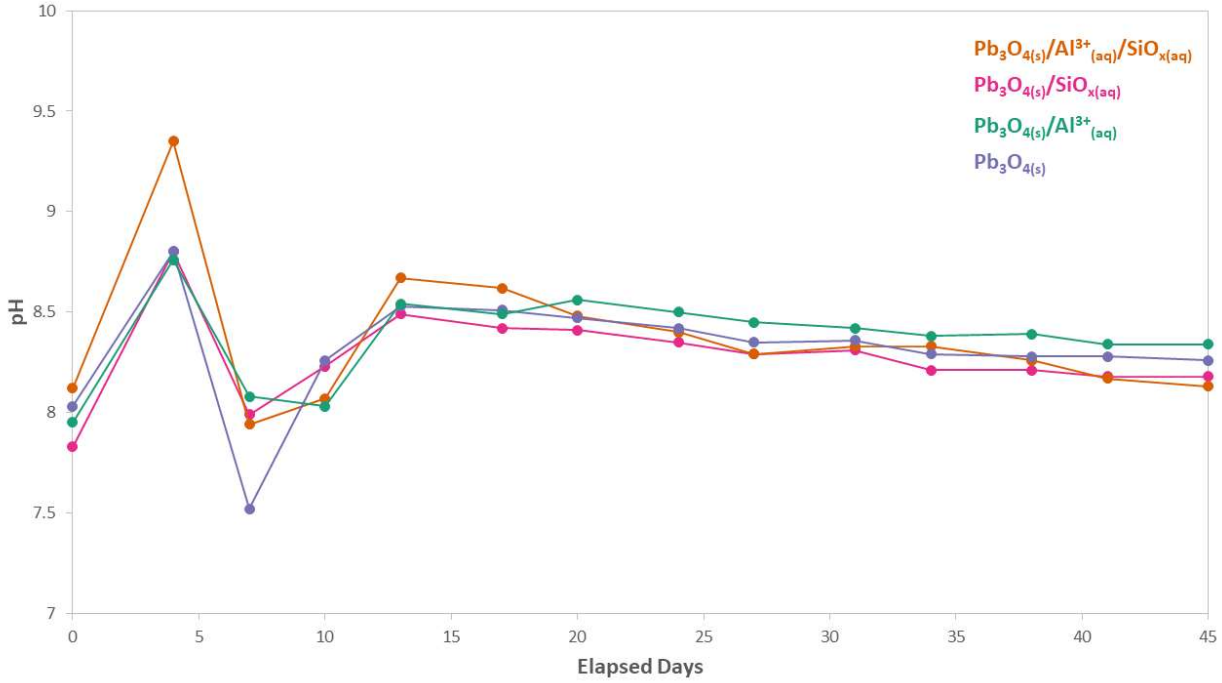


*Figure 33: pH levels over time for minium system exposed to chlorinated drinking water with and without silicates over 45 days (test four)*

## Appendix B: Si 2p and Al 2p XPS Fittings

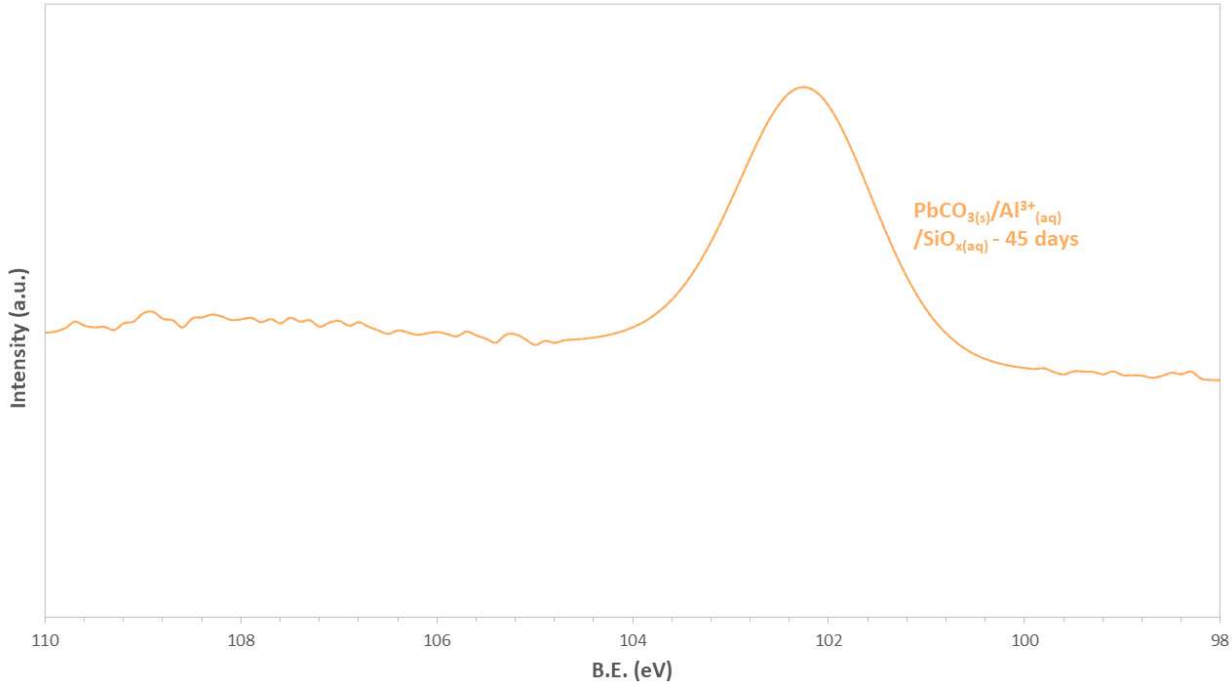


*Figure 34: High resolution Si 2p XPS fitting for $PbCO_{3(s)}/Al^{3+}{}_{(aq)}/SiO_{x(aq)}$ following 45 days exposure to chlorinated drinking water, indicating Si phase present is silicate.*

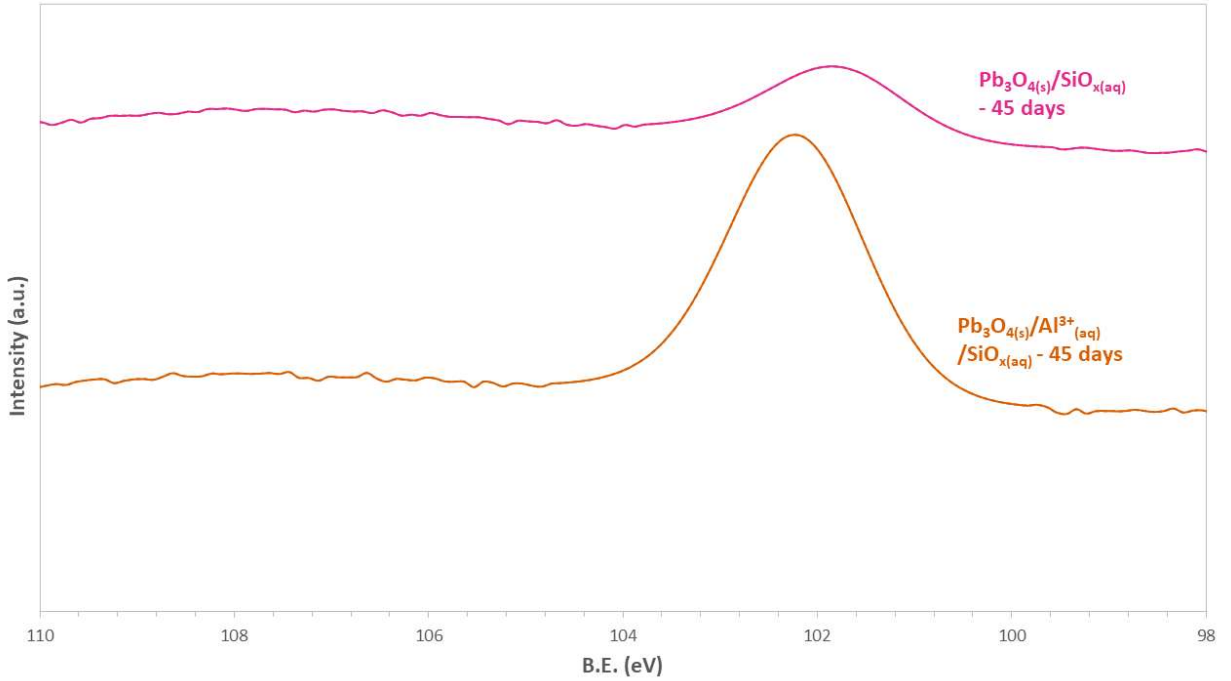


*Figure 35: High resolution Si 2p fitting for silicate-treated minium samples following 45 days exposure to chlorinated drinking water. Results indicate Si phase present is silicate and more Si is present when the solid phase is also exposed to aqueous aluminum.*

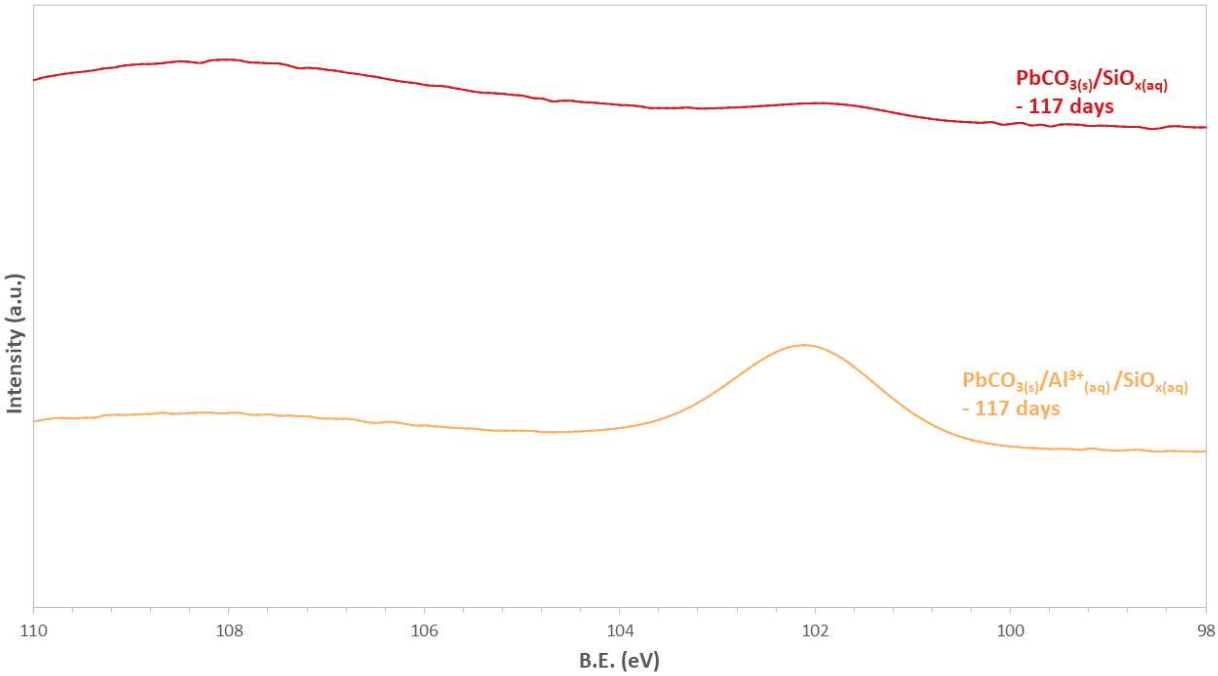


*Figure 36: High resolution Si 2p fitting for silicate-treated cerussite samples following 117 days exposure to chlorinated drinking water. Results indicate Si phase present is silicate and significantly more Si is present when the solid phase is also exposed to aqueous aluminum*

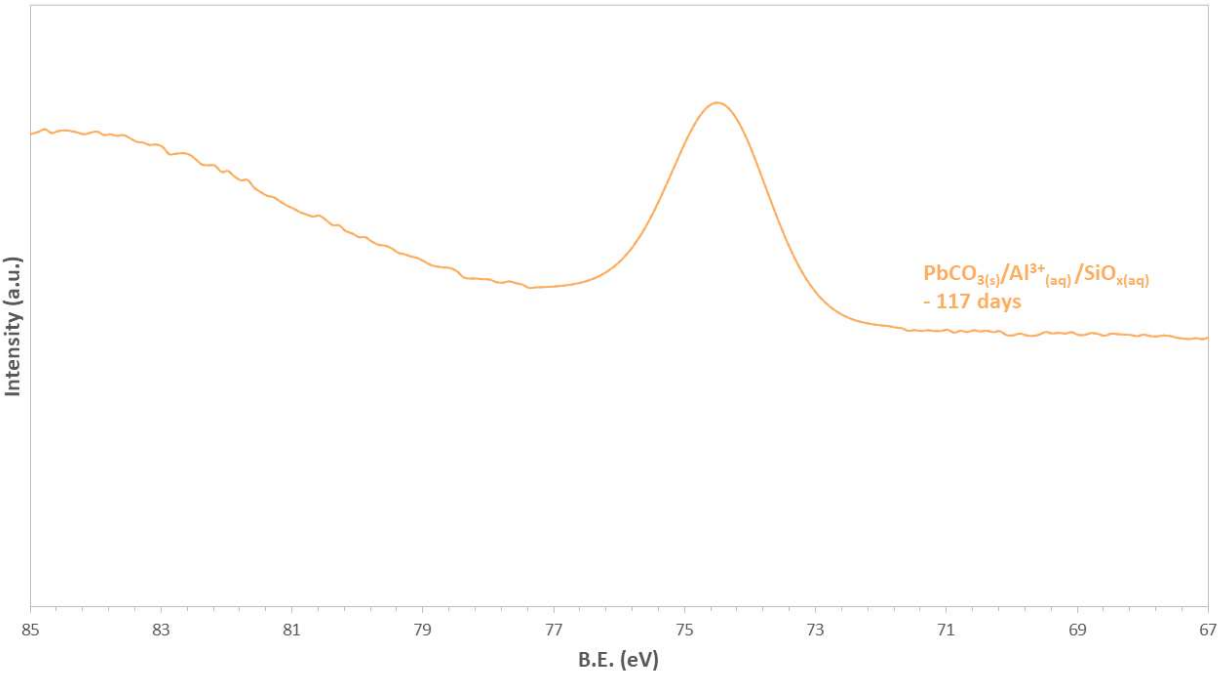


*Figure 37: High resolution Al 2p XPS fitting following 117-day exposure to chlorinated drinking water with cerussite as solid phase. Peak location indicates Al phase present is allophane.*

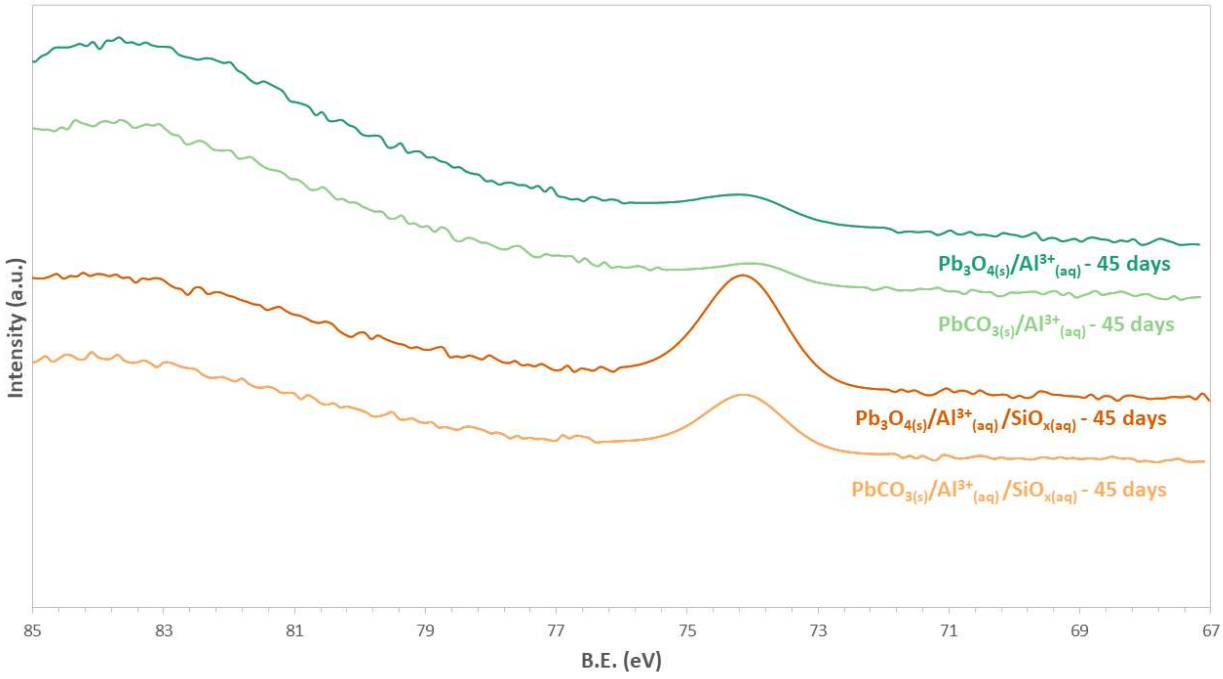


*Figure 38: High Resolution Al 2p XPS fitting for all 45-day samples exposed to aqueous aluminum. Peak location in the presence of silicates indicates Al phase is allophane. Peak location in absence of silicates indicates Al-OH phase present.*

## Curriculum Vitae

| | |
|---|---|
| **Name:** | Hailey (Overend) Holmes |
| **Post-Secondary Education and Degrees:** | Western University<br>London, ON, Canada<br>2019 – 2021 MESc Chemical Engineering (Environment and Sustainability)<br><br>Western University<br>London, ON, Canada<br>2014 – 2019 BESc Green Process Engineering, with Professional Internship, with Distinction |
| **Related Work Experience:** | Research Assistant<br>Western University<br>2019 – 2021<br><br>Teaching Assistant<br>Western University<br>2019 – 2021 |
| **Honors/ Awards:** | 3-Minute Thesis Engineering Heat 2nd place award, 2020<br><br>AER Graduate Scholarship in Environment and Sustainability, 2019 – 2020<br><br>Queen Elizabeth II Graduate Scholarship in Science and Technology, 2019 – 2020<br><br>Western University Gold Medal in Green Process Engineering, 2019 |
| **Conferences:** | Presented: Silicates as a Corrosion Control Option for Lead at EnviroCon 2021, hosted by Western University Center for Environment and Sustainability<br><br>Attended: Water Quality and Technology Conference 2019 in Dallas, TX hosted by the American Water Works Association |